

HU ISSN 1586–2070

# JOURNAL OF COMPUTATIONAL AND APPLIED MECHANICS

A Publication of the University of Miskolc

VOLUME 1, NUMBER 1 (2000)



MISKOLC UNIVERSITY PRESS



HU ISSN 1586–2070

# JOURNAL OF COMPUTATIONAL AND APPLIED MECHANICS

A Publication of the University of Miskolc

VOLUME 1, NUMBER 1 (2000)



MISKOLC UNIVERSITY PRESS

## EDITORIAL BOARD

- István PÁCZELT**, Editor in Chief, Department of Mechanics, University of Miskolc, 3515 MISKOLC, Hungary, mechpacz@uni-miskolc.hu
- László BARANYI, Department of Fluid and Heat Engineering, University of Miskolc, 3515 MISKOLC, Hungary, arambli@uni-miskolc.hu
- Edgár BERTÓTI, Department of Mechanics, University of Miskolc, 3515 MISKOLC, Hungary, mechber@uni-miskolc.hu
- Tibor CZIBERE, Department of Fluid and Heat Engineering, University of Miskolc, 3515 MISKOLC, Hungary, aramct@uni-miskolc.hu
- István ECSEDI, Department of Mechanics, University of Miskolc, 3515 MISKOLC, Hungary, mechecs@uni-miskolc.hu
- Wolfram FRANK, Institut für Fluid- und Thermodynamik, Universität Siegen, Paul-Bonatz-Strasse 9-11, 57076 SIEGEN, Germany, frank@ift.mb.uni-siegen.de
- Ulrich GABBERT, Institut für Mechanik, Otto-von-Guericke-Universität Magdeburg, Universitätsplatz 2, 39106 MAGDEBURG, Germany, ulrich.gabbert@mb.uni-magdeburg.de
- Zsolt GÁSPÁR, Department of Structural Mechanics, Budapest University of Technology and Economics, Műegyetem rkp. 3, 1111 BUDAPEST, Hungary, gaspar@ep-mech.me.bme.hu
- Robert HABER, Department of Theoretical and Applied Mechanics, University of Illinois at Urbana-Champaign, 216 Talbot Lab., 104 S. Wright Str., URBANA, IL 61801, USA, r-haber@uiuc.edu
- Gábor HALÁSZ, Department of Hydraulic Machines, Budapest University of Technology and Economics, Műegyetem rkp. 3, 1111 BUDAPEST, Hungary, HALASZ@vizgep.bme.hu
- Ji Huan HE, Department of Mathematics, College of Basic Science, Shanghai Donghua University, No. 1882 Yan'anxilu Road, 200051 SHANGHAI, China, jhhe@dhu.edu.cn
- Károly JÁRMAI, Department of Materials Handling and Logistics, University of Miskolc, 3515 MISKOLC, Hungary, altjar@uni-miskolc.hu
- László KOLLÁR, Department of Strength of Materials and Structures, Budapest University of Technology and Economics, Műegyetem rkpt. 3. K.II.42., 1521 BUDAPEST, Hungary, lkollar@eik.bme.hu
- Vladimir KOMPIŠ, Department of Mechanics, Faculty of Mechanical Engineering, University of Žilina, ŽILINA, Slovakia, kompiv@fstroj.utc.sk
- Imre KOZÁK, Department of Mechanics, University of Miskolc, 3515 MISKOLC, Hungary, mechkoz@uni-miskolc.hu
- József KÖVECSES, Mechanical Engineering Department 817 Sherbrooke Street West, MD163 Montreal, Quebec H3A 2K6, jozsef.kovecses@mcgill.ca
- Márta KURUTZ, Department of Structural Mechanics, Budapest University of Technology and Economics, Műegyetem rkp. 3, 1111 BUDAPEST, Hungary, kurutzm@eik.bme.hu
- R. Ivan LEWIS, Room 2-16 Bruce Building, Newcastle University, NEWCASTLE UPON TYNE, NE1 7RU, UK, R.I.Lewis@NCL.AC.UK
- Gennadij LVOV, Department of Mechanics, Kharkov Polytechnical Institute, 2 Frunze Str., 310002 KHARKOV, Ukraine, lvovgi@kpi.kharkov.ua
- Herbert MANG, Institute for Strength of Materials, University of Technology, Karlsplatz 13, 1040 VIENNA, Austria, Herbert.Mang@tuwien.ac.at
- Zenon MROZ, Polish Academy of Sciences, Institute of Fundamental Technological Research, Swietokrzyska 21, WARSAW, Poland, zmroz@ippt.gov.pl
- Tibor NAGY, Department of Physics, University of Miskolc, 3515 MISKOLC, Hungary, fiznagyt@uni-miskolc.hu
- Gyula PATKÓ, Department of Machine Tools, University of Miskolc, 3515 MISKOLC, Hungary, mechpgy@uni-miskolc.hu
- Jan SLADEK, Ústav stavbenictva a architektúry, Slovenskej akadémie vied, Dubróvska cesta 9, 842 20 BRATISLAVA, Slovakia, usarlad@savba.sk
- Gábor STÉPÁN, Department of Mechanics, Budapest University of Technology and Economics, Műegyetem rkp. 3, 1111 BUDAPEST, Hungary, stepan@mm.bme.hu
- Barna SZABÓ, Center for Computational Mechanics, Washington University, Campus Box 1129, St. LOUIS, MO63130, USA, szabo@me.wustl.edu
- Szilárd SZABÓ, Department of Fluid and Heat Engineering, University of Miskolc, 3515 MISKOLC, Hungary, aram2xsz@uni-miskolc.hu
- György SZEIDL, Department of Mechanics, University of Miskolc, 3515 MISKOLC, Hungary, Gyorgy.SZEIDL@uni-miskolc.hu

## LOCAL EDITORIAL COUNCIL

T. CZIBERE, I. KOZÁK, I. PÁCZELT, G. PATKÓ, G. SZEIDL

# APPLICABILITY OF A CONSTANT YOUNG'S MODULUS IN GEOMETRICALLY NONLINEAR ELASTICITY

EDGÁR BERTÓTI

Department of Mechanics, University of Miskolc  
3515 Miskolc – Egyetemváros, Hungary  
mechber@gold.uni-miskolc.hu

[Received: August 24, 1999]

*Dedicated to Professor István Páczelt on the occasion of his sixtieth birthday*

**Abstract.** The aim of this paper is to demonstrate through a simple problem that the use of a constant Young's modulus in numerical analyses of geometrically nonlinear elasticity problems should be considered as a potential source of inaccuracy, depending on what work-conjugate stress and strain measures the formulation uses. Importance of the Biot stresses and Jaumann strains as conjugate engineering stress and strain measures in nonlinear elasticity is emphasized.

*Keywords:* Stress and strain measures, constant Young's modulus, geometrically nonlinear elasticity

## 1. Introduction

In geometrically nonlinear elasticity problems the material is often considered to be linearly elastic and the nonlinearity usually enters into the formulation through the strain-displacement relations, due to the appearance of larger displacement derivatives (which are mostly related to the large local rotations). In the majority of numerical analyses, the preferred work-conjugate stress and strain measures are the second Piola-Kirchhoff stress tensor and the Green-Lagrange strain tensor.

When the stretches of the material curves of an elastic body are much smaller than unity, the constant Young's modulus measured for a given material can directly be applied between different work-conjugate stress and strain measures such as the popular Green-Lagrange strains and the second Piola-Kirchhoff stresses. For some modern materials, applied for instance in manufacturing advanced composite structures, the limit of the linearly elastic behavior in terms of stretches can, however, be much higher than that for classical materials (e.g. for metals). This means that in many geometrically nonlinear elasticity problems, the stretches in some parts of the body can be much larger than in other parts of the body and using the same constant Young's modulus for relating the second Piola-Kirchhoff stresses to the Green-Lagrange strains in each point of the body, independently of the local stretch value, can lead to incorrect numerical results [1].

In this paper we consider the uniaxial tension of a homogeneous isotropic prismatic beam in the elastic range. Although the material of the beam is assumed to be linearly

elastic, it is not assumed that the stretch of the beam is much smaller than unity. The deformation and the stress state of the beam will be described by stress and strain measures of finite elasticity, which is an important issue for the purpose of the present investigations. In contrast to [1], the relationship between the Cauchy stresses and the Euler-Almansi strains is, however, not assumed to be linear. Instead, as in reality, the dependence of the nominal stress on the stretch of the beam is considered to be linear and the tangent of this linear function is the (constant) Young's modulus of the material of the beam.

After writing down the different work-conjugate stress and strain tensors for the beam under uniaxial tension, the relationships between the normal stresses and strains in the axial direction are derived and the error resulting from the use of a constant Young' modulus at different stretch and strain levels is investigated.

## 2. Strain measures

Consider the elastic deformation of a homogeneous isotropic prismatic beam of length  $L$  under uniaxial tension. Let  $A_0$  and  $A$  be the cross-sectional areas of the beam in the reference (undeformed) and current (deformed) configurations, respectively. Let the two configurations of the beam be investigated in the same Cartesian frame. Coordinates of material points in the reference and current configurations are denoted by  $X, Y, Z$  and  $x, y, z$ , respectively, where  $Z$  and  $z$  are the axes of the beam in the two configurations. The axial force is denoted by  $F$  and the change in length  $L$  of the beam is denoted by  $\Delta L$ .

Plotting the nominal stress  $\sigma = F/A_0$  against the stretch  $\epsilon = \Delta L/L$  of the beam, the stress-strain curve is obtained. We restrict our investigations here to the elastic range of the deformation when the nominal stress  $\sigma$  is a linear function of the stretch  $\epsilon$ . The elasticity or Young's modulus  $E_Y$  of the material of the beam is defined as the tangent of this linear function  $\sigma = \sigma(\epsilon) = E_Y \epsilon$ .

The deformation gradient and the inverse deformation gradient of the beam under uniaxial tension are given by

$$\mathbf{F} = \begin{bmatrix} 1 - \nu\epsilon & 0 & 0 \\ 0 & 1 - \nu\epsilon & 0 \\ 0 & 0 & 1 + \epsilon \end{bmatrix}, \quad (2.1)$$

$$\mathbf{F}^{-1} = \begin{bmatrix} (1 - \nu\epsilon)^{-1} & 0 & 0 \\ 0 & (1 - \nu\epsilon)^{-1} & 0 \\ 0 & 0 & (1 + \epsilon)^{-1} \end{bmatrix}, \quad (2.2)$$

where  $\nu$  is the Poisson's ratio. Since the deformation of the beam is rotation-free, the polar decomposition of the deformation gradient reads

$$\mathbf{F} = \mathbf{R} \cdot \mathbf{U} = \mathbf{I} \cdot \mathbf{U} = \mathbf{U} \quad (2.3)$$

where  $\mathbf{U}$  is the right stretch tensor,  $\mathbf{I}$  is the unit tensor and  $\mathbf{R} = \mathbf{I}$  is the (orthogonal) rotation tensor and a dot denotes scalar product between two tensors.

The displacement gradient in the reference configuration is given by

$$\mathbf{H} = \mathbf{F} - \mathbf{I}; \quad \mathbf{H} = \begin{bmatrix} -\nu\epsilon & 0 & 0 \\ 0 & -\nu\epsilon & 0 \\ 0 & 0 & \epsilon \end{bmatrix}. \quad (2.4)$$

The Jaumann or engineering strain tensor  $\boldsymbol{\varepsilon}$  is defined in the reference configuration as

$$\boldsymbol{\varepsilon} = \mathbf{U} - \mathbf{I}; \quad \boldsymbol{\varepsilon} = \begin{bmatrix} -\nu\epsilon & 0 & 0 \\ 0 & -\nu\epsilon & 0 \\ 0 & 0 & \epsilon \end{bmatrix}. \quad (2.5)$$

Due to the rotation-free deformation of the beam, the Jaumann strain tensor is equivalent to the displacement gradient in the reference configuration, i.e.  $\mathbf{H} \equiv \boldsymbol{\varepsilon}$ .

The Green-Lagrange strain tensor  $\mathbf{E}^0$  is defined in the reference configuration as

$$\mathbf{E}^0 = \frac{1}{2}(\mathbf{F}^T \cdot \mathbf{F} - \mathbf{I}). \quad (2.6)$$

In view of (2.1),  $\mathbf{E}^0$  takes the form

$$\mathbf{E}^0 = \begin{bmatrix} -\nu\epsilon + \frac{1}{2}\nu^2\epsilon^2 & 0 & 0 \\ 0 & -\nu\epsilon + \frac{1}{2}\nu^2\epsilon^2 & 0 \\ 0 & 0 & \epsilon + \frac{1}{2}\epsilon^2 \end{bmatrix}. \quad (2.7)$$

The Almansi-Euler strain tensor  $\mathbf{E}$  is defined in the current configuration as

$$\mathbf{E} = \frac{1}{2}(\mathbf{I} - \mathbf{F}^{-T} \cdot \mathbf{F}^{-1}). \quad (2.8)$$

Taking into account that the Almansi-Euler and Green-Lagrange strain tensors are related to each other through

$$\mathbf{E} = \mathbf{F}^{-T} \cdot \mathbf{E}^0 \cdot \mathbf{F}^{-1} \quad (2.9)$$

and recalling that the reference and current configurations of the beam are investigated now in the same Cartesian frame, the Almansi-Euler strain components can be expressed in terms of the Green-Lagrange strain components as

$$E_{ij} = \begin{cases} \frac{1}{(F_{ij})^2} E_{ij}^0 & \text{if } i = j \\ 0 & \text{if } i \neq j \end{cases} \quad (2.10)$$

i.e. the non-zero components of  $\mathbf{E}$  are given by

$$\begin{aligned} E_{11} &= \frac{1}{(1 - \nu\epsilon)^2} E_{11}^0, & E_{22} &= \frac{1}{(1 - \nu\epsilon)^2} E_{22}^0, \\ E_{33} &= \frac{1}{(1 + \epsilon)^2} E_{33}^0. \end{aligned} \quad (2.11)$$

As is well known, for stretches close to zero the Green-Lagrange and Almansi-Euler strain tensors become identical with the engineering or Jaumann strain tensor. Note

that independently of how large  $\epsilon$  is, the structure of the Jaumann strain tensor is the same as that of the infinitesimal strain tensor.

### 3. Stress measures

Four important stress measures are considered here for the beam under uniaxial tension: the Cauchy (or true) stress tensor,  $\mathbf{S}$ , defined in the current configuration, the first Piola-Kirchhoff stress tensor,  $\mathbf{T}$ , which is a two-point tensor, the second Piola-Kirchhoff stress tensor,  $\mathbf{S}^0$ , defined in the reference configuration, and the less known, though very important, Biot stress tensor,  $\boldsymbol{\sigma}$ , defined in the reference configuration [2].

The relationships between these stress measures are well known and can be found in many books on continuum mechanics (see e.g.[3]): assuming that the Cauchy stress tensor  $\mathbf{S}$  is known, the first Piola-Kirchhoff stress tensor is obtained as

$$\mathbf{T} = J \mathbf{S} \cdot \mathbf{F}^{-T} \quad (3.1)$$

where  $J$  is the Jacobian of the deformation gradient, and the second Piola-Kirchhoff stress tensor as

$$\mathbf{S}^0 = \mathbf{F}^{-1} \cdot \mathbf{T} = J \mathbf{F}^{-1} \cdot \mathbf{S} \cdot \mathbf{F}^{-T} . \quad (3.2)$$

The Biot stress tensor  $\boldsymbol{\sigma}$  is obtained through the polar decomposition of the first Piola-Kirchhoff stress tensor

$$\mathbf{T} = \mathbf{R} \cdot \boldsymbol{\sigma} \quad \boldsymbol{\sigma} = \mathbf{R}^T \cdot \mathbf{T} \quad (3.3)$$

where  $\mathbf{R}$  is the proper orthogonal rotation tensor obtained from the polar decomposition of the deformation gradient. The Biot stress tensor is generally nonsymmetric. For isotropic materials  $\boldsymbol{\sigma}$  becomes coaxial with  $\mathbf{U}$  and is, therefore, symmetric.

For the isotropic beam under uniaxial tension, each stress tensor introduced above has only one non-zero component which is the normal stress in the axial ( $z$  or  $Z$ ) direction. In addition, since the deformation is rotation-free, the first Piola-Kirchhoff stress tensor is identical with the Biot stress tensor, i.e.

$$\mathbf{T} = \mathbf{R} \cdot \boldsymbol{\sigma} = \mathbf{I} \cdot \boldsymbol{\sigma} = \boldsymbol{\sigma} . \quad (3.4)$$

The only non-zero component of the first Piola-Kirchhoff as well as the Biot stress tensor is the nominal stress  $\sigma$ , which is the quotient of the axial force and the cross sectional area of the undeformed beam:

$$T_{33} = \sigma_{33} = \sigma = \frac{F}{A_0} \quad (3.5)$$

The non-zero components of the two other stress tensors can be obtained by applying the transformation formulas (3.1) and (3.2). Taking into account that the Jacobian of the deformation (2.1) is

$$J = \det \mathbf{F} = (1 + \epsilon)(1 - \nu\epsilon)^2 , \quad (3.6)$$

the Cauchy normal stress in the  $z$  direction of the beam is

$$S_{33} = \frac{1}{(1 - \nu\epsilon)^2} T_{33} = \frac{1}{(1 - \nu\epsilon)^2} \sigma \quad (3.7)$$

and the second Piola-Kirchhoff normal stress in the  $Z$  direction of the beam is

$$S_{33}^0 = \frac{1}{1 + \epsilon} T_{33} = \frac{1}{1 + \epsilon} \sigma. \quad (3.8)$$

The first Piola-Kirchhoff-, the Biot-, the Cauchy- and the second Piola-Kirchhoff stress tensors for the beam are given by

$$\mathbf{T} \equiv \boldsymbol{\sigma} = \begin{bmatrix} 0 & 0 & 0 \\ 0 & 0 & 0 \\ 0 & 0 & \sigma \end{bmatrix}; \quad \mathbf{S} = \begin{bmatrix} 0 & 0 & 0 \\ 0 & 0 & 0 \\ 0 & 0 & \sigma(1 - \nu\epsilon)^{-2} \end{bmatrix}; \quad \mathbf{S}^0 = \begin{bmatrix} 0 & 0 & 0 \\ 0 & 0 & 0 \\ 0 & 0 & \sigma(1 + \epsilon)^{-1} \end{bmatrix} \quad (3.9)$$

The relationship between the Cauchy normal stress  $S_{33}$  and the second Piola-Kirchhoff normal stress  $S_{33}^0$  can be obtained from (3.7)-(3.8):

$$S_{33} = \frac{1 + \epsilon}{(1 - \nu\epsilon)^2} S_{33}^0. \quad (3.10)$$

#### 4. Relations between conjugate stress and strain measures

The strain energy density of a hyperelastic body can be expressed by the inner product of different, appropriate stress and strain tensors. We are interested here in the relations between the following work-conjugate stress and strain measures:

- second Piola-Kirchhoff stress tensor  $\Leftrightarrow$  Green-Lagrange strain tensor
- first Piola-Kirchhoff stress tensor  $\Leftrightarrow$  displacement gradient tensor
- Cauchy stress tensor  $\Leftrightarrow$  Almansi-Euler strain tensor
- Biot stress tensor  $\Leftrightarrow$  Jaumann strain tensor.

As mentioned in the Introduction, the relation between the nominal stress and the stretch of the beam under uniaxial tension is considered to be linear and this relation is expressed by Hooke's law:

$$\sigma = E_Y \epsilon \quad (4.1)$$

where  $E_Y$  is the Young's or elasticity modulus of the material of the beam and  $\epsilon$  is not necessarily infinitesimal. In view of the previous sections, the Hooke's law between the different work-conjugate stress and strain components of the beam can easily be derived. Taking into account that – according to (3.5) – the nominal stress  $\sigma$  is equal to the first Piola-Kirchhoff normal stress  $T_{33}$  as well as the Biot normal stress  $\sigma_{33}$  in the axial direction, and also that the stretch of the beam  $\epsilon$  is equal to

the displacement gradient component  $H_{33}$  as well as the Jaumann normal strain  $\varepsilon_{33}$  in the axial direction, we obtain the following stress-strain relationships between the appropriate conjugate stress and strain components:

I. Piola-Kirchhoff stress – displacement gradient:

$$T_{33} = E_Y H_{33} \quad (4.2)$$

Biot stress – Jaumann strain:

$$\sigma_{33} = E_Y \varepsilon_{33} \quad (4.3)$$

Cauchy stress – Almansi-Euler strain:

$$S_{33} = \frac{2(1+\epsilon)^2}{(2+\epsilon)(1-\nu\epsilon)^2} E_Y E_{33} = E_Y^{\text{cur}} E_{33} \quad (4.4)$$

II. Piola-Kirchhoff stress – Green-Lagrange strain:

$$S_{33}^0 = \frac{2}{(1+\epsilon)(2+\epsilon)} E_Y E_{33}^0 = E_Y^{\text{ref}} E_{33}^0 \quad (4.5)$$

where

$$E_Y^{\text{cur}}(\epsilon) = \frac{2(1+\epsilon)^2}{(2+\epsilon)(1-\nu\epsilon)^2} E_Y \quad (4.6)$$

and

$$E_Y^{\text{ref}}(\epsilon) = \frac{2}{(1+\epsilon)(2+\epsilon)} E_Y \quad (4.7)$$

are the actual moduli of elasticity in the current and reference configurations, respectively. It can be seen from (4.2) and (4.3) that, independently of how large the stretch of the beam is, the I. Piola-Kirchhoff normal stress  $T_{33}$  and the displacement gradient component  $H_{33}$  as well as the Biot normal stress  $\sigma_{33}$  and the Jaumann strain  $\varepsilon_{33}$  are related to each other by the same (known and constant) Young's modulus  $E_Y$ . This is not the case, however, for either the Cauchy normal stress  $S_{33}$  and Almansi-Euler strain  $E_{33}$  or the II. Piola-Kirchhoff stress  $S_{33}^0$  and Green-Lagrange strain  $E_{33}^0$ . They are related to each other through the 'modified' Young's moduli  $E_Y^{\text{cur}}$  and  $E_Y^{\text{ref}}$ , respectively, and, as it is seen from (4.6) and (4.7), neither  $E_Y^{\text{cur}}$  nor  $E_Y^{\text{ref}}$  is constant with respect to the stretch  $\epsilon$ . The functions  $E_Y^{\text{cur}}(\epsilon)$  and  $E_Y^{\text{ref}}(\epsilon)$  for stretch values  $0 \leq \epsilon \leq 0.5$  are shown in Figure 1, assuming that the measured Young's modulus  $E_Y$  is constant and unity.

Relative errors in the Cauchy stress (at  $\nu = 0.0$ ) as well as in the II. Piola-Kirchhoff stress for relatively small stretch values are given in Table 1 with the assumption that the measured constant Young's modulus  $E_Y$  is used instead of the actual moduli  $E_Y^{\text{cur}}$  and  $E_Y^{\text{ref}}$ . As expected, for very small stretches the error is not significant; approximately 1% error is obtained in both stresses when the stretch  $\epsilon$  attains the value of 0.0065.

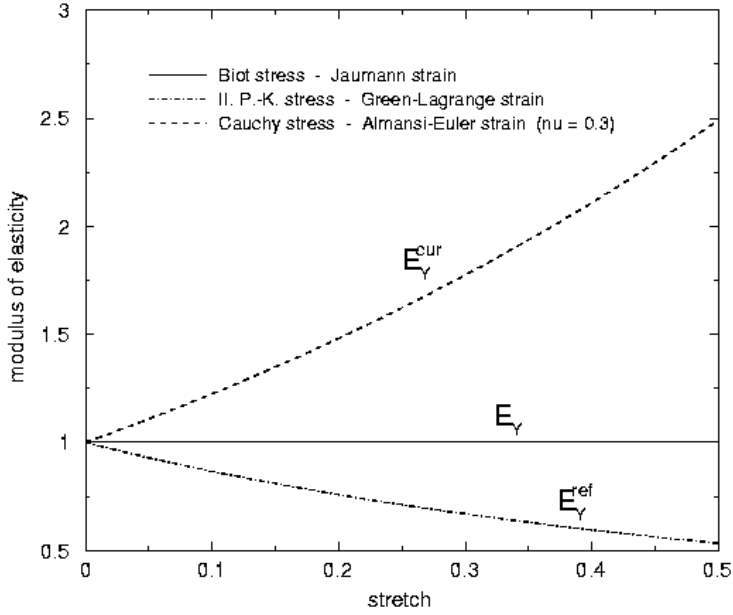


Figure 1. Modulus of elasticity for different conjugate stress and strain measures

$\epsilon$	rel. error in $S_{33}$ (%)	rel. error in $S_{33}^0$ (%)
0.0001	0.015	0.015
0.0005	0.075	0.075
0.001	0.15	0.15
0.005	0.75	0.75
0.01	1.50	1.50
0.05	7.56	7.56
0.1	15.24	13.42

Table 1. Relative error in the Cauchy stress (at  $\nu = 0.0$ ) and in the II. Piola-Kirchhoff stress

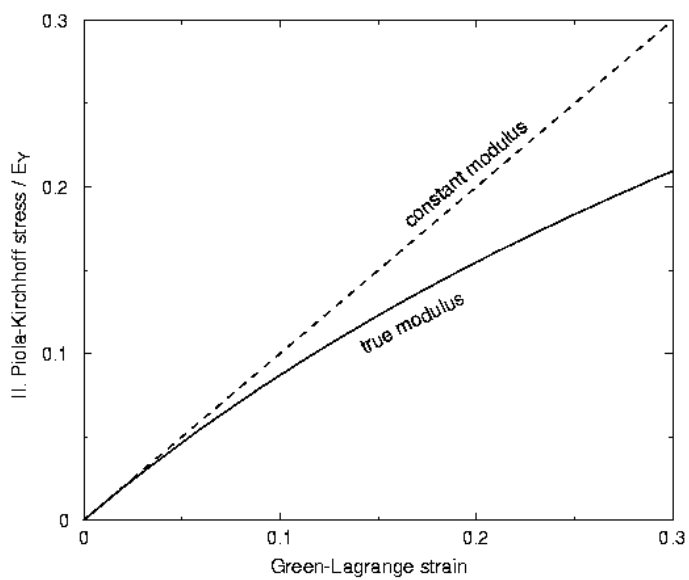


Figure 2. II. Piola-Kirchhoff stress against the Green-Lagrange strain with  $E_Y$  fixed

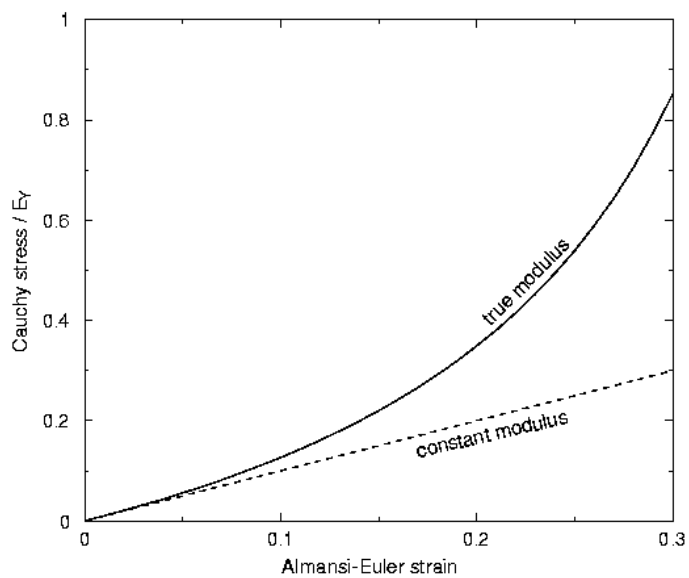


Figure 3. Cauchy stress against the Almansi-Euler strain with  $E_Y$  fixed

Taking into account that the stretch  $\epsilon$  can be expressed by the Green-Lagrange strain  $E_{33}^0$  as [3]

$$\epsilon = \sqrt{2E_{33}^0 + 1} - 1 \quad (4.8)$$

and inserting (4.8) in (4.5), the II. Piola-Kirchhoff stress  $S_{33}^0$  can be obtained directly in terms of the Green-Lagrange strain  $E_{33}^0$ . The  $S_{33}^0(E_{33}^0)$  function is plotted in Figure 2 for Green-Lagrange strain values  $0 \leq E_{33}^0 \leq 0.3$ . The Cauchy stress  $S_{33}$  can also be expressed directly in terms of the Almansi-Euler strain  $E_{33}$  by utilizing the fact that stretch  $\epsilon$  can be expressed by the Almansi-Euler strain  $E_{33}$  as [3]

$$\epsilon = \frac{1}{\sqrt{1 - 2E_{33}}} - 1. \quad (4.9)$$

Inserting (4.9) in (4.4), the function  $S_{33}(E_{33})$  is obtained which is shown in Figure 3 for Almansi-Euler strain values  $0 \leq E_{33} \leq 0.3$ . Dashed lines in both Figures 2 and 3 indicate the linear (incorrect) stress-strain curves when the constant Young's modulus  $E_Y$  is used for obtaining the II. Piola-Kirchhoff stresses from the Green-Lagrange strains and the Cauchy stresses from the Euler-Almansi strains.

## 5. Conclusions

In advanced materials it is not unusual that the limit of the linearly elastic behavior in terms of stretches is much higher than for classical materials like metals. Independently of the stress and strain measures applied by the underlying formulation, an accurate numerical analysis of geometrically nonlinear problems involving materials of that kind requires the use of correct elasticity modulus in the stress-strain relations at different stretch and strain levels.

Considering a homogeneous isotropic prismatic beam under uniaxial tension, the Young's modulus of the linearly elastic material is the tangent of the nominal stress versus stretch function. Independently of how large the stretches are, the constant Young's modulus measured that way can always be applied between the Biot stresses and Jaumann strains, being work-conjugate engineering stress and strain measures. (The I. Piola-Kirchhoff stress and displacement gradient components can also be related to each other through that constant Young's modulus, provided the deformation is rotation-free.) The constant Young's modulus cannot, however, be used for relating other stress and strain measures, such as the widely used second Piola-Kirchhoff stresses and Green-Lagrange strains or the Cauchy stresses and Euler-Almansi strains, without the restriction that the stretches in the material should be very small. This paper investigated the error resulting from the use of a constant Young's modulus for relating the above mentioned different conjugate stress and strain measures at different stretch levels.

**Acknowledgement.** This work was supported in part by the Hungarian Scientific Research Fund under Grant No. OTKA T026292.

**REFERENCES**

- [1] GUMMADI, L.M.B. and PALAZOTTO A.N.: *Large strain analysis of beams and arches undergoing large rotations*, Int. J. Non-Linear Mechanics, **33**, (1998), 615–645.
- [2] BIOT, M. A.: *The mechanics of incremental deformations*, John Wiley & Sons, Inc., New York, 1965.
- [3] MALVERN, L.E.: *Introduction to the mechanics of a continuous medium*, Prentice Hall, Englewood Cliffs, New Jersey, 1969.

## STRESS FUNCTIONS FOR TORSION-FREE AXISYMMETRIC STATE OF STRESS

ISTVÁN ECSEDI

Department of Mechanics, University of Miskolc  
3515 Miskolc – Egyetemváros, Hungary  
mechecs@gold.uni-miskolc.hu

[Received: August 15, 1999]

*Dedicated to Professor István Páczelt on the occasion of his sixtieth birthday*

**Abstract.** The solution of problems of the theory of elasticity in terms of stresses requires the solution of equations of equilibrium. In two and three-dimensional application, the components of stress are frequently expressed in terms of partial derivatives of stress function, the correct expressions being chosen so that the conditions of static equilibrium become a consequence of partial derivatives independent of the order of differentiation. In this manner the solution of an equilibrium equation can be obtained without any difficulty. In this paper a systematic process is devised to derive the stress functions for the problems of torsion-free axisymmetric state of stresses. The applied method is based on the theory of total differentials. The stress boundary conditions are also formulated in terms of stress functions. The relations between the strain compatibility conditions and the stress functions are discussed. Different forms of solutions of equilibrium equations in terms of stress functions are also analyzed.

*Keywords:* Stress functions, axisymmetric, strain compatibility, virtual work

### 1. Introduction

For torsion-free axisymmetric state of stress the equilibrium equations can be written as

$$\frac{\partial}{\partial r}(r\sigma_r) + \frac{\partial}{\partial z}(r\tau_{rz}) - \sigma_\varphi + rq_r = 0 \quad (r, z) \in T, \quad (1.1)$$

$$\frac{\partial}{\partial r}(r\tau_{rz}) + \frac{\partial}{\partial z}(r\sigma_z) + rq_z = 0 \quad (r, z) \in T. \quad (1.2)$$

Here, we have used cylindrical coordinates  $(r, \varphi, z)$  with  $z$  as the axis of symmetry. In equations (1.1) and (1.2)  $\sigma_r, \sigma_\varphi, \sigma_z$  are the normal stresses,  $\tau_{rz}$  is the shearing stress and the body forces are denoted by  $q_r$  and  $q_z$ . All these quantities depend on the polar coordinates  $r$  and  $z$  only. We remark that for torsion-free axisymmetric state of stress the shearing stresses  $\tau_{r\varphi}$  and  $\tau_{z\varphi}$  vanish in all points of the body. In the sequel we shall assume that  $T$  is a simply connected plane region in the meridian section of the body of rotation and  $T$  has not any point in common with the axis  $z$ . The boundary of the meridian section  $T$  is the closed curve  $\partial T$ . The unit tangent

and the outward unit normal to  $\partial T$  are denoted by  $\mathbf{t}$  and  $\mathbf{n}$ , respectively. Let

$$R = R(s), \quad Z = Z(s) \quad 0 \leq s \leq L \quad (1.3)$$

be the parametric equation of the curve  $\partial T$ , where  $s$  is the arc length measured on  $\partial T$ , and  $L$  is the total length of curve  $\partial T$ . The unit vectors in the radial and longitudinal directions are denoted by  $\mathbf{e}_r$  and  $\mathbf{e}_z$ . It can be shown with ease that

$$\mathbf{t} = \frac{dR}{ds}\mathbf{e}_r + \frac{dZ}{ds}\mathbf{e}_z, \quad \mathbf{n} = \frac{dZ}{ds}\mathbf{e}_r - \frac{dR}{ds}\mathbf{e}_z \quad (1.4)$$

and

$$t_r = -n_z = \frac{dR}{ds}, \quad t_z = n_r = \frac{dZ}{ds}. \quad (1.5)$$

Let  $\partial T_p$  ( $\partial T_p \in \partial T$ ) be the arc of  $\partial T$  on which tractions are imposed. The corresponding boundary conditions take the form

$$\sigma_r n_r + \tau_{rz} n_z = p_r, \quad \tau_{rz} n_r + \sigma_z n_z = p_z \quad (r, z) \in \partial T_p \quad (1.6)$$

where

$$\mathbf{p} = p_r(r, z)\mathbf{e}_r + p_z(r, z)\mathbf{e}_z \quad (1.7)$$

is prescribed on  $\partial T_p$ .

It is the purpose of the present paper to find the general solution in terms of stress functions to equations (1.1) and (1.2) and to analyze how the tractions and stress functions are related to each other. Langhaar and Stippes [3] presented a complete representation of stresses for axisymmetric stress states. The same problem was analyzed by Filonenko-Borodich [2]. The complete representation given in this paper is different from the solution derived by the two authors mentioned.

In Section 2 the stress function solution of equilibrium equations (1.1), (1.2) is derived and is shown to be complete. The degree of arbitrariness of the stress functions for a given state of stresses is then discussed. In Section 3 the traction boundary conditions are formulated in terms of stress functions. In Section 4 the stress function solution is derived from the principle of virtual work. Section 5 is devoted to the problem how the different solutions to the equilibrium equations in the terms of stress functions are related to each other. Section 6 contains some conclusions.

## 2. Stress Functions

In this paper we will not formulate explicitly the smoothness and continuity properties which are required. They may be deduced from known theorems of calculus (see, for example Courant [1], Rudin [4]).

We shall assume that the body forces can be represented as

$$r q_r = -\frac{\partial Q_r}{\partial r}, \quad r q_z = -\frac{\partial Q_z}{\partial z} \quad (2.1)$$

where  $Q_r = Q_r(r, z)$  and  $Q_z = Q_z(r, z)$  are potential functions for the body forces  $q_r$  and  $q_z$ , respectively. Without loss of generality we can consider the stress component  $\sigma_\varphi$  as the partial derivative of a function  $B = B(r, z)$  with respect to  $r$ , that is

$$\sigma_\varphi = \frac{\partial B}{\partial r} \quad (r, z) \in T \cup \partial T . \quad (2.2)$$

Upon substitution of (2.1) and (2.2) into the equilibrium equations (1.1), (1.2) we obtain

$$\frac{\partial}{\partial r}(r\sigma_r - B - Q_r) + \frac{\partial}{\partial z}(r\tau_{rz}) = 0 \quad (r, z) \in T , \quad (2.3a)$$

$$\frac{\partial}{\partial r}(r\tau_{rz}) + \frac{\partial}{\partial z}(r\sigma_z - Q_z) = 0 \quad (r, z) \in T . \quad (2.3b)$$

The stress function solution of equations (1.1), (1.2) is supplied by the following theorem.

*Theorem 2.1.* Let the stresses be represented by

$$r\sigma_r = \frac{\partial^2 A}{\partial z^2} + B + Q_r , \quad (2.4a)$$

$$\sigma_\varphi = \frac{\partial B}{\partial r} , \quad (2.4b)$$

$$r\sigma_z = \frac{\partial^2 A}{\partial r^2} + Q_z , \quad (2.4c)$$

$$r\tau_{rz} = -\frac{\partial^2 A}{\partial r \partial z} , \quad (2.4d)$$

where  $A = A(r, z)$  and  $B = B(r, z)$  are arbitrary functions. This stress representation identically satisfies the equilibrium equations (1.1), (1.2).

The proof of this theorem can be obtained by direct substitution. The next theorem, which is motivated by stress representation (2.4a,b,c,d), states that if the body forces are obtainable from (2.1) then every solution of the equilibrium equations (1.1), (1.2) can be given by equations (2.4a,b,c,d).

*Theorem 2.2.* Let the stresses satisfy (1.1), (1.2). Then there exist functions  $A = A(r, z)$  and  $B = B(r, z)$  such that the stresses can be represented by equations (2.4a,b,c,d), and the stress functions  $A = A(r, z)$  and  $B = B(r, z)$  are single-valued.

*Proof.* According to the theory of total differentials (Courant [1], Rudin [4]), (2.3a) implies the existence of a single-valued function in  $\bar{T} = T \cup \partial T$  such that

$$r\tau_{rz} = \frac{\partial a}{\partial r} , \quad r\sigma_r - B - Q_r = -\frac{\partial a}{\partial z} . \quad (2.5)$$

Similarly, by equation (2.3b) there exists a function  $b = b(r, z)$  in  $\bar{T}$  such that

$$r\sigma_z - Q_z = \frac{\partial b}{\partial r} , \quad r\tau_{rz} = -\frac{\partial b}{\partial z} . \quad (2.6)$$

From the equality of the two different expressions for  $\tau_{rz}$  – these follow from (2.5)<sub>1</sub> and (2.6)<sub>2</sub> – we obtain

$$\frac{\partial a}{\partial r} + \frac{\partial b}{\partial z} = 0 . \quad (2.7)$$

A repeated application of the theory of total differentials gives that there exists a single-valued function  $A = A(r, z)$  such that

$$a = -\frac{\partial A}{\partial z} , \quad b = \frac{\partial A}{\partial r} . \quad (2.8)$$

A combination of equations (2.5), (2.6) and (2.8) leads to stress representation (2.4a, b, c, d) which gives all the stress components. This last step completes the proof of Theorem 2.2. The degree of arbitrariness of the stress functions for a given state of stress is formulated in the following theorem.

*Theorem 2.3.* Let a given set of stresses which meet the equations (1.1), (1.2) be represented by (2.4a, b, c, d) in terms of the stress functions  $A = A(r, z)$ ,  $B = B(r, z)$  and in terms of different stress functions  $A' = A'(r, z)$ ,  $B' = B'(r, z)$ . Then

$$A(r, z) = A'(r, z) + \alpha(z) + \beta_0 + \beta_1 r , \quad (2.9)$$

$$B(r, z) = B'(r, z) - \frac{d^2 \alpha}{dz^2} , \quad (2.10)$$

where  $\beta_0, \beta_1$  are arbitrary constants and  $\alpha = \alpha(z)$  is an arbitrary function of  $z$ .

*Proof.* Using stress representation (2.4a, b, c, d) one finds that

$$\frac{\partial^2 A}{\partial z^2} + B + Q_r = \frac{\partial^2 A'}{\partial z^2} + B' + Q_r , \quad (2.11a)$$

$$\frac{\partial B}{\partial r} = \frac{\partial B'}{\partial r} , \quad (2.11b)$$

$$\frac{\partial^2 A}{\partial r^2} = \frac{\partial^2 A'}{\partial r^2} , \quad (2.11c)$$

$$\frac{\partial^2 A}{\partial r \partial z} = \frac{\partial A'}{\partial r \partial z} . \quad (2.11d)$$

Equation (2.11d) yields

$$A - A' = \alpha(z) + \beta(r) \quad (2.12)$$

where  $\alpha = \alpha(z)$  and  $\beta = \beta(r)$  are arbitrary functions,  $\alpha$  depends only on  $z$ , and  $\beta$  depends only on  $r$ . Equation (2.11c) gives

$$\beta = \beta_0 + \beta_1 r , \quad (2.13)$$

where  $\beta_0, \beta_1$  are the arbitrary constants. We obtain from equation (2.11b)

$$B = B' + \gamma(z) . \quad (2.14)$$

Inserting equations (2.12) and (2.14) into equation (2.11a) we arrive at

$$\gamma(z) = -\frac{d^2\alpha}{dz^2}. \quad (2.15)$$

which completes the proof of Theorem 2.3.

It is important to emphasize that the theorems proven are independent of any constitutive and compatibility equations which the stresses should also satisfy since we have been dealing with equilibrium equations only.

### 3. Stress boundary condition

In order to formulate the stress boundary conditions we start from equations (1.6) and (2.4a,b,c,d). By a simple substitution we obtain

$$\begin{aligned} r\sigma_r n_r + r\tau_{rz} n_z &= \frac{\partial^2 A}{\partial z^2} n_r + B n_r + Q_r n_r - \frac{\partial^2 A}{\partial r \partial z} n_z = \\ &= \frac{d}{ds} \left( \frac{\partial A}{\partial z} \right) + B \frac{dZ}{ds} + Q_r \frac{dZ}{ds} \quad (r, z) \in \partial T_p, \end{aligned} \quad (3.1a)$$

$$\begin{aligned} r\tau_{rz} n_r + r\sigma_z n_z &= -\frac{\partial^2 A}{\partial r \partial z} n_r + \frac{\partial^2 A}{\partial r^2} n_z + Q_z n_z = \\ &= -\frac{d}{ds} \left( \frac{\partial A}{\partial r} \right) - Q_z \frac{dR}{ds} \quad (r, z) \in \partial T_p. \end{aligned} \quad (3.1b)$$

Here we have used equation (1.5). Combination of equations (1.6) and (3.1a,b) leads to the result

$$\frac{d}{ds} \left( \frac{\partial A}{\partial z} \right) = r p_r - B \frac{dZ}{ds} - Q_r \frac{dZ}{ds}, \quad (3.2a)$$

$$-\frac{d}{ds} \left( \frac{\partial A}{\partial r} \right) = r p_z + Q_z \frac{dR}{ds}. \quad (3.2b)$$

After integrating these equations on  $\partial T_p$  we have

$$\left( \frac{\partial A}{\partial z} \right)_P - \left( \frac{\partial A}{\partial z} \right)_{P_0} = \int_{\widehat{P_0 P}} r p_r ds - \int_{\widehat{P_0 P}} (B + Q_r) \frac{dZ}{ds} ds, \quad (3.3a)$$

$$\left( \frac{\partial A}{\partial r} \right)_{P_0} - \left( \frac{\partial A}{\partial r} \right)_P = \int_{\widehat{P_0 P}} r p_z ds + \int_{\widehat{P_0 P}} Q_z \frac{dR}{ds} ds. \quad (3.3b)$$

In formulae (3.3a,b) the integrals are taken over an arc  $P_0 P$  of  $\partial T_p$ . The lower limit  $P_0$  is fixed and the upper limit  $P$  is regarded as a parameter. According to Theorem 2.3 we can set the starting values for the partial derivatives of the stress function  $A$  to

$$\left( \frac{\partial A}{\partial r} \right)_{P_0} = \left( \frac{\partial A}{\partial z} \right)_{P_0} = 0. \quad (3.4)$$

#### 4. Derivation of stress functions from the principle of virtual work

In this section we derive the solution of the homogeneous equilibrium equation in terms of stress functions from the principle of virtual work. The line of thought is based on that of Washizu [7]. The general solution of the homogeneous equilibrium equations is given in terms of stress functions  $A$  and  $B$ . In the absence of body forces one can write that

$$q_r = q_z = 0, \quad Q_r = Q_z = 0. \quad (4.1)$$

The strain compatibility equations for torsion-free axisymmetric deformation are as follows [6]:

$$C_a = \frac{\partial^2 \varepsilon_r}{\partial z^2} + \frac{\partial^2 \varepsilon_z}{\partial r^2} - \frac{\partial^2 \gamma_{rz}}{\partial r \partial z} = 0 \quad (r, z) \in T, \quad (4.2a)$$

$$C_b = \frac{\partial}{\partial r}(r\varepsilon_\varphi) - \varepsilon_r = 0 \quad (r, z) \in T. \quad (4.2b)$$

Here  $\varepsilon_r, \varepsilon_\varphi, \varepsilon_z$  are direct strains and  $\gamma_{rz}$  is the shear strain. The strain components depend on the radial coordinate  $r$ , and the longitudinal coordinate  $z$ . Washizu [7] proposes to introduce the strain compatibility conditions instead of the displacement components  $u$  and  $w$  into the principle of virtual work by the use of Lagrange multipliers. Since the problem is axisymmetric for the volume and the surface elements, one can write

$$dV = 2\pi r dT, \quad dS = 2\pi r ds.$$

The principle of virtual work has the form

$$\int_T r(\sigma_r \delta\varepsilon_r + \sigma_\varphi \delta\varepsilon_\varphi + \sigma_z \delta\varepsilon_z + \tau_{rz} \delta\gamma_{rz}) dT - \int_{\partial T_p} r(p_r \delta u + p_z \delta w) ds = 0. \quad (4.3)$$

Here the infinitesimal virtual displacements  $\delta u, \delta w$  and the infinitesimal virtual strains  $\delta\varepsilon_r, \delta\varepsilon_\varphi, \delta\varepsilon_z, \delta\gamma_{rz}$  should satisfy the strain-displacement relationships and the homogeneous geometrical boundary conditions imposed on the boundary segment  $\partial T_u$ . Consequently

$$\delta u = \delta w = 0 \quad \text{on } \partial T_u. \quad (4.4)$$

We remark that

$$\partial T_p \cup \partial T_u = \partial T \quad \text{and} \quad \partial T_p \cap \partial T_u = \{\emptyset\}.$$

We apply equations (4.2a,b) as the field conditions of compatibility instead of the strain-displacement relationship. We can now transform equation (4.3) into the form

$$\int_T r(\sigma_r \delta\varepsilon_r + \sigma_\varphi \delta\varepsilon_\varphi + \sigma_z \delta\varepsilon_z + \tau_{rz} \delta\gamma_{rz}) dT - \int_T (\lambda_a \delta C_a + \lambda_b \delta C_b) dT + \{\text{boundary terms}\} = 0 \quad (4.5)$$

where  $\lambda_a$  and  $\lambda_b$  are the Lagrange multipliers which depend on the coordinates  $r$  and  $z$ . After some calculations including repeated partial integrations, equation (4.5) is manipulated into its final form:

$$\int_T \left[ \left( r\sigma_r - \frac{\partial^2 \lambda_a}{\partial z^2} - \lambda_b \right) \delta\varepsilon_r + r \left( \sigma_\varphi - \frac{\partial \lambda_b}{\partial r} \right) \delta\varepsilon_\varphi + \left( r\sigma_z - \frac{\partial^2 \lambda_a}{\partial r^2} \right) \delta\varepsilon_z + \left( r\tau_{rz} + \frac{\partial^2 \lambda_a}{\partial r \partial z} \right) \delta\gamma_{rz} \right] dT + \{\text{boundary terms}\} = 0. \quad (4.6)$$

Since the variations  $\delta\varepsilon_r, \delta\varepsilon_\varphi, \delta\varepsilon_z$  and  $\delta\gamma_{rz}$  are arbitrary, we have

$$\begin{aligned} r\sigma_r &= \frac{\partial^2 \lambda_a}{\partial z^2} + \lambda_b, & \sigma_\varphi &= \frac{\partial \lambda_b}{\partial r}, \\ r\sigma_z &= \frac{\partial^2 \lambda_a}{\partial r^2}, & r\tau_{rz} &= -\frac{\partial^2 \lambda_a}{\partial r \partial z}. \end{aligned} \quad (4.7)$$

A comparison of equations (4.7) and (2.4a,b,c) – in the latter case  $Q_r = Q_z = 0$  – shows that

$$\lambda_a = A \quad \text{and} \quad \lambda_b = B, \quad (4.8)$$

thus the Lagrange multipliers  $\lambda_a$  and  $\lambda_b$  are stress functions.

## 5. Comparison of various formulations

It follows from the general axisymmetric solution of the homogeneous equilibrium equations (due to symmetry  $\tau_{r\varphi} = \tau_{\varphi z} = 0$ ) given by Filonenko-Borodich that

$$r\sigma_r = \frac{\partial^2 f_1}{\partial z^2}, \quad (5.1a)$$

$$\sigma_\varphi = \frac{\partial^2 f_2}{\partial z^2}, \quad (5.1b)$$

$$r\sigma_z = -\frac{\partial}{\partial r} \left( f_2 - \frac{\partial f_1}{\partial r} \right), \quad (5.1c)$$

$$r\tau_{rz} = \frac{\partial}{\partial z} \left( f_2 - \frac{\partial f_1}{\partial r} \right). \quad (5.1d)$$

Here,  $f_1 = f_1(r, z)$  and  $f_2 = f_2(r, z)$  are stress functions. Formulas (5.1a,b,c,d) can be obtained from formula (1.10) of paper [2] by putting  $f_3 = 0$ . The next theorem relates the stress functions  $f_1 = f_1(r, z)$ ,  $f_2 = f_2(r, z)$  to the stress functions  $A = A(r, z)$ ,  $B = B(r, z)$  assuming that the stress state is the same.

*Theorem 5.1.* If the stress functions  $f_1 = f_1(r, z)$ ,  $f_2 = f_2(r, z)$  and  $A = A(r, z)$ ,  $B = B(r, z)$  produce the same stress state then the following equations hold

$$f_1 = A + b, \quad f_2 = \frac{\partial b}{\partial r}, \quad \frac{\partial^2 b}{\partial z^2} = B. \quad (5.2)$$

In the absence of body forces and assuming an axisymmetric stress state, H. L. Langhaar and M. Stippes also gave a solution in terms of stress functions for the equilibrium equations [3]:

$$\sigma_r = \frac{\partial^2 F}{\partial z^2} + \frac{1}{r} \frac{\partial H}{\partial r}, \quad (5.3a)$$

$$\sigma_\varphi = \frac{\partial^2 F}{\partial z^2} + \frac{\partial^2 H}{\partial r^2}, \quad (5.3b)$$

$$\sigma_z = \frac{\partial^2 F}{\partial r^2} + \frac{1}{r} \frac{\partial F}{\partial r}, \quad (5.3c)$$

$$\tau_{rz} = -\frac{\partial^2 F}{\partial r \partial z}. \quad (5.3d)$$

Theorem 5.2 gives the connection between the stress functions  $F = F(r, z)$ ,  $H = H(r, z)$  and  $A = A(r, z)$ ,  $B = B(r, z)$ .

*Theorem 5.2.* If the stress state is the same, then the following equations hold between the stress functions  $F = F(r, z)$ ,  $H = H(r, z)$  and  $A = A(r, z)$ ,  $B = B(r, z)$ :

$$A(r, z) = r \frac{\partial f}{\partial r} - f, \quad (5.4a)$$

$$B(r, z) = \frac{\partial^2 f}{\partial z^2} + \frac{\partial H}{\partial r}, \quad (5.4b)$$

where

$$F = \frac{\partial f}{\partial r}. \quad (5.5)$$

The proof of Theorem 5.1 and 5.2 can be obtained from the comparison of the various stress function solutions (4.7), (4.8), (5.1a,b,c,d) and (5.3a,b,c,d).

It is obvious that the substitution of the expressions giving  $f_1$  and  $f_2$  in terms of  $A$ ,  $b$  and  $B$  into the Filonenko-Borodich solution leads immediately to the solution of the homogeneous equilibrium equation established in this paper.

A similar statement can be formulated for the Langhaar-Stippes solution. In the absence of body forces the stress representation suggested in this paper leads to the Langhaar-Stippes solution in terms of stress functions  $F = F(r, z)$  and  $H = H(r, z)$  if we use the stress functions  $A = A(r, z)$  and  $B = B(r, z)$  given by (5.4a,b), (5.5).

## 6. Conclusions

In this paper the general solution of equilibrium equation is presented for torsion-free axisymmetric state of stress. It has been shown that the solution given is complete

and its degree of arbitrariness is also analyzed. The stress boundary conditions in terms of stress functions are also given. In the absence of body forces the stress representation we have found – solution to the homogenous equilibrium equations in terms of stress functions – can also be derived from the principle of virtual work. The presented stress function solution is then compared with other stress function solutions. The solution of equilibrium equations for axisymmetric torsion-free state of stress is very similar to the Airy solution of equilibrium equations for plane problems [5]. The results presented in the paper are all independent of any constitutive and compatibility equations which the stresses should satisfy in order to be the solution of a given boundary-value problem. If the body is elastic, then the field equations the stress functions should meet are the Beltrami-Mitchell equations under the prescribed boundary conditions. The stress functions solution of equilibrium equations gives a possibility to use the variational method elaborated by A. Castigliano. Another field of applications is the formulation of stress-based finite element models.

**Acknowledgement.** This work was supported by the Hungarian Ministry of Education under grant FKFP OO40/1999.

## REFERENCES

- [1] COURANT, R.: *Differential and Integral Calculus*, Vol. II, Interscience, New York, 1939.
- [2] FILONENKO-BORODICH, M. M.: *Some generalisation of Lamé's problem for an elastic parallelepiped*, Prikl. Matem. i Mekh., **17** (4), (1953), 465-469.
- [3] LANGHAAR, H. L. and STIPPES, M.: *Three-dimensional stress functions*, Journal Franklin Inst., **258** (5), (1954), 371-382.
- [4] RUDIN, W.: *Principles of Mathematical Analysis*, 2nd Edition., McGraw-Hill. New York. 1961.
- [5] TIMOSHENKO, S. AND GOODIER, J. N.: *Theory of Elasticity*, McGraw-Hill. New-York, 1952.
- [6] VASILJEV, B. AND CHERNIH, B. A. AND KOLTUNOV, M. A.: *Elasticity and Strength of Cylindrical Bodies*, Higher School, Moscow, 1975. (in Russian)
- [7] WASHIZU, K.: *Variational Methods in Elasticity and Plasticity*, Second Ed., Pergamon Press, New York, 1975.



# COMPARISON OF SOME CONTACT ELEMENTS AND ITERATIVE ALGORITHMS FOR THE SOLUTION OF FRICTIONLESS CONTACT PROBLEMS

JÁNOS ÉGERT

Department of Mechanics and Machine Structures, Széchenyi István College Győr,  
5 Kovács Pál Str., 9021 GYŐR, Hungary

egert@rs1.szif.hu

[Received: August 15, 1999]

**Abstract.** The paper presents three different iterative algorithms for the numerical solution of contact problems. Each algorithm is based on the use of the finite element method. It is assumed that the contact conditions are fulfilled by means of special contact elements. Numerical results for the various contact elements and solution algorithms are then compared by solving 2D elasticity problems.

*Keywords:* Iterative algorithms, frictionless contact problems, finite element method

## 1. Introduction

A machine structure consists of several parts, which are connected with each other by surface contact. It is very important to determine the displacements, strains and stresses in the contact area, because they can exert a powerful influence on the reliability, failsafety and lifetime of the construction.

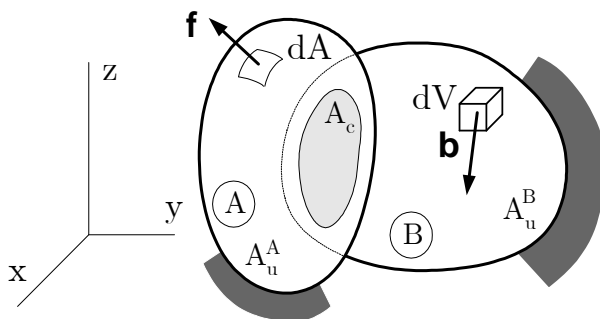


Figure 1.

An elastic contact problem can be formulated as follows. The system under consideration – see Figure 1 for details – consists of two bodies denoted by  $\mathcal{A}$  and  $\mathcal{B}$ . These bodies are in contact on the surface  $A_c$ . The body forces  $\mathbf{b}$  and surface tractions  $\mathbf{f}$  on  $A_t^A$  and  $A_t^B$  are given for each body. The kinematic boundary conditions (support conditions) are also known on the corresponding surfaces  $A_u^A$  and

$A_u^{\mathcal{B}}$ . ( $V = V^{\mathcal{A}} \cup V^{\mathcal{B}}$ ;  $V^{\mathcal{A}} \cap V^{\mathcal{B}} = 0$ ;  $A^{\mathcal{A}} = A_c^{\mathcal{A}} \cup A_u^{\mathcal{A}} \cup A_t^{\mathcal{A}}$ ;  $A^{\mathcal{B}} = A_c^{\mathcal{B}} \cup A_u^{\mathcal{B}} \cup A_t^{\mathcal{B}}$ ;  $A_t = A_t^{\mathcal{A}} \cup A_t^{\mathcal{B}}$ ). Though it is assumed that the equations of linear elasticity are valid for each body (the material is homogenous and isotropic) due to the surface contact the relation between loading and displacements is a non-linear one. Consequently the problem is also non-linear.

For non-linear problems the incremental version of the principle of virtual work is the basis of solution. For the structure made up of the two bodies  $\mathcal{A}$  and  $\mathcal{B}$ , the principle is of the form

$$\int_{(V)} \Delta \mathbf{T} \cdot \cdot \delta(\Delta \mathbf{E}) dV = \int_{(V)} \Delta \mathbf{b} \cdot \delta(\Delta \mathbf{u}) dV + \int_{(A_t)} \Delta \mathbf{f} \cdot \delta(\Delta \mathbf{u}) dV. \quad (1.1a)$$

In addition it holds for body  $\mathcal{A}$  (and  $\mathcal{B}$ ) that

$$\begin{aligned} \int_{(V^{\mathcal{A}})} \Delta \mathbf{T} \cdot \cdot \delta(\Delta \mathbf{E}) dV + \int_{(A_c)} \Delta \mathbf{p} \cdot \delta(\Delta \mathbf{u}) dV = \\ \int_{(V^{\mathcal{A}})} \Delta \mathbf{b} \cdot \delta(\Delta \mathbf{u}) dV + \int_{(A_t^{\mathcal{A}})} \Delta \mathbf{f} \cdot \delta(\Delta \mathbf{u}) dA \end{aligned} \quad (1.1b)$$

where  $\mathbf{T}$  is the stress tensor,  $\mathbf{E}$  is the strain tensor,  $\mathbf{p}$  is the contact pressure,  $\mathbf{u}$  is the displacement field, the double scalar product is denoted by  $\cdot \cdot$ . Greek  $\delta$  stands for the variation of a quantity while  $\Delta$  identifies the increment of a quantity.

There are two typical groups of solution methods used to solve elastic contact problems of the above type. Methods in the first group reduce the contact problem to a mathematical programming problem [3] [4]. Procedures in the second group are iterative methods based on the use of special contact elements [5] - [9]. This paper is going to apply and compare three different iterative methods and three types of contact elements for solving frictionless elastic contact problems. The main goal of the author was to implement two known iterative methods [5] - [9] and three types of contact elements into a FEM code and to compare those with a new iterative solution algorithm.

With the iterative solutions the contact conditions for each increment and iteration step are satisfied using special contact elements. These special contact elements – see Figure 2 – are fictitious elements with proper stiffness or material properties which ensure the fulfillment of contact conditions. Thus they are not real finite elements, but can be considered as an appropriate numerical help for the solution process.

In order to fulfil the contact condition in each load increment, two known iterative solution algorithms were implemented: iteration with varying stiffness, iteration with constant stiffness and a new method was developed: iteration with kinematic load.

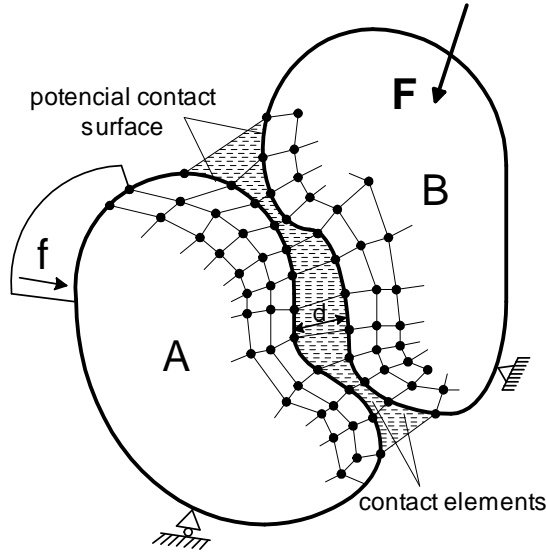


Figure 2.

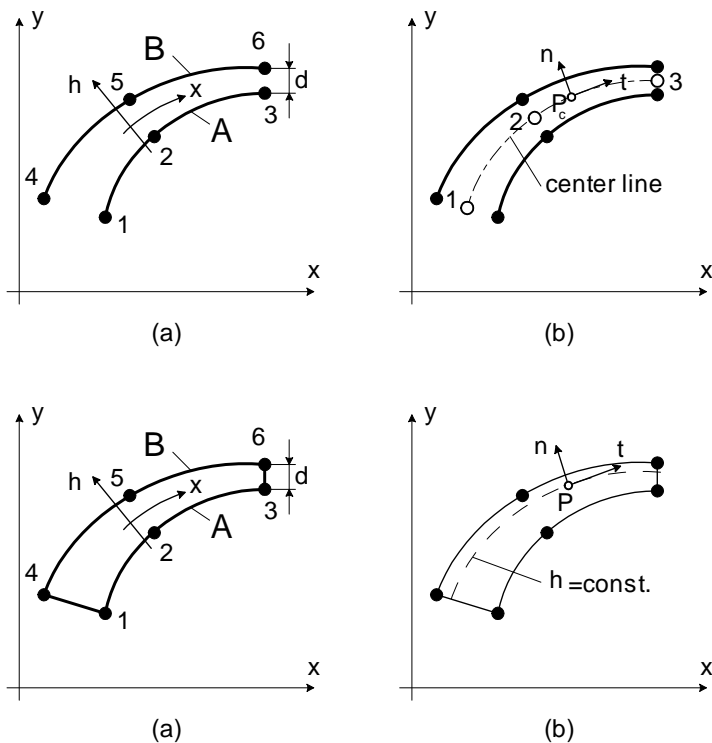
Every contact elements and solution algorithms was installed in the *FEM-3D* finite element program system [13] developed under *Páczelt's* leadership. The effective application of the above iterative algorithms with contact elements assumes that the FEM code makes substructuring possible. During the solution of contact problems it is very useful to select the nodes on the potential contact area (Figure 2) as external nodes while the other nodes can be considered as internal nodes. In this case one should carry out the iteration steps taking only the variables of external nodes into consideration.

## 2. Features of 2D contact elements

Three types of contact elements, namely line contact elements, layer contact elements and node (or spring) contact elements were applied during the computations. These special elements have already been applied in the literature [5] - [9]. Figures 3-5 illustrate the elements for 2D case.

The line contact elements (Figure 3) consist of two lines which represent real element sides on bodies *A* and *B* and are attached to each other via a distributed spring system. The corresponding spring stiffnesses are denoted by  $k_t$  and  $k_n$  in the local co-ordinate system  $t, n$  (Figure 3/b).

During the contact iteration the stiffnesses  $k_t$  and  $k_n$  must be modified until the tangential (frictional) and normal contact conditions are fulfilled. For the characteris



Figures 3 and 4

tic block of stiffness matrix of line contact element we obtain

$$\mathbf{K}_{c_{ij}} = \begin{bmatrix} k_t & 0 \\ 0 & k_n \end{bmatrix}_{ij} \quad (2.2)$$

where the nodes attached to each other by the spring are denoted by  $i$  and  $j$ .

When using line contact elements the fulfillment of contact conditions is ensured in the  $tn$  co-ordinate system along the center line of the contact element.

The layer contact elements (Figure 4) are made of special fictitious material for which the modulus of elasticity  $E$  and the shear modulus  $G$  do not depend on each other. Fulfillment of the normal contact condition can be reached by modifying  $E$  and by giving a proper value to the shear modulus  $G$  one can satisfy the frictional contact conditions. The form of the layer contact element stiffness matrix is similar to that expressed in equation (1.1b). The contact conditions are again fulfilled along the  $\eta = 0$  co-ordinate line.

The node contact elements (Figure 5) consist of a couple of nodes, which are connected in tangential and normal direction by springs with stiffnesses  $k_t$  and  $k_n$ .

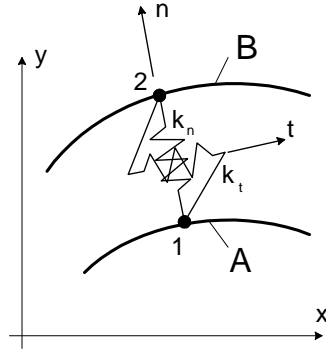


Figure 5.

The contact iteration procedure is the same as for the case of the above two contact elements, consequently the stiffness matrix has the same form with only one characteristic block.

### 3. Iterative solution algorithms

The basic FEM equation of the investigated system of bodies  $A$  and  $B$  for the  $i$ -th load increment  $\Delta \mathbf{f}^i$  may be written as

$$(\mathbf{K}_{AB} + \mathbf{K}_c) \Delta \mathbf{q}^i = \Delta \mathbf{f}^i \quad (3.1)$$

where  $\mathbf{K}_{AB}$  is the super-structure stiffness matrix of the bodies  $A$  and  $B$  and  $\mathbf{K}_c$  is the stiffness matrix of the contact elements. If  $\mathbf{K}_c$  takes the "proper" value, (i.e., each contact condition is fulfilled), these (the above) equations will allow for the computation of the real displacement increment of the external nodes. It follows that our task is now to determine this "proper" value for  $\mathbf{K}_c$ . For this purpose, three iterative solution methods have been developed:

a) *Iteration with varying stiffness* [5] - [8]

In the 1-st step we solve the linear algebraic equation system (3.1) with an initial value  $\mathbf{K}_{c_0}$ :

$$\Delta \mathbf{q}_0^i = (\mathbf{K}_{AB} + \mathbf{K}_{c_0})^{-1} \Delta \mathbf{f}^i. \quad (3.2)$$

Then the fulfillment of contact conditions is checked for the solution  $\Delta \mathbf{q}_0^i$  and in case they are not fulfilled, the stiffness matrix of contact elements must be modified by  $\mathbf{K}_{c_1}$  - as regards its choice see [12] - :

$$(\mathbf{K}_{AB} + \mathbf{K}_{c_0} + \mathbf{K}_{c_1}) \Delta \mathbf{q}_1^i = \Delta \mathbf{f}^i \quad (3.3)$$

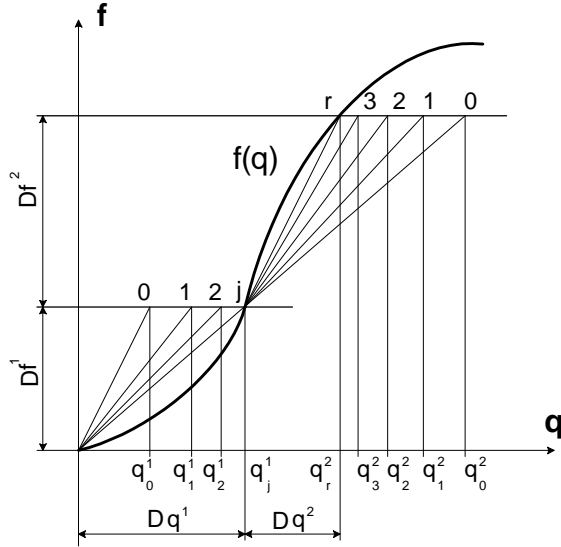


Figure 6.

After solving equation system (3.3) we obtain a new approach for the nodal displacement increment:

$$\Delta \mathbf{q}_1^i = (\mathbf{K}_{AB} + \mathbf{K}_{c_o} + \mathbf{K}_{c_1})^{-1} \Delta \mathbf{f}^i . \quad (3.4)$$

In the  $(j+1)$ -th iteration step the displacement increment can be computed as follows:

$$\Delta \mathbf{q}_j^i = (\mathbf{K}_{AB} + \mathbf{K}_{c_o} + \mathbf{K}_{c_1} + \dots + \mathbf{K}_{c_j})^{-1} \Delta \mathbf{f}^i . \quad (3.5)$$

From this equation it is obvious that the iteration algorithm with varying stiffness needs a new matrix inversion procedure in each iteration step since the stiffness of the contact elements is changed step by step. The qualitative character of the above procedure is shown in Figure 6.

*b) Iteration with constant stiffness [9]*

The 1-st step is the same as for the case of the iteration with varying stiffness – see equation (3.2). Rearranging equation (3.3) we obtain a new equation with an unchanged left side system matrix (stiffness matrix):

$$(\mathbf{K}_{AB} + \mathbf{K}_{c_o}) \Delta \mathbf{q}_1^i = \Delta \mathbf{f}^i - \mathbf{K}_{c_1} \Delta \mathbf{q}_0^i . \quad (3.6)$$

Introducing a new notation for the right side of the above linear equation system

$$\Delta \mathbf{f}_1^i = \Delta \mathbf{f}^i - \mathbf{K}_{c_1} \Delta \mathbf{q}_0^i , \quad (3.7)$$

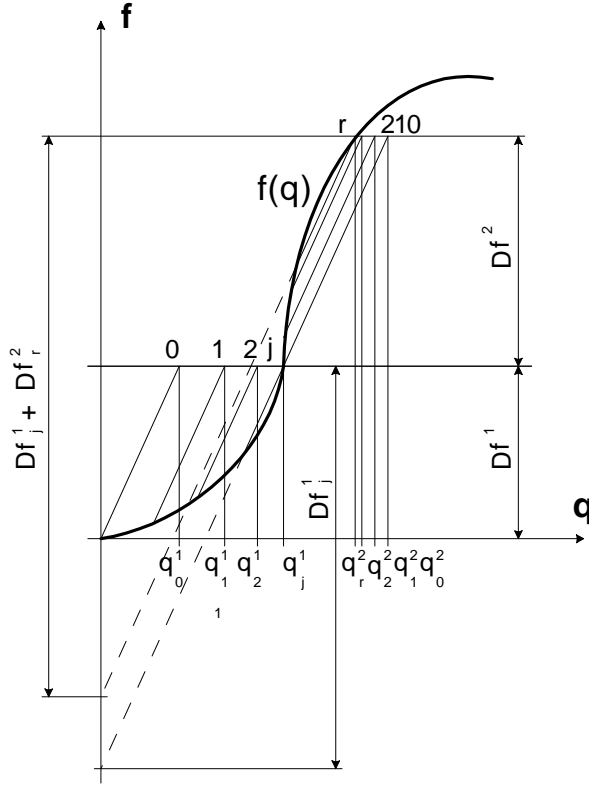


Figure 7.

a recursive formula with constant stiffness matrix and varying load increment is obtained:

$$(\mathbf{K}_{AB} + \mathbf{K}_{c_o}) \Delta \mathbf{q}_1^i = \Delta \mathbf{f}_1^i \quad (3.8)$$

For the  $(j + 1)$ -th iteration step the displacement increment can be computed from the following equation:

$$\Delta \mathbf{q}_j^i = (\mathbf{K}_{AB} + \mathbf{K}_{c_o})^{-1} \Delta \mathbf{f}_j^i \quad (3.9)$$

where the current value of load increment is

$$\Delta \mathbf{f}_j^i = \Delta \mathbf{f}^i - \mathbf{K}_{c_1} \Delta \mathbf{q}_0^i - \dots - \mathbf{K}_{c_j} \Delta \mathbf{q}_{(j+1)}^i \quad (3.10)$$

It is seen from equation (3.10) that the iteration procedure with constant stiffness requires only one matrix inversion for each load increment and that, step by step, only the right side is modified. In this manner, it is possible to save a great deal of computing operations and time. Figure 7. represents the qualitative character of the above algorithm.

*c) Iteration with kinematic load*

This algorithm is based on *Páczelt's* idea [14]. Using this idea an appropriate kinematic loading is applied in the 1-st iteration step:

$$(\mathbf{K}_{AB} + \mathbf{K}_{c_o}) \Delta \mathbf{q}_0^i = \Delta \mathbf{f}_0^i + \mathbf{f}_{g_o} \quad (3.11)$$

The kinematic loading can be computed as

$$\mathbf{f}_{g_o} = \mathbf{K}_{c_o} \mathbf{g}_0 \quad (3.12)$$

where  $\mathbf{g}_0$  is the matrix of the initial gaps of normal direction on the potential contact area. This kinematic loading is set to a value which makes the initial normal gaps disappear.

Solving the algebraic equation (3.11) one can check the fulfillment of the contact condition and after performing the necessary modifications in the contact stiffness matrix a new equation system is obtained:

$$(\mathbf{K}_{AB} + \mathbf{K}_{c_o} + \mathbf{K}_{c_1}) \Delta \mathbf{q}_1^i = \Delta \mathbf{f}^i + (\mathbf{K}_{c_o} + \mathbf{K}_{c_1}) \mathbf{g}_0 \quad (3.13)$$

In the  $(j + 1)$ -th iteration step the  $i$ -th displacement increment is computed from the following equation system:

$$(\mathbf{K}_{AB} + \mathbf{K}_{c_o} + \dots + \mathbf{K}_{c_j}) \Delta \mathbf{q}_j^i = \Delta \mathbf{f}^i + (\mathbf{K}_{c_o} + \dots + \mathbf{K}_{c_j}) \mathbf{g}_0 \quad (3.14)$$

It is seen from equation (3.14) that both the stiffness matrix and the load vector are modified step by step in this iteration procedure.

#### 4. Numerical examples

The comparison of efficiency and capability of the above algorithms and contact elements are carried out through the use of two numerical tests.

*a) Elastic cylinder - rigid plane*

In this example we have solved the contact problem of an infinite elastic cylinder and a rigid plane pressed to each other by a uniform load  $\mathbf{q}$  (Figure 8). Thus the problem is a plane strain one.

*H. Hertz* [15] found an exact solution (closed form solution) for this frictionless contact problem, which allows us to compare our results with the exact solution. Taking advantage of the symmetrical properties of the problem, as a finite element model we can regard half a cylinder loaded by half of the given loading. The top part of the cylinder does not influence the behavior of the contact area, therefore we are allowed to neglect the top quarter of our half cylinder. Figure 9 shows the FEM model of the investigated problem.

In Figure 10 we have compared Hertz's exact solution with various approximate solutions – see Figure 10 for the details concerning the methods of the approximate so-

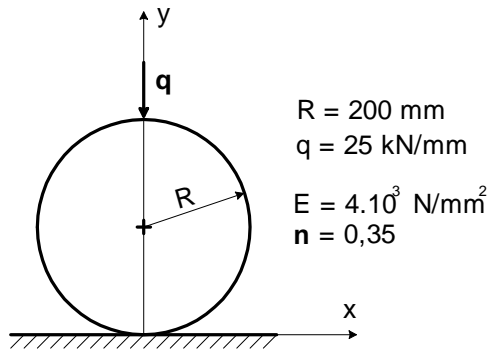


Figure 8.

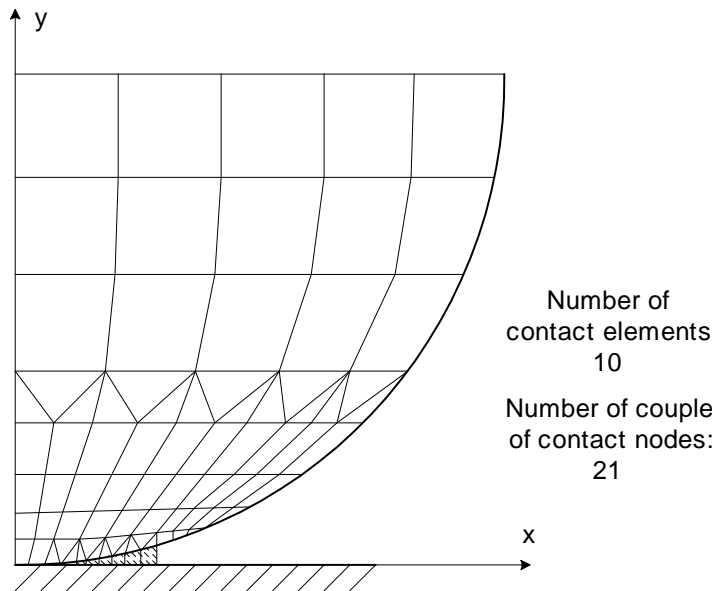


Figure 9.

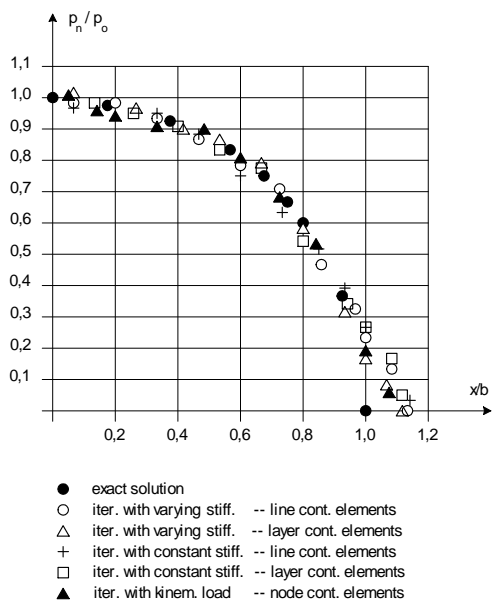


Figure 10.

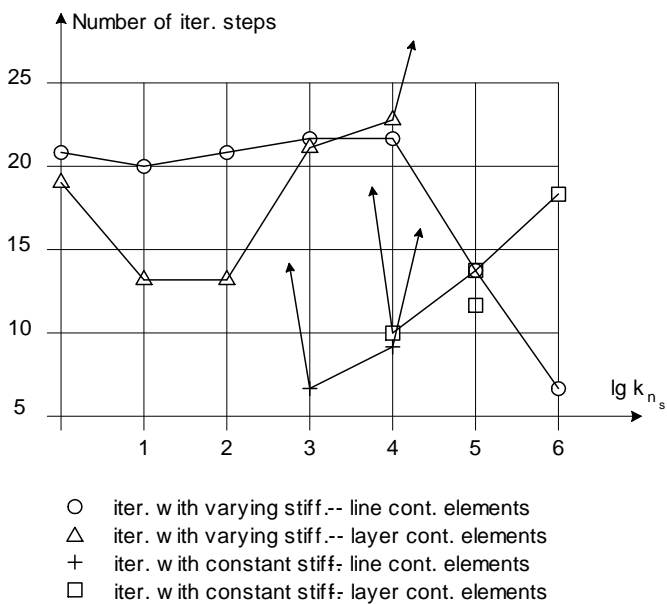


Figure 11.

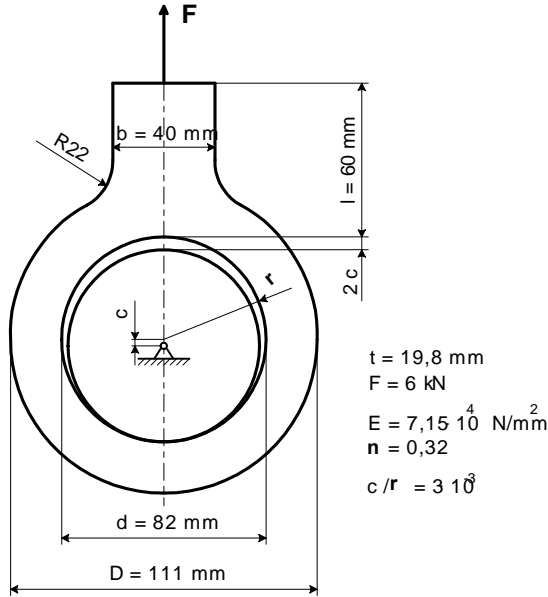


Figure 12.

lutions. It can be seen that we have obtained a good agreement for every combination of the applied contact elements and iterative algorithms.

At the same time, the number of iteration steps required to reach convergence has differed to a great extent, and it has strongly depended on the initial value of the normal stiffnesses of contact elements (Figure 11). In some cases there was no convergence found at all. From Figure 11 it is seen that the iteration with varying stiffness is much more stable than the iteration with constant stiffness. For the iteration with varying stiffness and using line contact elements, convergence was found in every case. The best results are obtained using the iteration with kinematic load. They are not seen in Figure 11, because with this iterative algorithm the convergence was reached in two steps for any initial normal stiffness.

#### b) Pin - connecting rod problem

In this problem, (Figure 12) a connecting rod acts on a supported pin with a radial eccentricity  $c$ . Both the pin and the rod (housing) are assumed to have the same thickness  $t$ . Thus it is, from a mechanical point of view, a plane stress problem.

The load is a concentrated force  $\mathbf{F}$  exerted on the rod. Figure 13. shows the finite element model which takes advantage of the symmetry of both parts of the joint.

In Figures 14 and 15, solutions obtained using the presented solution methods are compared with each other and with Gaertner's FEM and experimental results [16]. Both figures show a reasonable agreement in computation accuracy of the different solutions.

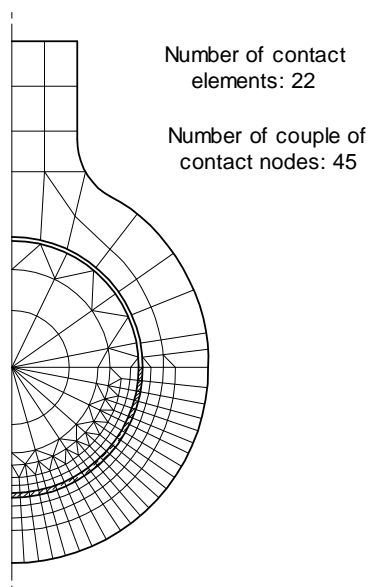


Figure 13.

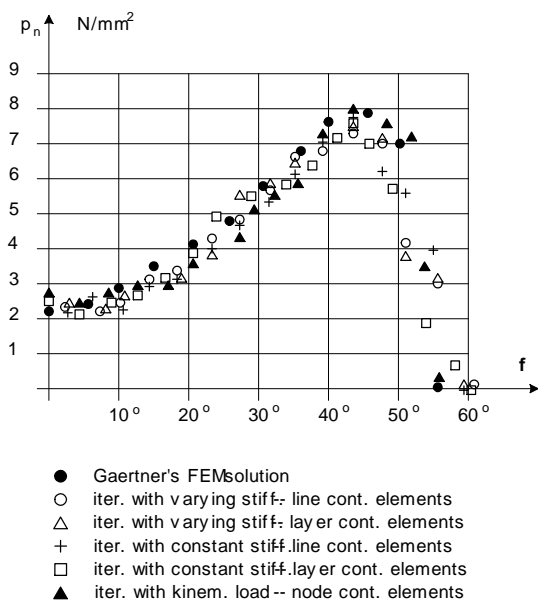


Figure 14.

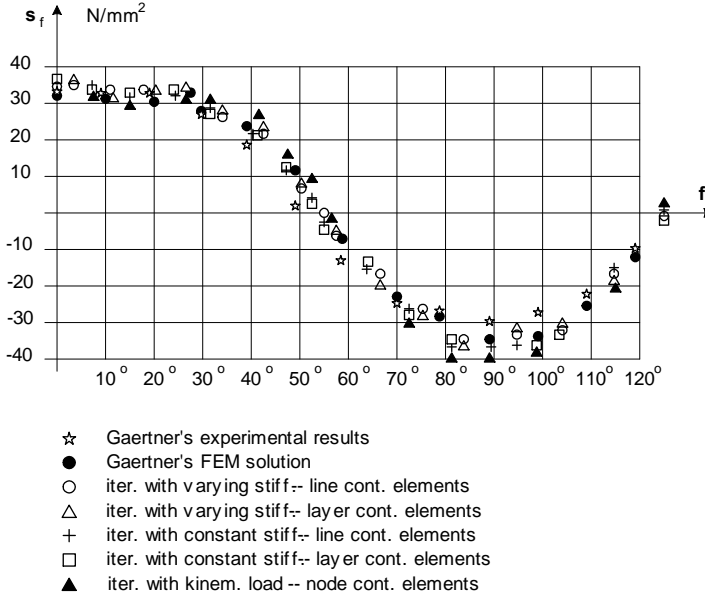


Figure 15.

For the latter problem the number of iteration steps required to reach convergence depends on the initial value of the normal stiffnesses of the contact elements. The applied algorithms and contact elements have shown the same convergence properties as for the first sample problem. When solving this problem we obtained the least iteration steps using an iteration algorithm with kinematic load. This iterative algorithm was convergent in two steps independently of the initial value of normal stiffnesses.

### 5. Concluding remarks

All of the applied iterative algorithms and contact elements have given a good approximation for the investigated sample problems. Within the prescribed accuracy, there is no remarkable difference between the implemented iterative methods or between the applied contact elements.

But there is a great difference in the number of iteration steps required to reach convergence. As regards the methods taken from the literature the number of iteration steps strongly depends on the initial value of the normal stiffnesses of the contact elements. In some cases there was no convergence found at all. The iteration procedure with varying stiffnesses has proved to be convergent in all cases provided that line contact elements have been used.

The new algorithm suggested in this paper, i.e., the iteration with kinematic load using node contact elements has also proved to be convergent in every case. In

addition it always works independently of the initial value of the normal stiffness. It is a further advantage that the number of iteration steps to be carried out and the computational time are much less than those for the other solution algorithms.

## REFERENCES

1. BATHE, K. J.: *Finite Element Procedures*, Upper Saddle River, New Jersey, 1996.
2. KLEIBER, M.: *Handbook of Computational Solid Mechanics - Survey and Comparison of Contemporary Methods*, Springer-Verlag, Berlin Heidelberg New York, 1998.
3. PÁCZELT, I.: *Some remarks to the solution of quadratic programmings problems*, Publications Techn. Univ. Heavy Ind. Miskolc, Ser. D. Natural Sciences, **33**, (1979), 137-156.
4. FISCHER, U., HOYER, U. and MELOSH, R.-J.: *Lösung diskretisierter Kontaktprobleme unter Verwendung der linearen Optimierung*, Technische Mechanik, **8**, (1987), 52-56.
5. KATONA, M. G.: *A simple contact-friction interface element with applications to buried culverts*, Int. Journ. Num. Meth. Geomech., **7**, (1983), 371-384.
6. DESAI, C. S., ZAMAN, M. M., LIGHTNER, J. G. and SIRIWARDANE, H. J.: *Thin-layer element for interfaces and joints*, Int. Journ. Num. Anal. Meth. Geomech., **8**, (1984), 19-43.
7. KEUSER, M.: *Verbundelemente für nichtlineare Finite-Element-Berechnungen vom Stahlbaukonstruktionen*, VDI Fortschrittberichte, Reihe 4., Bauingenieurwesen Nr. 71. VDI Verlag Düsseldorf, 1985.
8. STADTER, J. T. and WEISS, R. O.: *Analysis of contact through finite element gaps*, Comp. & Struct., **10**, (1979), 867-873.
9. GNUTSHI, J. B.: *Solution of contact problems of the theory of elasticity and plasticity*, Problemi prochnosti, **12**, (1982), 99-104.
10. ÉGERT, J. and ALTENBACH, J.: *Inkrementelle Iterationsmethoden zur Lösung elastischer Kontaktaufgaben mit Reibung mittels spezieller isoparametrischer 2D- und 3D Kontaktelemente*, Technische Mechanik, **10**, (1989), 120-137.
11. ALTENBACH, J., ÉGERT, J. and PÁCZELT, I.: *Lösung ebener und rotationssymmetrischer elastischer Kontaktaufgaben mit Hilfe spezieller finiter Kontaktelemente*, Z. angew. Math. Mech. **70**, (1990), T671-T674.
12. ALTENBACH, J., ÉGERT, J. and PÁCZELT, I.: *Vergleich unterschiedlicher Iterationsmethoden zur Lösung elastischer Kontaktaufgaben mit Reibung*, Z. angew. Math. Mech., **72**, (1992), T137-141.
13. ÉGERT, J., HERPAI, B., NÁNDORI, F., PÁCZELT, I., SÁRKÖZI, L. and SZABÓ, T.: *Characteristics of a substructural finite element programming system for IBM AT compatible PC*, Proc. of Int. Conference on Eng. Design (ICED '88), Budapest, 23-25 August 1988, Series WDK 16, Vol. 3.
14. PÁCZELT I.: *Oral communication*, 1990.
15. PONOMAREW, S. D., BIDERMANN, W. L., LIHAREW, K. K., MAKUSHIN, W. M., MALININ, H. H. and FEODOSEW, W. I.: *Rascheti na prochnost w mashinostroenii*, Tom 3., Gl. 6., Mashgiz, Moskva, 1958. (in Russian)
16. GAERTNER, R.: *Investigation of plane elastic contact allowing for friction*, Comp. & Struct., **7**, (1977), 59-63.

# A FINITE ELEMENT MODEL FOR STABILITY ANALYSIS OF SYMMETRICAL ROTOR SYSTEMS WITH INTERNAL DAMPING

LÁSZLÓ FORRAI

Department of Mechanics, University of Miskolc  
3515 Miskolc – Egyetemváros, Hungary  
mechfl@gold.uni-miskolc.hu

[Received: September 22, 1999]

*Dedicated to Professor István Páczelt on the occasion of his sixtieth birthday*

**Abstract.** This paper deals with the stability analysis of self-excited bending vibrations of linear symmetrical rotor-bearing systems with internal damping using the finite element method. The rotor system consists of uniform circular Rayleigh shafts with internal viscous damping, symmetric rigid disks, and discrete isotropic damped bearings. The effect of rotatory inertia and gyroscopic moment are also included in the mathematical model. By combining the sensitivity analysis and the eigenvalue problem of the rotor dynamics equations presented in complex form, it is proved theoretically that the whirling motion of the rotor system becomes unstable at all speeds beyond the threshold speed of instability. In addition, the latter is always greater than the corresponding whirling speed. It is found that the rotor stability is improved by increasing the damping provided by the bearings, whereas increasing internal damping may reduce the stability threshold. It is also shown that the whirling speed of the rotor is higher than the first forward critical speed. Numerical examples are given to confirm the validity of the theoretical results.

*Keywords:* rotor dynamics, stability analysis, internal damping, threshold speed, finite elements

## 1. Introduction

It is well known that the stability of rotors is influenced by internal damping. The early works of Kimball [1] and Newkirk [2] showed that internal damping destabilizes the whirling motion of the rotor at speeds above the first critical speed. The stability problems of rotors with both internal and external damping have been discussed by several authors [3-7]. In most of the works by the investigators listed above, however, the gyroscopic effects are neglected.

Of the many researchers studying the stability problems of rotors using finite elements, Zorzi and Nelson [8] carried out first the numerical stability analysis of such rotor systems including the effects of rotatory inertia, gyroscopic moments, and both internal viscous and hysteretic damping. By using the numerical examples of a uniform circular shaft with viscous material damping, supported at its ends by two identical undamped isotropic bearings, they found that the first and second forward precessional modes become unstable at the first and second critical speeds, respec-

tively. The author [9] of this paper generalized the above results for symmetric rotor systems with viscous internal damping, supported by isotropic undamped bearings. By applying the sensitivity analysis and the eigenvalue problem of the rotor dynamics equation in complex form, it has been proved that the *stability threshold speed*, at which the rotor loses its stability, coincides with *the first forward critical speed* regardless of the magnitude of the internal viscous damping coefficient.

The main purpose of this paper is to demonstrate that the finite element simulation and the sensitivity analysis are adequate methods to study the combined effect of internal damping and isotropic bearing damping on the stability of complex symmetrical rotor systems. By combining the sensitivity analysis and the matrix representation of the rotor dynamics equations in complex form to assess stability, it is proved theoretically that the whirling motion of the rotor system becomes unstable at all speeds above the threshold speed of instability. In addition, the latter is always greater than the corresponding whirling speed (frequency). It is found that the rotor stability is improved by increasing the bearing damping, whereas increasing internal viscous damping may reduce the stability threshold speed. Furthermore, it is shown that the whirling speed of the rotor is higher than the first forward critical speed. Numerical examples are given to show the validity of the theoretical results of the present work. The threshold speeds and the whirling speeds of the rotor model are calculated using a computer program written in real form, which utilizes a standard QR-algorithm and an iterative technique developed by the author [10].

## 2. Equations of motion in complex form

**2.1. Preliminaries and notations.** In this section, the equations of motion for a rigid disk, finite shaft element with internal viscous damping, isotropic damped bearing, and the complete rotor system are written solely in complex form by making use of a note by Nelson [11] and the paper by Zorzi and Nelson [8]. Note that the equation of motion for the shaft element in complex form [11] does not contain internal damping, whereas the effects of both viscous and hysteretic internal damping are included into the finite element model in the work by Zorzi and Nelson [8].

Consider a symmetric rotor system as shown in Figure 1. The rotor system consists of symmetrical rigid disks with negligible thicknesses, uniform circular Rayleigh shafts with viscous internal damping, and  $n$  isotropic damped bearings with stiffnesses  $k_i$  and damping coefficients  $c_i$  ( $i = 1, 2, \dots, n$ ). The rotor is balanced, and rotates at a constant speed  $\Omega$  ( $\Omega > 0$ ). The reference system  $Oxyz$  is fixed in space with the horizontal  $x$ -axis coinciding with the undeformed rotor centerline. The external damping, axial load and gravity are neglected.

Any node  $i$  of the rotor system has four degrees of freedom: two translations ( $v_i, w_i$ ) in the  $(y, z)$  directions, and two rotations ( $\varphi_{yi}, \varphi_{zi}$ ) about the  $(y, z)$  axes, respectively. The complex displacement vector of the  $i$ th node is defined by complex coordinates [11]

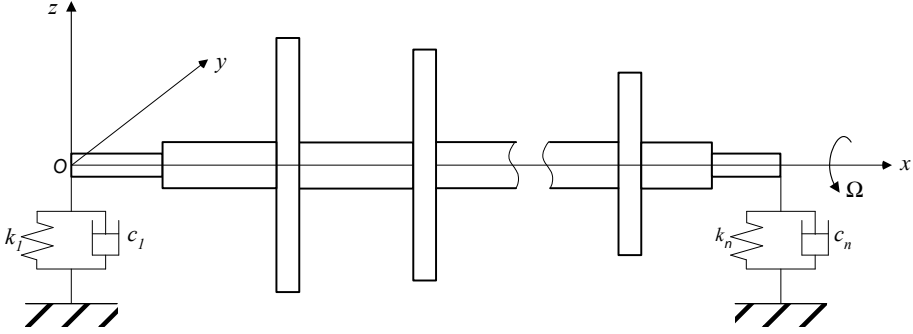


Figure 1: Symmetric rotor in isotropic damped bearings

as

$$\mathbf{p}_i = \begin{bmatrix} r_i \\ \varphi_i \end{bmatrix} = \begin{bmatrix} v_i + iw_i \\ \varphi_{yi} + i\varphi_{zi} \end{bmatrix}, \quad i = \sqrt{-1} \quad (2.1)$$

The component equations and the system equation in complex form may be written as presented below.

**2.2. Rigid disk.** The equation of motion for a rigid disk in complex form is given by

$$(\mathbf{M}_t^d + \mathbf{M}_r^d) \ddot{\mathbf{p}}^d - \Omega \mathbf{G}^d \dot{\mathbf{p}}^d = \mathbf{F}^d, \quad (2.2)$$

where  $\mathbf{p}^d$  is the complex displacement vector corresponding to the four degrees of freedom ( $v^d, w^d, \varphi_y^d, \varphi_z^d$ ) of the node at which the disk is attached. The translational and rotational mass matrices ( $\mathbf{M}_t^d, \mathbf{M}_r^d$ ), and the gyroscopic matrix  $\mathbf{G}^d$  are defined as

$$\mathbf{M}_t^d = \begin{bmatrix} m^d & 0 \\ 0 & 0 \end{bmatrix}, \quad (2.3)$$

$$\mathbf{M}_r^d = \begin{bmatrix} 0 & 0 \\ 0 & J_D \end{bmatrix}, \quad (2.4)$$

$$\mathbf{G}^d = \begin{bmatrix} 0 & 0 \\ 0 & iJ_P \end{bmatrix}, \quad (2.5)$$

where  $m^d$ ,  $J_D$  and  $J_P$  are the mass, the diametral and polar moments of inertia of the disk, respectively.

**2.3. Finite shaft element.** The equation of motion for the finite rotating shaft element with internal viscous damping takes the form [9]

$$(\mathbf{M}_t^e + \mathbf{M}_r^e) \ddot{\mathbf{p}}^e + (\eta \mathbf{K}_b^e - \Omega \mathbf{G}^e) \dot{\mathbf{p}}^e + (\mathbf{K}_b^e + \eta \Omega \mathbf{K}_c^e) \mathbf{p}^e = \mathbf{F}^e, \quad (2.6)$$

where

$$\mathbf{p}^e = \begin{bmatrix} \mathbf{p}_i \\ \mathbf{p}_j \end{bmatrix} \quad (2.7)$$

is the  $(4 \times 1)$  complex nodal displacement vector of the shaft element with nodes  $i$  and  $j$ ,  $\eta$  is the internal viscous damping coefficient,

$$\mathbf{K}_c^e = -i\mathbf{K}_b^e \quad (2.8)$$

is the complex circulation matrix of the shaft element.

The translational and rotational mass matrices  $(\mathbf{M}_t^e, \mathbf{M}_r^e)$ , the gyroscopic matrix  $\mathbf{G}^e$ , and the bending stiffness matrix  $\mathbf{K}_b^e$  of the shaft element are defined as

$$\mathbf{M}_t^e = \frac{\mu l}{420} \begin{bmatrix} 156 & & & & & \\ & i22l & 4l^2 & & & \\ & 54 & -i13l & 156 & & \\ & -i13l & -3l^2 & -i22l & 4l^2 & \\ & & & & & \end{bmatrix}, \quad (2.9)$$

$$\mathbf{M}_r^e = \frac{\mu r^2}{120l} \begin{bmatrix} 36 & & & & & \\ & i3l & 4l^2 & & & \\ & -36 & -i3l & 36 & & \\ & i3l & -l^2 & -i3l & 4l^2 & \\ & & & & & \end{bmatrix}, \quad (2.10)$$

$$\mathbf{G}^e = i2\mathbf{M}_r^e, \quad (2.11)$$

$$\mathbf{K}_b^e = \frac{EI}{l^3} \begin{bmatrix} 12 & & & & & \\ & i6l & 4l^2 & & & \\ & -12 & i6l & 12 & & \\ & i6l & 2l^2 & -i6l & 4l^2 & \\ & & & & & \end{bmatrix}, \quad (2.12)$$

where  $\mu$  is the mass per unit length,  $l$  is the length of shaft element,  $r$  is the element radius,  $EI$  is the bending rigidity of the shaft element.

**2.4. Linear isotropic damped bearings.** The linear isotropic damped bearings can be modeled by the equation:

$$\mathbf{C}^b \dot{\mathbf{p}}^b + \mathbf{K}^b \mathbf{p}^b = \mathbf{F}^b, \quad (2.13)$$

where  $\mathbf{p}^b$  is the complex displacement vector at the bearing location (node),  $\mathbf{F}^b$  is the complex bearing force vector. The damping and stiffness matrices  $(\mathbf{C}^b, \mathbf{K}^b)$  of the isotropic bearings are defined as

$$\mathbf{C}^b = \begin{bmatrix} c^b & 0 \\ 0 & 0 \end{bmatrix}, \quad \mathbf{K}^b = \begin{bmatrix} k^b & 0 \\ 0 & 0 \end{bmatrix}, \quad (2.14)$$

where  $c^b$  and  $k^b$  are the direct damping and stiffness coefficients for the translational displacements, respectively.

**2.5. System equations.** The equations of motion of the complete rotor-bearing system can be obtained by assembling all component equations of the form equations (2.2), (2.6) and (2.13). The resulting equation is of the form

$$\mathbf{M} \ddot{\mathbf{p}} + (\eta \mathbf{K}_b + \mathbf{C} - \Omega \mathbf{G}) \dot{\mathbf{p}} + [\mathbf{K}_B + (1 - i\eta\Omega) \mathbf{K}_b] \mathbf{p} = 0, \quad (2.15)$$

where

$$\mathbf{p}^T = [\mathbf{p}_1^T \mathbf{p}_2^T \dots \mathbf{p}_N^T] \quad (2.16)$$

is the  $(2N \times 1)$  complex nodal displacement vector of the rotor system ( $N$  equals the number of nodes), the letter “ $T$ ” denotes the transpose.

**2.6. Positive definite matrices.** Since kinetic energy and strain energy cannot be negative, the system matrices  $(\mathbf{M}, \mathbf{K}_b)$  are positive definite Hermitian matrices [9]. Thus the following relations hold:

$$\bar{\mathbf{p}}^T \mathbf{M} \mathbf{p} > 0, \quad \bar{\mathbf{p}}^T \mathbf{K}_b \mathbf{p} > 0, \quad (\mathbf{p} \neq 0), \quad (2.17)$$

where the bar denotes the complex conjugate operator.

Note that the system gyroscopic matrix  $\mathbf{G}$  is not Hermitian. However, by using the definitions of the component gyroscopic matrices presented by equations (2.5) and (2.11) it can be expressed as

$$\mathbf{G} = i\mathbf{M}_g, \quad (2.18)$$

where

$$\bar{\mathbf{p}}^T \mathbf{M}_g \mathbf{p} > 0, \quad (\mathbf{p} \neq 0). \quad (2.19)$$

Evidently  $\mathbf{C}$  and  $\mathbf{K}_B$  are positive definite diagonal matrices, the nonzero elements of which are the damping coefficients and the stiffnesses of the isotropic bearings, respectively

### 3. Stability analysis

**3.1. Stability threshold speed determination.** On seeking a solution to equation (2.15) of the form

$$\mathbf{p} = \mathbf{P}e^{\lambda t}, \quad (3.1)$$

we obtain the eigenvalue problem

$$[\lambda^2 \mathbf{M} + \lambda(\eta \mathbf{K}_b + \mathbf{C} - \Omega \mathbf{G}) + \mathbf{K}_B + (1 - i\eta\Omega)\mathbf{K}_b] \mathbf{P} = 0 \quad (3.2)$$

with  $4N$  eigenvalues  $\lambda_j$  and the corresponding eigenvectors  $\mathbf{P}_j$  ( $j = 1, 2, \dots, 4N$ ). The eigenvalues  $\lambda$  are of the form

$$\lambda = \alpha + i\omega, \quad (3.3)$$

where  $\alpha$  is the damping coefficient or decay rate,  $\omega$  is the damped natural frequency or whirl speed.

For later use, the eigenvalue problem will be given in a modified form. To this end, we premultiply equation (3.2) by the complex conjugate eigenvector  $\bar{\mathbf{P}}^T$ . Then we obtain the following scalar equation:

$$\bar{\mathbf{P}}^T [\lambda^2 \mathbf{M} + \lambda(\eta \mathbf{K}_b + \mathbf{C} - \Omega \mathbf{G}) + \mathbf{K}_B + (1 - i\eta\Omega)\mathbf{K}_b] \mathbf{P} = 0, \quad (3.4)$$

which can be rewritten as

$$m\lambda^2 + (\eta k_b + c - ig\Omega)\lambda + k_B + (1 - i\eta\Omega)k_b = 0, \quad (3.5)$$

where the scalars  $m, k_b, c, g$  and  $k_B$  are in all positive real quantities defined by

$$\bar{\mathbf{P}}^T \mathbf{M} \mathbf{P} = m > 0, \quad (3.6)$$

$$\bar{\mathbf{P}}^T \mathbf{K}_b \mathbf{P} = k_b > 0, \quad (3.7)$$

$$\bar{\mathbf{P}}^T \mathbf{C} \mathbf{P} = c > 0, \quad (3.8)$$

$$\bar{\mathbf{P}}^T \mathbf{G} \mathbf{P} = ig (g > 0) \quad (3.9)$$

$$\bar{\mathbf{P}}^T \mathbf{K}_B \mathbf{P} = k_B > 0. \quad (3.10)$$

Note that the inequalities (3.6) - (3.10) hold on account of the positive definite matrices of the rotor system (see Section 2.5.).

Instability occurs if one of the eigenvalues has a positive real part. Thus, the problem of determining the limit of stability of the rotor system is reduced to finding the shaft speed  $\Omega_s$  (stability threshold speed), at which the greatest real part of all eigenvalues  $\lambda_j$  equals zero. The corresponding imaginary part  $\omega_s$  is the *whirling speed*.

For the possible limit  $\omega$ , the substitution of the eigenvalue of the form

$$\lambda = i\omega \quad (3.11)$$

into equation (3.5) yields

$$-m\omega^2 + g\Omega\omega + k_b + k_B + i[(\eta k_b + c)\omega - \eta\Omega k_b] = 0. \quad (3.12)$$

After separating equation (3.12) into real and imaginary parts, we obtain

$$-m\omega^2 + g\omega\Omega + k_b + k_B = 0, \quad (3.13)$$

$$\omega(\eta k_b + c) = \eta\Omega k_b \quad (3.14)$$

It is clear from equation (3.14) and inequalities (3.7) and (3.8) that

$$\Omega = \omega \left( 1 + \frac{c}{\eta k_b} \right) > \omega (\omega > 0). \quad (3.15)$$

Consequently, the threshold speed is greater than the corresponding whirling speed. Furthermore, from inequality (3.15) it is seen that the particular undamped whirl mode induced at the stability threshold speed is forward and asynchronous. It is noteworthy that all backward precessional modes of the rotor are stable for any rotational speed.

Now we shall prove that the rotor loses its stability at all speeds above the possible stability limit. Here, we apply the eigenvalue sensitivity analysis. Let us suppose that the shaft speed  $\Omega$  is an independent parameter, and let us differentiate equation (3.5) with respect to  $\Omega$ :

$$\begin{aligned} \lambda' (2m\lambda + \eta k_b + c - ig\Omega) - ig\lambda - i\eta k_b + m'\lambda^2 + \\ + (\eta k_b' + c' - ig'\Omega)\lambda + k_B' + (1 - i\eta\Omega)k_b' = 0, \end{aligned} \quad (3.16)$$

where primes denote differentiation with respect to  $\Omega$ . The quantity  $\lambda' = \partial\lambda/\partial\Omega$  is referred to as an eigenvalue sensitivity coefficient [12], which can be written, with the aid of equation (3.3), in the form:

$$\frac{\partial\lambda}{\partial\Omega} = \frac{\partial\alpha}{\partial\Omega} + i\frac{\partial\omega}{\partial\Omega}. \quad (3.17)$$

To calculate  $\partial\lambda/\partial\Omega$  from equation (3.16) at the possible limit  $\Omega$ , we substitute again equation (3.11) into equation (3.16):

$$\frac{\partial\lambda}{\partial\Omega} [\eta k_b + c + i(2m\omega - g\Omega)] + g\omega - i\eta k_b + \underbrace{(-m'\omega^2 + g'\omega\Omega + k'_b + k'_B)}_{+i[\omega(\eta k'_b + c') - \eta\Omega k'_b]} = 0. \quad (3.18)$$

Since the eigenvalue derivative  $\partial\lambda/\partial\Omega$  represents the unique solution of equation (3.18) at the possible limit of stability and hence its value is not influenced by any normalization criterion for the eigenvector  $\mathbf{P}$ , therefore the underlined terms will vanish:

$$-m'\omega^2 + \omega\Omega g' + k'_b + k'_B = 0, \quad (3.19)$$

$$\omega(\eta k'_b + c') = \eta\Omega k'_b. \quad (3.20)$$

We then obtain the following expression for the damping sensitivity coefficient  $\partial\alpha/\partial\Omega$ :

$$\frac{\partial\alpha}{\partial\Omega} = \frac{2\eta k_b(m\omega - g\Omega)}{(\eta k_b + c)^2 + (2m\omega - g\Omega)^2}. \quad (3.21)$$

It is easy to show that the nominator of the above ratio is positive. By using equation (3.13), the bracketed term in the nominator can be written as

$$m\omega - g\Omega = \frac{k_b + k_B}{\omega}. \quad (3.22)$$

By making use of inequalities (3.6) - (3.10), it is clear that the right-hand side of equation (3.22) is positive. Therefore, the damping sensitivity coefficient  $\partial\alpha/\partial\Omega$  is positive at each possible limit of stability. Thus, the lowest value of the above stability limits for the particular forward whirl modes is considered to be the *stability threshold speed* of the rotor-bearing system. Consequently, the whirling motion of the rotor becomes unstable at all speeds above the stability threshold speed.

**3.2. Effect of bearing damping on rotor stability.** Now we shall prove that an increase in the bearing damping coefficients results in an increase in the whirl threshold speed, thus the rotor stability will be improved.

Let us consider the bearing damping coefficient  $c_i (i = 1, 2, \dots, n)$  of the  $i$ th isotropic damped bearing as an independent parameter, and differentiate equations (3.13) and (3.14) with respect to  $c_i$ :

$$\omega'(g\Omega - 2m\omega) + \omega g\Omega' + \underbrace{(-m'\omega^2 + \omega\Omega g' + k'_b + k'_B)}_{=0} = 0, \quad (3.23)$$

$$\omega'(c + \eta k_b) - \eta k_b \Omega' + \underbrace{\omega(\tilde{c} + \eta k'_b) - \eta\Omega k'_b}_{=0} = -\omega c^*, \quad (3.24)$$

where prime denotes differentiation with respect to  $c_i$ ,

$$\tilde{c} = \frac{\partial \bar{\mathbf{P}}^T}{\partial c_i} \mathbf{C} \mathbf{P} + \bar{\mathbf{P}}^T \mathbf{C} \frac{\partial \mathbf{P}}{\partial c_i} \quad (3.25)$$

and

$$c^* = \bar{\mathbf{P}}^T \frac{\partial \mathbf{C}}{\partial c_i} \mathbf{P} > 0. \quad (3.26)$$

By using the same reasoning that we have applied in connection with equation (3.18), it is clear that the underlined terms in equations (3.23) and (3.24) will vanish at the threshold speed  $\Omega$ . The whirling speed sensitivity coefficient  $\omega'$  and the threshold speed sensitivity coefficient  $\Omega'$  can now be obtained from the above two equations as

$$\frac{d\omega}{dc_i} = \frac{gc^*\omega^2}{2(m\omega - g\Omega)\eta k_b}, \quad (3.27)$$

$$\frac{d\Omega}{dc_i} = \frac{\omega(2m\omega - g\Omega)c^*}{2(m\omega - g\Omega)\eta k_b}. \quad (3.28)$$

By using equation (3.22) and inequalities (3.7) and (3.9), it is easy to see that the above sensitivity coefficients are positive. Thus, the addition of bearing damping improves the rotor stability. It is also clear that the whirling speed is always greater than the first forward bending critical speed of the rotor system. The latter statement follows from the fact that the threshold speed of symmetrical rotors with viscous internal damping, supported by undamped isotropic bearing, coincides with the first forward critical speed [9]. It can further be concluded from equation (3.27) that when the gyroscopic moments of the rotor are neglected ( $g = 0$ ), then the whirling speed remains constant (the first critical speed of the rotor) regardless of the magnitude of the bearing damping coefficients.

**3.3. Influence of internal damping on threshold speed.** We shall now prove that increasing the internal viscous damping coefficient  $\eta$  causes reduction in the stability threshold speed of the rotor. We assume that  $\eta$  is an independent system parameter. By differentiating equations (3.13) and (3.14) with respect to  $\eta$ , we get

$$\omega'(g\Omega - 2m\omega) + \omega g \Omega' + \underline{(-m'\omega^2 + \omega\Omega g' + k'_b + k'_B)} = 0, \quad (3.29)$$

$$\omega'(c + \eta k_b) - \eta k_b \Omega' + \underline{\omega(c' + \eta k'_b)} - \eta \Omega k'_b = (\Omega - \omega)k_b, \quad (3.30)$$

where prime denotes differentiation with respect to  $\eta$ . Since the underlined expressions vanish at the stability threshold, the whirling speed and threshold speed sensitivity coefficients are determined by

$$\frac{d\omega}{d\eta} = -\frac{\omega g(\Omega - \omega)}{2(m\omega - g\Omega)\eta}, \quad (3.31)$$

$$\frac{d\Omega}{d\eta} = -\frac{(2m\omega - g\Omega)(\Omega - \omega)}{2(m\omega - g\Omega)\eta}. \quad (3.32)$$

By using inequalities (3.9), (3.15), and equation (3.22), it is clear that both the whirling speed sensitivity coefficient and the threshold speed sensitivity coefficient

are negative at the stability threshold speed  $\Omega = \Omega_s$ . Consequently, internal viscous damping has a destabilizing effect on the rotor stability.

From equation (3.31) we also see that a change of  $\Delta\eta$  leads to an opposite change in the whirling speed  $\omega_s$ . Further, when the gyroscopic moments are neglected ( $g = 0$ ), the whirling speed remains constant regardless of the magnitude of the internal viscous damping coefficient.

#### 4. Numerical examples

**4.1.** To demonstrate the validity of the above theoretical results, two numerical examples are provided. In both examples, the simply supported uniform shaft studied by Zorzi [8] is considered. The rotor model consists of a 10.16 cm diameter and 127 cm long steel shaft supported by two identical isotropic damped bearings at both ends. The stiffnesses of the bearings are:  $k_1 = 1.75 \times 10^{11}$  N/m. The material properties of the shaft are: Young's modulus  $E = 2.06 \times 10^{11}$  N/m<sup>2</sup>, and density  $\rho = 7800$  kg/m<sup>3</sup>. The rotor is modeled as an assembly of four finite elements of equal length. In the calculations, the damping coefficients  $c_1$  of the bearings and the internal viscous damping coefficient  $\eta$  for the shaft are considered to be parameters.

**4.2.** As a first example, we shall examine the influence of the damping coefficient  $c_1$  on the rotor stability for the viscous internal damping coefficient  $\eta = 0.0002$  s. Table 1 shows the numerical values of the whirling speed  $\omega_s$  and the stability threshold speed  $\Omega_s$  of the rotor for different values of  $c_1$ . The first forward bending critical speed of the rotor was found to be  $\Omega_{F1} = 521.392$  rad/s.

bearing damping (Ns/m)	threshold speed (rad/s)	whirling speed (rad/s)
0	521.392	521.392
100	544.085	521.397
200	566.798	521.410
300	589.518	521.430
400	612.254	521.457
500	635.006	521.492

Table 1. Effect of bearing damping ( $c_1$ ) on rotor stability

As can be seen from Table 1, the introduction of bearing damping will increase the stability threshold speed, thus the stability of the rotor system will be improved. The numerical results also illustrate that the threshold speeds are greater than the corresponding whirling speeds, which are only slightly greater than the first forward critical speed of the rotor. Clearly the numerical results of Table 1 are in quite good agreement with the theoretical results obtained in Section 3.2.

**4.3.** As a second example, we consider the influence of the internal viscous damping  $\eta$  on the rotor stability for the bearing damping coefficient  $c_1 = 1750$  Ns/m. Table 2 presents the calculated values of the threshold speeds and whirling speeds for different values of  $\eta$ .

viscous internal damping (s)	threshold speed (rad/s)	whirling speed (rad/s)
0.0002	922.335	522.565
0.0003	789.012	522.556
0.0004	722.375	522.551
0.0005	682.396	522.548

Table 2. Effect of internal damping on rotor stability

The numerical results show clearly that the stability of the rotor is greatly reduced by increasing internal damping. For example, for the viscous internal damping coefficient of  $\eta = 0.0002$  s, the rotor becomes unstable at the threshold speed  $\Omega_s = 922.335$  rad/s. By increasing the viscous internal damping coefficient to  $\eta = 0.0003$  s, the rotor stability threshold speed will be reduced to  $\Omega_s = 789.012$  rad/s. It should be noted that increasing internal damping produces only a small reduction in the whirling speed  $\omega_s$ . Table 2 also confirms the validity of inequality (3.15). ( $\Omega_s > \omega_s$ ). Evidently the numerical results summarized in Table 2 are in good agreement with the theoretical results derived in Section 3.3.

## 5. Summary and conclusions

In this paper a finite element stability analysis of self-excited bending vibrations of symmetric rotors with viscous internal damping, supported by isotropic damped bearings has been presented. By combining the sensitivity method and the eigenvalue problem of the rotor dynamics equations in complex form, it is proved theoretically that the whirling motion of the rotor becomes unstable at all speeds above the stability threshold speed.

In addition, the latter is always greater than the corresponding whirling speed. Further, the rotor stability is improved by increasing the damping provided by the bearings, whereas internal viscous damping destabilizes the whirling motion of the rotor.

It is also shown that the whirling speed of the rotor system is higher than the first forward bending critical speed. Numerical examples are provided to confirm the validity of the above theoretical results.

**Acknowledgement.** This research has been partially supported by the National Fund for Scientific Research of Hungary (OTKA) under grants T 016836 and T 030096.

## REFERENCES

1. KIMBALL, A.L.: *Internal friction theory of shaft whirling*, General Electric Review, **27**, (1924), 244-251.
2. NEWKIRK, B.L.: *Shaft Whipping*, General Electric Review, **27**, (1924), 169-178.
3. SMITH, D.M.: *The motion of a rotor carried by a flexible shaft in flexible bearings*, Proceedings of the Royal Society of London, Series A, **142**, (1933), 92-118.
4. DIMENTBERG, F.M.: *Flexural Vibrations of Rotating Shafts*, Butterworths, London 1961.
5. EHRICH, F.F.: *Shaft whirl induced by rotor internal damping*, ASME Journal of Applied Mechanics **31**, (1964), 279-282.
6. TONDL, A.: *Some Problems of Rotor Dynamics*, Publishing House of the Czechoslovak Academy of Sciences, Prague 1965.
7. GUNTER, E.J. and TRUMPLER, P.R.: *The influence of internal friction on the stability of high speed rotors with anisotropic supports*, ASME Journal of Engineering for Industry **91**, (1969), 1105-1113.
8. ZORZI, E.S. and NELSON, H.D.: *Finite element simulation of rotor-bearing systems with internal damping*, ASME Journal of Engineering for Power, **99**, (1977) 71-76.
9. FORRAI, L.: *Stability analysis of symmetrical rotor-bearing systems with internal damping using finite element method*, Presented at the International Gas Turbine and Aero-engine Congress and Exhibition, Birmingham, UK (1996), ASME Paper No. 96-GT-407.
10. FORRAI, L.: *Stability of rotor-bearing systems with internal damping using finite elements*, Proc. 9th World Congress on the Theory of Machines and Mechanisms, Milano, Italy (1995), 1204-1208.
11. NELSON, H.D.: *Rotor dynamics equations in complex form*, ASME Journal of Vibration, Acoustics, Stress and Reliability in Design, **107**, (1985), 460-461.
12. RAJAN, M., NELSON, H.D. and CHEN, W.J.: *Parameter sensitivity in the dynamics of rotor-bearing systems*, Journal of Vibration, Acoustics, Stress, and Reliability in Design, April 1986, Vol. 108, 197-206.



## OPTIMUM DESIGN OF STIFFENED PLATES

KÁROLY JÁRMAI

Department of Materials Handling and Logistics, University of Miskolc  
3515 Miskolc – Egyetemváros, Hungary  
altjar@gold.uni-miskolc.hu

[Received: August 4, 1999]

*Dedicated to Professor István Páczelt on the occasion of his sixtieth birthday*

**Abstract.** The aim of this paper is to show how to make real structural optimizations on a strong theoretical background. Using stiffened plates one can get a lightweight and stiff structure. Several calculations have been developed for stiffened plates. All of them are approximations: the Massonnet and the Gienke techniques. Cost calculation is also important, due to the expensive welding technologies. Two applications are shown: shipdeck panel and compressed stiffened plate. It is shown that using optimization, one can reduce the total cost of the structure. In countries where fabrication costs are high the number of stiffeners is small and the thickness is large. In countries where fabrication costs are low the number of stiffeners is large and the thickness is small [1, 1999].

*Keywords:* Structural optimization, stiffened plates, cost calculation

### 1. Introduction

A stiffened plate has low mass and high bending stiffness. The use of welding made it possible to produce different constructions. To increase the torsional rigidity, cellular plates have been introduced. Stiffened plates can be applied as roof structures of supermarkets, petrol stations, etc. (Figure 1), orthotropic bridge decks (Figure 2), airplane wing structures (Figure 3), ship wall and deck structures (Figure 4), roof structure of tanks (Figure 5) [2, 1966], [3, 1968].

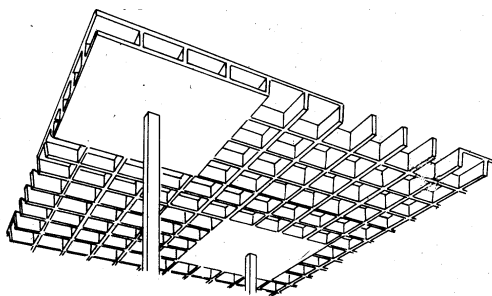


Figure 1.

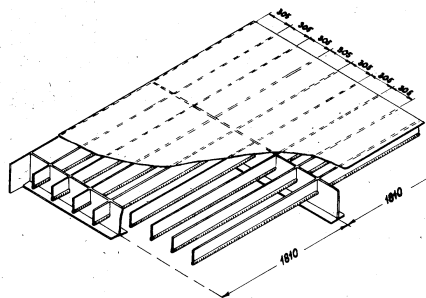


Figure 2.



- deflections are small compared to the thickness of the plate,
- normal stresses orthogonal to the plate can be neglected,
- shear deformations can be neglected,
- stresses from torsion can be calculated from Saint-Venant theory,
- number of stiffeners in both directions is large enough to assume that the effective plate width is equal to the distance between stiffeners.

The stiffness matrix of a plate stiffened on one side in two directions can be formulated from three matrixes: cover plate and stiffeners in  $x$ - and  $y$ -directions. The reference plane is the mid cover plane. The equilibrium equations concerning the deflections are as follows:

$$(D + D_{bx}) u'' - z_{Sx} D_{bx} w''' + \frac{1 - \nu}{2} D \ddot{u} + \frac{1 - \nu}{2} D \dot{v}' = 0, \quad (2.1)$$

$$(D + D_{by}) \ddot{v} - z_{Sy} D_{by} \ddot{w} + \frac{1 - \nu}{2} D v'' + \frac{1 - \nu}{2} D \dot{u}' = 0, \quad (2.2)$$

$$\begin{aligned} & z_{Sx} D_{bx} u''' + z_{Sy} D_{by} \ddot{v} - (B + B_{bx} + z_{Sx}^2 D_{bx}) w'''' - \\ & - (B + B_{by} + z_{Sy}^2 D_{by}) \ddot{\ddot{w}} - (2B + B_{xy} + B_{yx}) \ddot{w}'' + p = 0 \end{aligned} \quad (2.3)$$

where  $D$  is the tensional stiffness of the isotropic plate,  $t_f$  is the thickness of the cover plate,  $u$ ,  $v$  and  $w$  are deflections in  $x$ ,  $y$  and  $z$  directions,  $\nu$  is the Poisson ratio,  $z_{Sx} D_{bx}$ ,  $z_{Sy} D_{by}$  are related to the linear moment,  $\dot{w}$  and  $w'$  are derivatives of  $w$  in  $x$  and  $y$  directions,  $E$  is the Young modulus,  $p$  is the uniformly distributed load, perpendicular to the cover plate.

Introducing the notations

$$D + D_{bx} = D_x, \quad D + D_{by} = D_y \quad (2.4)$$

the bending stiffnesses of the cover plate and the stiffener in  $x$ - and  $y$  directions are

$$B_x = B + e_x^2 D + B_{bx} + D_{bx} (z_{Sx} - e_x)^2 \quad (2.5a)$$

$$B_y = B + e_y^2 D + B_{by} + D_{by} (z_{Sy} - e_y)^2 \quad (2.5b)$$

where  $B$ ,  $B_x$ ,  $B_y$  are bending stiffnesses,  $D_{bx}$ ,  $D_{by}$  are tensional stiffnesses of the stiffeners in  $x$ - and  $y$  directions,  $e_x$ ,  $e_y$  are eccentricities.

Substituting equations (2.4-2.5b) into (2.1-2.3) we obtain

$$\begin{aligned} B_x w'''' + 2(B + B_{xy} + B_{yx}) \ddot{w}'' + B_y \ddot{\ddot{w}} + \frac{D}{2} (1 - \nu) e_y \ddot{u}' + \\ + \frac{D}{2} [(1 + \nu) e_x + (1 - \nu) e_y] \dot{v}'' = p \end{aligned} \quad (2.6)$$

For a symmetrically stiffened plate on both sides,  $e_x = e_y = 0$  then (2.6) will have a simpler form referred to as Huber equation

$$B_x w'''' + 2(B + B_{xy} + B_{yx}) \ddot{w}'' + B_y \ddot{\ddot{w}} = p. \quad (2.7)$$

For an isotropic plate  $B_x = B_y = B$  and  $B_{xy} = B_{yx} = 0$ .

**2.3. Calculation of eccentrically stiffened plates.** For an eccentrically stiffened plate (2.1-2.3), eliminating  $u$  and  $v$ , gives the following form

$$a_1 \frac{\partial^8 w}{\partial x^8} + a_2 \frac{\partial^8 w}{\partial x^6 \partial x^2} + a_3 \frac{\partial^8 w}{\partial x^4 \partial y^4} + a_4 \frac{\partial^8 w}{\partial x^2 \partial y^6} + a_5 \frac{\partial^8 w}{\partial y^8} = f \left( \frac{\partial^4 p}{\partial x^4}, \frac{\partial^4 p}{\partial x^2 \partial y^2}, \frac{\partial^4 p}{\partial y^4} \right) \quad (2.8)$$

where  $a_1, a_2, a_3$  are parameters and  $f$  is the loading function.

The 8th order partial differential equation shows the complexity of the general problem. For a symmetrical structure the equation can be solved by infinite mathematical series. The other solution is to introduce approximations, like reduced stiffnesses, which leads to a Huber equation. This kind of method was developed by [5, 1959] and [6, 1955].

*2.3.1. Massonnet technique.* The elastic energy of the plate is given by

$$U = \frac{E}{2(1-\nu^2)} \iiint_{\text{cover plate}} \left( \varepsilon_x^2 + \varepsilon_y^2 + 2\nu\varepsilon_x\varepsilon_y + \frac{1-\nu}{2}\gamma_{xy}^2 \right) dx dy dz + \frac{E}{2} \iiint_{\text{stiffeners}} (\varepsilon_x^2 + \varepsilon_y^2) dx dy dz + \frac{1}{2} \iint_A (B_{xy} + B_{yx}) \dot{w}' dx dy \quad (2.9)$$

where  $\varepsilon_x, \varepsilon_y$  and  $\gamma_{xy}$  are the strains. The displacements in the  $x, y$  and  $z$  directions are denoted by  $u, v$  and  $w$ . Massonnet assumes that

$$u = c_x w', \quad v = c_y \dot{w}$$

where  $c_x$  and  $c_y$  are parameters.

Due to the shear stiffness of the cover plate, the eccentricities are less than  $e_x$  and  $e_y$ .

While we want to determine  $u$  and  $v$  for a given  $w$ , in the equation of  $U$  we should consider the parts, which depend on  $u$  and  $v$ . Solving equation (2.9) we get the reduced Huber equations

$$B_x^* w'''' + 2H^* \ddot{w}'' + B_y^* \dot{w}'' = p, \quad (2.10a)$$

$$B_x^* = B_x + (e_x - c_x)^2 D_x, \quad (2.10b)$$

$$B_y^* = B_y + (e_y - c_y)^2 D_y, \quad (2.10c)$$

$$2H^* = 2B + B_{xy} + B_{yx} + \frac{1-\nu}{2} D(c_x + c_y)^2 + 2\nu D c_x c_y. \quad (2.10d)$$

This is an iteration procedure: first take an approximation function to  $w$ , determination of  $c_x, c_y$  calculation the reduced stiffnesses, get a better approximation to  $w$  and start a new iteration.

*2.3.2. Gienke technique.* In order to simplify calculation Gienke suggested considering  $D_x$  and  $D_y$  as infinitely great quantities. It means that we neglect the deformation

of the fibre in gravity center to  $w$ :

$$1/D_x = 1/D_y = 0, \quad (2.11)$$

$$c_x = e_x, \quad c_y = e_y \quad (2.12)$$

where  $c_x, c_y$  are parameters.

The bending stiffnesses are now given by

$$B_{x^*} = B_x, \quad B_y^* = B_y \quad (2.13)$$

while for the half torsional stiffness  $H$  one can write

$$2H^* = 2B + B_{xy} + B_{yx} + \frac{1-\nu}{2}D(e_x + e_y)^2 + 2\nu D e_x e_y. \quad (2.14)$$

The Gienke calculation is less accurate, but simpler than that of Massonnet, because there is no need for iterations.

*2.3.3. Navier solution of square stiffened plates subject to bending.* We are looking for  $w = w(x, y)$  function as a solution of the equation

$$B_x w'''' + 2H^* \ddot{w}'' + B_y \ddot{w} = p(x, y) \quad (2.15)$$

$$2H^* = B + B_{xy} + B_{yx} \quad (2.16)$$

If the plate is a square one and is simply supported, equation (2.15) is associated with the boundary conditions

$$\begin{aligned} w &= 0, & m_x &= 0 & \text{if } x = 0 \text{ and } x = b_x \\ w &= 0, & m_y &= 0 & \text{if } y = 0 \text{ and } y = b_y \end{aligned}$$

As is well known, the solution assumes the form

$$w(x, y) = \sum_{m=1}^{\infty} \sum_{n=1}^{\infty} c_{mn} \sin \frac{m\pi x}{b_x} \sin \frac{n\pi y}{b_y} \quad (2.17)$$

where  $b_x$  and  $b_y$  are the sizes of the plate in  $x$  and  $y$  directions. We remark that the load can also be given in this form

$$p(x, y) = \sum_{m=1}^{\infty} \sum_{n=1}^{\infty} a_{mn} \sin \frac{m\pi x}{b_x} \sin \frac{n\pi y}{b_y} \quad (2.18)$$

The coefficients  $a_{mn}$  and  $c_{mn}$  are related to each other via the equation

$$c_{mn} = \frac{a_{mn}}{\pi^4 \left( B_x \frac{m^4}{b_x^4} + 2H \frac{m^2 n^2}{b_x^2 b_y^2} + B_y \frac{n^4}{b_y^4} \right)} \quad (2.19)$$

We can get the solution that for uniformly distributed load  $p(x, y) = p$

$$a_{mn} = 16p/\pi^2 mn. \quad (2.20)$$

### 3. Cost calculation of stiffened plates

**3.1. Fabrication costs.** The cost function can be expressed as

$$K = K_m + K_f = k_m \rho V + k_f \sum_i T_i \quad (i = 1, 2, \dots, 7) \quad (3.1)$$

where  $K_m$  and  $K_f$  are the material and fabrication costs, respectively,  $k_m$  and  $k_f$  are the corresponding cost factors,  $\rho$  is the material density,  $V$  is the volume of the structure,  $T_i$  are the production times [7, 1997], [8, 1999].

**3.2. Welding times.** Time for preparation, assembly and tacking is given by

$$T_1 = C_1 \delta \sqrt{\kappa \rho V} \quad (3.2)$$

where  $\delta$  is a difficulty factor,  $\kappa$  is the number of structural elements to be assembled [9, 1992]. For the welding time one can write

$$T_2 = \sum_i C_{2i} a_{wi}^n L_{wi} \quad (3.3)$$

in which  $a_{wi}$  is the weld size,  $L_{wi}$  is the weld length and  $C_{2i}$  are constants determined by the welding technology. Time for additional fabrication activities such as changing the electrode, deslagging and chipping can be calculated as

$$T_3 = \sum_i C_{3i} a_{wi}^n L_{wi} \quad (3.4)$$

in which [10, 1985] proposed for the constants that  $C_3 = (0.2-0.4)C_2$  and  $C_3 = 0.3C_2$ . Neglecting  $\sqrt{\Theta_d}$  one obtains

$$T_2 + T_3 = 1.3 \sum_i C_{2i} a_{wi}^2 L_{wi} \quad (3.5)$$

which is a modified formula for  $T_2 + T_3$ .

Table 1. Applied welding technologies

SMAW	Shielded Metal Arc Welding
SMAW HR	Shielded Metal Arc Welding High Recovery
GMAW-C	Gas Metal Arc Welding with CO <sub>2</sub>
GMAW-M	Gas Metal Arc Welding with Mixed Gas
FCAW	Flux Cored Arc Welding
FCAW-MC	Metal Cored Arc Welding
SSFCAW (ISW)	Self Shielded Flux Cored Arc Welding
SAW	Submerged Arc Welding
GTAW	Gas Tungsten Arc Welding

Different welding technologies are shown in Table 1.

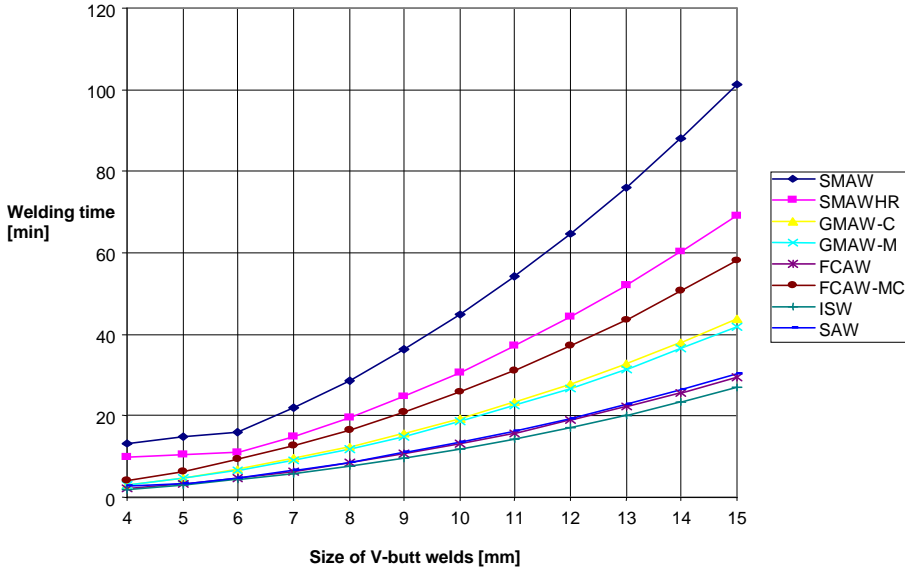


Figure 7. Welding time  $T_2$  (min) for different welding technologies plotted against the weld size  $a_w$  (mm) for longitudinal V butt welds downhand position

In Figure 7 data are given for eight welding techniques and for a given weld type.

Using COSTCOMP [11, 1990] software we have calculated the welding time  $T_2$  (min) as a function of weld size  $a_w$  (mm) for longitudinal fillet welds, for 1/2 V and V butt welds, for K and X butt welds, for T butt welds, for U and double U butt welds, in downhand position [12, 1990].

The welding time  $T_2$  (min/mm) as a function of weld size  $a_w$  (mm) for longitudinal V butt welds is increasing in positional welding, which means not downhand, but vertical or overhead positions. Figure 7 shows that the welding time for longitudinal V butt welds in decreasing order is the highest for SMAW, SMAW-HR, GMAW-C, GMAW-M, FCAW, FCAW-MC, ISW and the lowest for SAW.

**3.3. Time for flattening plates.** In the catalogues of different companies one can find the times for flattening plates ( $T_4$  [min]) as the function of the plate thickness ( $t$  [mm]) and the area of the plate ( $A_p$  [mm<sup>2</sup>]). The time function can be written in the form:

$$T_4 = \Theta_{de} \left( a_e + b_e t^3 + \frac{1}{a_e t^4} \right) A_p, \quad (3.6)$$

where  $a_e = 9.2 * 10^{-4}$  [min/mm<sup>2</sup>],  $b_e = 4.15 * 10^{-7}$  [min/mm<sup>5</sup>],  $\Theta_{de}$  is the difficulty parameter ( $\Theta_{de} = 1, 2$  or  $3$ ). The difficulty parameter depends on the form of the plate.

**3.4. Surface preparation time.** Surface preparation means the surface cleaning, painting, ground coat, top coat, sand-spraying, etc. The surface cleaning time can be

given in terms of the surface area ( $A_s$  [mm<sup>2</sup>]) as follows:

$$T_5 = \Theta_{ds} a_{sp} A_s \quad (3.7)$$

where  $a_{sp} = 3 * 10^{-6}$  [min/mm<sup>2</sup>],  $\Theta_{ds}$  is a difficulty parameter.

**3.5. Painting time.** Painting means making the ground and the topcoat. The painting time depends on the surface area ( $A_s$  [mm<sup>2</sup>]) as follows:

$$T_6 = \Theta_{dp}(a_{gc} + a_{tc})A_s \quad (3.8)$$

where  $a_{gc} = 3 * 10^{-6}$  [min/mm<sup>2</sup>],  $a_{tc} = 4.15 * 10^{-6}$  [min/mm<sup>2</sup>],  $\Theta_{dp}$  is a difficulty factor,  $\Theta_{dp}=1,2$  or  $3$  for horizontal, vertical or overhead painting.

**3.6. Cutting and edge grinding times.** Cutting and edge grinding can be done by different technologies, like Acetylene, Stabilized gasmix and Propane with normal and high speed. The cutting time can be calculated also by COSTCOMP. The normal speed acetylene has the highest time and the high speed propane has the smallest cutting time.

The cutting cost function can be formulated as a function of the thickness ( $t$  [mm]) and cutting length ( $L_c$  [mm]):

$$T_7 = \sum C_{7i} t_i^n L_{ci} \quad (3.9)$$

where  $t_i$  is the thickness in [mm],  $L_{ci}$  is the cutting length in [mm].

**3.7. Total cost function.** The total cost function is defined according to (3.1). Taking  $k_m = 0.5 \div 1$  \$/kg,  $k_f = 0 \div 1$  \$/min, the  $k_f/k_m$  ratio varies between 0 - 2 kg/min. If  $k_f/k_m = 0$ , we get the mass minimum.  $k_f/k_m = 2.0$  means a very high labor cost (Japan, USA),  $k_f/k_m = 1.5$  and  $1.0$  mean a West European labor cost,  $k_f/k_m = 0.5$  means the labor cost in developing countries.

## 4. Welded stiffened plate

**4.1. Main data for the optimization.** The cost function is calculated according to (3.1), where  $A = b_0 t_f + \varphi h_s t_s$ ,  $\Theta_a = 3$ ,  $\kappa = \varphi + 1$ ,  $L_w = 2L\varphi$  and  $\varphi$  is the number of stiffeners. The stiffeners are welded to the plate by double fillet welds.

The main data for the optimization are as follows:

The Young modulus of the steel is  $E = 2.1 * 10^5$  MPa, the density is  $\rho = 7.85 * 10^{-6}$  kg/mm<sup>3</sup>, the Poisson ratio is  $\nu = 0.3$ , the yield stress is  $f_y = 235$  MPa, the width of the plate is  $b_0 = 4200$  mm and the plate length is  $L = 4000$  mm.

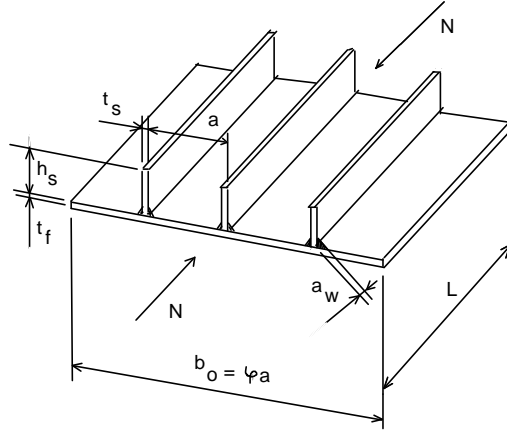


Figure 8. Stiffened plate

The compression force is

$$N = f_y b_0 t_f \max = 235 * 4200 * 20 = 1.974 * 10^7 \text{ (N)} \quad (4.1)$$

The independent design variables are as follows (Figure 8): The plate thickness  $t_f$ , the height  $h_s$  and thickness  $t_s$  of the stiffeners and the number of stiffeners  $\varphi = b_0/a$ .

#### 4.2. Design constraints.

a) According to API [13, 1987] the overall buckling constraint for the compressed plate with uniform distance stiffeners is (Figure 8)

$$N \leq \chi f_y A \quad (4.2)$$

where the buckling factor  $\chi$  is a function of the reduced slenderness factor  $\bar{\lambda}$  :

$$\chi = \begin{cases} 1 & \text{if } \bar{\lambda} \leq 0.5 \\ 1.5 - \bar{\lambda} & \text{if } 0.5 < \bar{\lambda} \leq 1 \\ 0.5/\bar{\lambda} & \text{if } \bar{\lambda} > 1 \end{cases} \quad (4.3)$$

The factor  $\bar{\lambda}$  is given by

$$\bar{\lambda} = \frac{b_0}{t_f} \sqrt{\frac{12(1 - \nu^2) f_y}{E \pi^2 k_{\min}}} \quad (4.4)$$

in which

$$k_{\min} = \min(k_F, k_R) \quad (4.5)$$

$$k_R = 4\varphi^2, \quad k_F = \begin{cases} \frac{(1 + \alpha^2)^2 + \varphi\gamma}{\alpha^2(1 + \varphi\delta_P)} & \text{if } \alpha = \frac{L}{b_0} \leq 4\sqrt{1 + \varphi\gamma} \\ \frac{2(1 + \sqrt{1 + \varphi\gamma})}{1 + \varphi\gamma} & \text{if } \alpha \geq 4\sqrt{1 + \varphi\gamma} \end{cases} \quad (4.6)$$

and

$$\delta_P = \frac{h_s t_s}{b_0 t_f}, \quad \gamma = \frac{EI_s}{b_0 D}, \quad I_s = \frac{h_s^3 t_s}{3}, \quad D = \frac{Et_f^3}{12(1-\nu^2)}. \quad (4.7)$$

Equation (4.7)<sub>2</sub> can be rewritten as

$$\gamma = 4(1-\nu^2) \frac{h_s^3 t_s}{b_0 t_f^3} = 3.64 \frac{h_s^3 t_s}{b_0 t_f^3}, \quad (4.8)$$

where  $I_s$  is the moment of inertia of one stiffener about an axis parallel to the plate surface at the base of the stiffener,  $D$  is the torsional stiffness of the main plate.

Optimization was made using Hillclimb technique [14, 1989].

Table 2. Optimum rounded sizes of welded stiffened plates in mm with fillet welds using different welding technologies for  $k_f/k_m = 2.0$

Welding technology	$k_f/k_m$	$h_s$	$t_f$	$\varphi$	$t_s$	$\rho V$ (kg)	$K/k_m$ (kg)
Same for each technology	0.0	210	17	13	11	2737	2737
	0.5	230	17	6	19	3242	6313
SMAW	1.0	235	17	6	19	3258	9409
	1.5	235	17	6	19	3258	12484
	2.0	235	17	6	19	3258	15559
	0.5	230	17	6	19	3242	5749
SMAW HR	1.0	230	17	6	19	3242	8257
	1.5	230	17	6	19	3242	10764
	2.0	235	17	6	19	3258	13306
	0.5	230	17	6	19	3242	5553
FCAW-MC	1.0	230	17	6	19	3242	7864
	1.5	230	17	6	19	3242	10175
	2.0	235	17	6	19	3258	12521
	0.5	230	17	6	19	3242	5299
GMAW-C	1.0	230	17	6	19	3242	7357
GMAW-M	1.5	235	17	6	19	3258	9444
	2.0	230	17	6	19	3242	11471
SAW	0.5	230	17	6	19	3242	5064
ISW	1.0	230	17	6	19	3242	6886
FCAW	1.5	230	17	6	19	3242	8707
	2.0	235	17	6	19	3258	10564

b) The buckling constraint of the stiffener is

$$\frac{h_s}{t_s} \leq \frac{1}{\beta_s} = 14 \sqrt{\frac{235}{f_y}}. \quad (4.9)$$

The size ranges for the variables are as follows:

$$t_f = 6 \div 20 \text{ mm}, \quad h_s = 84 \div 280 \text{ mm}, \quad t_s = 6 \div 25 \text{ mm} \quad \text{and} \quad \varphi = 4 \div 15 \text{ mm}.$$

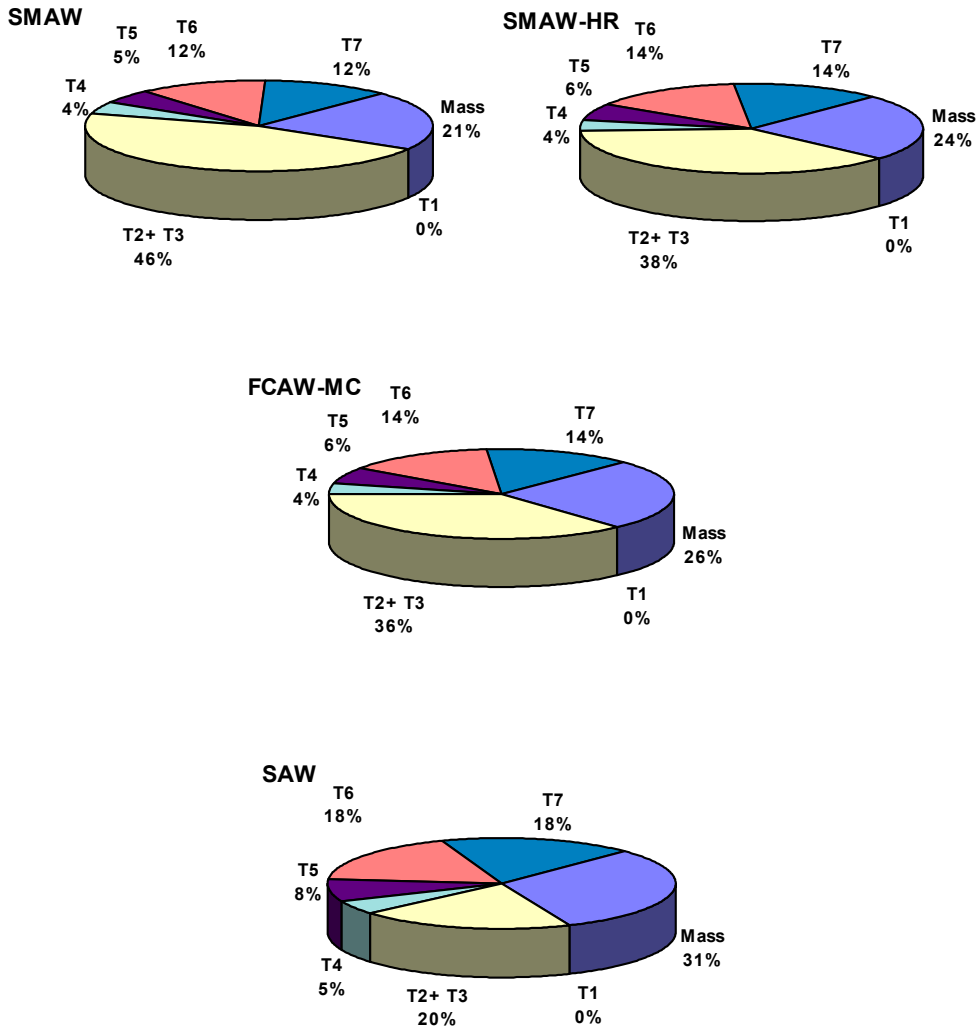


Figure 9. The total cost distribution of the welded stiffened plate with fillet welds using different welding technologies for  $k_f/k_m=2.0$

The elements of cost function for the welded stiffened plate are as follows:

Size of welded joint	$a_w = t_s$	Cross section area	$A = b_0 t_f + \varphi h_s t_s$
Material cost	$\rho V = \rho L A$	Fabrication costs	$k_f/k_m \sum_i T_i$

Further data

Formula for $T_i$	Data for $T_i$
$T_1 = C_1 \delta \sqrt{\kappa \rho V}$	$\rho = 7.85 * 10^{-6}, C_1 = 1, \kappa = \varphi + 1, \Theta_d = 2$
$T_2 + T_3 = 1.3 \sum C_{2i} a_{wi}^2 L_{wi}$	$C_{2i} = 0.7889 * 10^{-3}$ for SMAW and $L_{wi} = 2L\varphi, L$ in mm
$T_4 = \Theta_{de} \left( a_e + b_e t^3 + \frac{1}{a_e t^4} \right) A_p$	$a_e = 9.2 * 10^{-4}, b_e = 4.15 * 10^{-7},$ $t = t_s, \text{ or } t_f, A_p = \varphi h_s L \text{ or } b_0 L$
$T_5 = \Theta_{ds} a_{sp} A_s = 5 * 10^{-7}$	$a_{sp} = 3 * 10^{-6}, A_s = \varphi h_s L + b_0 L$
$T_6 = \Theta_{dp} (a_{gc} + a_{tc}) A_s$	$a_{gc} = 3 * 10^{-6}, a_{tc} = 4.15 * 10^{-6}$ and $A_s = \varphi h_s L + b_0 L$
$T_7 = \sum C_{7i} t_i^n L_{ci}$	$C_7 = 1.1388, t = t_s \text{ or } t_f, n = 0.25,$ $L_{ci} = (h_s + L) \text{ or } (b_0 + L)$

Table 2 shows the optimum discrete sizes of the stiffened plate made with different welding technologies. Figure 9 shows the distribution of the total cost. The diagrams illustrate that this distribution depends on the welding technologies, the type of welding, the ratio of material and fabrication specific costs and the structure type as well.

The welding technologies in Figure 9 are given in decreasing order related to the welding time and cost. The differences between them are great. The welding time and cost are the greatest for SMAW, the quickest and cheapest are SAW, FCAW and ISW. For stiffened plates using SMAW, 46% of the total cost is the welding cost, using SAW, it is only 20%. The fabrication costs of stiffened plates have a larger ratio in total cost, because stiffened plates contain more elements, which need more welding time.

The mass of stiffened plate is  $\rho LA = 3258$  kg (Table 2), the fabrication cost is 100 (15559-3258) / 15559 = 79 % of the total cost. Cost savings can be achieved using a cheaper welding technology, like SAW instead of SMAW or GMAW, if it is possible. Table 3 shows the cost savings for the two different structures and for the five different groups of welding. For stiffened plates the cost savings can be 32 % of the total cost. All compared results are optimized.

Table 3. Cost savings for different welding technologies

Welding technology $k_f/k_m=2.0$	Total cost	Cost savings in %
SMAW	15559	0
SMAW-HR	13305	14
FCAW-MC	12521	20
GMAW-C	11471	27
SAW	10560	32

## 5. Ship deck optimization

**5.1. Structural elements.** Cellular plates consist of two face sheets and a grid of ribs welded between them. The main advantage of such a plate structure is that the

cells have a large torsional stiffness, which allows designers to construct plates of small height. The disadvantage of cellular plates lies in fabrication difficulty, since, when the height is smaller than 800÷1000 mm, it is impossible to weld the ribs to the face sheets from inside.

Some applications of cellular plates are as follows: double bottoms of ships, rudders of ships, floating roofs of cylindrical storage tanks, box gates for dry docks, wings of aircraft structures, bridge decks, floating bridges, offshore platforms, elements of machine tool structures (press tables, mounting desks, base plates), mining shields, floors of buildings, lightweight roofs, etc.

Regarding the fabrication of cellular plates there are several possibilities to join the ribs to the face sheets. The simplest but not the cheapest solution is to use faceplate elements and weld them to ribs from outside by fillet welds. Special welds such as arc-spot welds, slot or plug welds as well as electron-beam or laser welds can be used without cutting larger face sheet parts. A combination of fillet and arc-spot welds is shown in Figure 10.

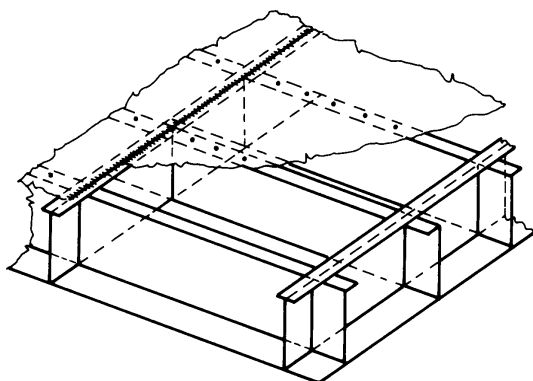


Figure 10. Cellular plate with a combination of fillet and arc spot welds

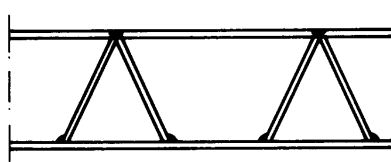


Figure 11. A special cellular plate with longitudinal stiffeners proposed by Suruga and Maeda [15, 1976]

Suruga and Maeda proposed a special cellular plate construction for bridge decks (Figure 11), but this solution is too expensive.

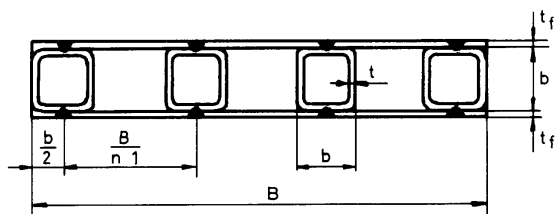


Figure 12. Cross-section of the ship deck panel

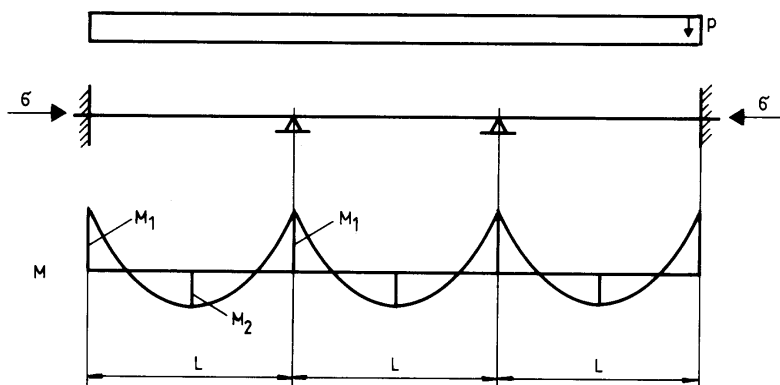


Figure 13. Bending moment diagram of the ship deck panel

An interesting application of cellular plates is the ship deck panels. The main specialties of this application are as follows: 1) only longitudinal ribs of square hollow section (SHS) are used joined to the face sheets by arc-spot welding, thus, in the cost function the fabrication cost of arc-spot welds should be included; 2) to avoid the vibration resonance, the first eigenfrequency of the plate should be larger than a prescribed value.

The aim of the present study is to work out a minimum cost design of such cellular plates considering, in addition to the stress constraint, the eigenfrequency constraint as well, and the fabrication cost of arc-spot welds.

**5.2. The cost function.** The cross-section of the deck panel is shown in Figure 12. The cellular plate consists of two face sheets of thickness  $t_f$  and longitudinal SHS ribs of number  $n$  with dimensions of  $b$  and  $t$ .

In the longitudinal direction the plate ends are clamped and the panel is supported in two points, thus, it can be calculated as a three-span beam (Figure 13) loaded axially with a compression stress  $\sigma = N/A_{eff}$ ,  $A_{eff}$  being the effective cross-section for compression (Figure 15), and transversely by a uniformly distributed normal load of a factored intensity  $p$ .

The cost is calculated according to (3.1). The volume of the structure is

$$V = 3l(nA_{SHS} + 2Bt_f). \quad (5.1)$$

Considering the corner roundings according to a formula given by DAST [16, 1986], the cross-sectional area of a SHS is approximately

$$A_{SHS} = 0.99 * 4(b - t)t \left( 1 - 0.43 \frac{t}{b - 3t} \right). \quad (5.2)$$

The fabrication times are as follows. The time of preparation, assembly and tacking can be expressed as

$$T_1 = C_1 \Theta_d (\kappa \rho V)^{0.5}, \quad (5.3)$$

where  $C_1 = 1.0 \text{ min/kg}^{0.5}$  is the difficulty factor expressing the effect of the type of structure (planar or spatial),  $\kappa$  is the number of assembled structural elements, in our case  $\kappa = n + 2$ .

The time of arc-spot welding is given by

$$T_2 = n_s T_s \quad (5.4)$$

where  $n_s$  is the number of spots,  $T_s$  is the time of welding of one spot weld and of the electrode transfer to the next spot.

The additional time for deslagging, chipping and changing the electrode can be calculated as

$$T_3 = 0.3 T_2. \quad (5.5)$$

Since data for  $T_s$  cannot be found in literature, we take  $T_s = 0.3 \text{ min}$  noting that it depends on the welding equipment and the degree of automation.

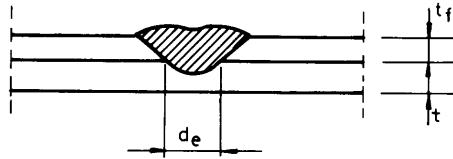


Figure 14. Effective diameter of an arc-spot weld

The number of spots can be calculated by means of the spot pitch  $a$ . The required minimum spot pitch can be determined considering a spot weld as a pin [17, 1978], [18, 1990].

Limiting forces for a pin, according to Eurocode 3 (EC3) [19, 1992] are as follows:

– for bearing

$$F_b = 1.5t_f d_e f_y / \gamma_{Mp} \quad (5.6)$$

with  $d_e = 2t_f$  (Figure 14) and  $\gamma_{Mp} = 1.25$ ;  $F_b = 2.4t_f^2 f_y$

– for shear

$$F_Q 0.6t \frac{\pi d_e^2}{4} \frac{f_u}{\gamma_{Mp}} = 1.508t_f^2 t f_u. \quad (5.7)$$

For steel Fe 360 the ultimate strength is  $f_u = 360$  and the yield stress is  $f_y = 235$  MPa, for steel Fe 510 they are  $f_u = 510$  and  $f_y = 355$  MPa.

The spot weld is loaded by the force FW from the shear acting in a bent beam

$$F_w = \frac{Q S_\xi}{I_\xi} a \quad (5.8)$$

where  $Q$  is the shear force,  $S_\xi$  and  $I_\xi$  are the first moment and moment of inertia of an effective cross-section as shown in Figure 16 and given by (5.21), respectively, while  $a$  is the spot pitch. From the condition one obtains the required maximum spot pitch

$$a_{\max} = \frac{F_b Q I_\xi}{Q S_\xi} \quad \text{but} \quad a_{\max} \leq 50t_f. \quad (5.9)$$

The number of spots in (5.4) can be expressed as

$$n_s = 6nL/a. \quad (5.10)$$

**5.3. Constraint on eigenfrequency.** A serviceability constraint can be defined expressing that the first eigenfrequency of a simply supported bent beam of span length  $L$  should be larger than a prescribed value

$$f_1[\text{Hz}] = \frac{\pi}{2L^2} \left( \frac{10^3 E I_x}{m} \right)^{1/2} \geq f_0, \quad (5.11)$$

where  $E$  is the modulus of elasticity and  $I_x$  is the moment of inertia of the whole cross-section:

$$I_x = nI_{SHS} + Bt_f(b + t_f)^2/2. \quad (5.12)$$

According to DASt (1986) the moment of inertia of a SHS is approximately

$$I_{SHS} = \frac{2}{3}(b - t)^3 t \left( 1 - 0.86 \frac{t}{b - 3t} \right). \quad (5.13)$$

In the formula for the mass  $m$  an additive mass  $m_{add}$  should be involved, thus

$$m = \rho(nA_{SHS} + 2Bt_f) + m_{add}. \quad (5.14)$$

It should be mentioned that  $f_1$  is larger than the value obtained from the formula (5.11) because the beam is clamped and not simply supported. In spite of that, one can use the above approximation since it is obvious from Table 1 that this constraint is not active.

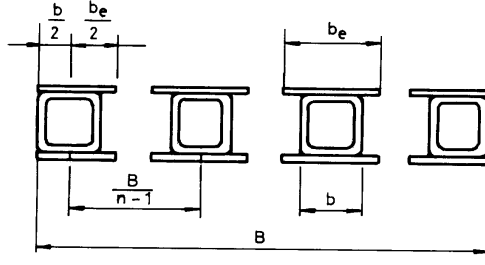


Figure 15. Effective cross-section for compression

**5.4. Constraint on stress due to compression and bending.** According to EC3, the stress constraint should be defined for a section of class 4 as follows:

$$\frac{N}{\chi A_{eff} f_{y1}} + \frac{k_x \psi M_1}{W_\xi f_{y1}} \leq 1 \quad (5.15)$$

where  $\chi$  is the overall buckling factor and

$$\chi = \frac{1}{\Phi + (\Phi^2 - \bar{\lambda}^2)^{1/2}}, \quad \Phi = 0.5 \left[ 1 + 0.34(\bar{\lambda} - 0.2) + \bar{\lambda}^2 \right], \quad \bar{\lambda} = \frac{KL}{\lambda_1 r} \beta_A^{1/2}. \quad (5.16)$$

Here  $K$  depends on the supports – for a beam with clamped ends  $K = 0.5$  – and

$$\lambda_1 = \pi(E/f_y)^{1/2} \beta_A^{1/2}, \quad r = (I_{eff}/A_{eff})^{1/2}, \quad \beta_A = \frac{A_{eff}}{nA_{SHS} + 2Bt_f}. \quad (5.17)$$

To obtain the effective cross-section, the effective width of face sheets should be calculated according to EC3

$$b_e = \rho_P \frac{B}{n-1}, \quad \bar{\lambda}_P = \frac{B/[(n-1)t_f]}{28.4\varepsilon k_\sigma^{1/2}}, \quad \varepsilon = \sqrt{\frac{235}{f_y}} \quad (5.18)$$

with

$$k_\sigma = 4, \quad \bar{\lambda}_P = \frac{B}{56.8\varepsilon(n-1)t_f} \quad (5.19)$$

where

$$\rho_P = \begin{cases} 1 & \text{if } \bar{\lambda}_P \leq 0.673 \\ \frac{1}{\bar{\lambda}_P} - \frac{0.22}{\bar{\lambda}_P^2} & \text{if } \bar{\lambda}_P \geq 0.673 \end{cases}. \quad (5.20)$$

Considering the effective cross-section shown in Figure 15 we get

$$A_{eff} = nA_{SHS} + 2B_e t_f, \quad B_e = b + (n-1)b_e, \quad I_{eff} = nI_{SHS} + B_e t_f (b + t_f)^2 / 2. \quad (5.21)$$

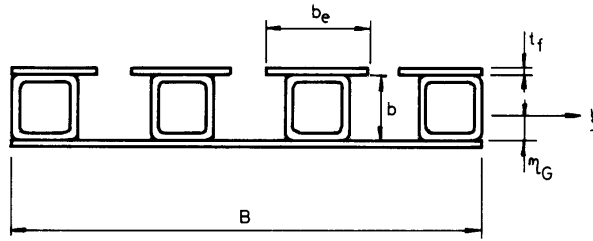


Figure 16. Effective cross-section for bending

According to the moment diagram shown in Figure 13

$$M_1 = BpL^2/12. \quad (5.22)$$

This bending moment should be multiplied by a dynamic factor

$$k_x = 1 - \frac{\mu_x N}{\chi(nA_{SHS} + 2Bt_f)f_y}, \quad \text{but} \quad k_x \leq 1.5 \quad (5.23)$$

$$\mu_x = \bar{\lambda}(2\beta_M - 4), \quad \text{but} \quad \mu_x \leq 0.9. \quad (5.24)$$

For our case  $\beta_M = 1.3$  and  $\mu_x = -1.4 \bar{\lambda}$ , thus

$$k_x = 1 + \frac{1.4\bar{\lambda}\beta_A N}{\chi A_{eff} f_y}. \quad (5.25)$$

For bending another asymmetric effective cross-section should be taken into account as shown in Figure 16. The distance of gravity centre  $G$  is

$$\eta_G = \frac{nA_{SHS}(b + t_f)/2 + B_e t_f (b + t_f)}{nA_{SHS} + (B + B_e)t_f}. \quad (5.26)$$

The moment of inertia is given by

$$I_\xi = nI_{SHS} + nA_{SHS} \left( \frac{b + t_f}{2} - \eta_G \right)^2 + Bt_f \eta_G + Bt_f (b + t_f - \eta_G)^2. \quad (5.27)$$

The first moment of the cross sectional area for the calculation of (5.18) and (5.26) and the corresponding section modulus are

$$S_\xi = b_e (b + t_f - \eta_G) \quad \text{and} \quad W_\xi = \frac{I_\xi}{b + t_f - \eta_G}, \quad (5.28)$$

respectively.

**5.5. The optimization procedure.** In the minimum cost design the optimum values of  $b, t, t_f$  and  $n$  are sought, which minimize the cost function (3.1) and fulfil the design constraints (5.11) and (5.15). In the first phase the above mentioned variables are treated as continuous ones and the optima are determined using the Rosenbrock's

hillclimb mathematical programming method. In the second phase the discrete values of variables are calculated using a complementary search method. In this search the minimum values are taken as

$$b_{min} = 30, t_{min} = 2, t_{fmin} = 2 \text{ mm and } n_{min} = 4.$$

The discrete values of SHS are sought according to the pre-standard prEN 10219-2 [20, 1992].

The numerical data are as follows:  $f_0 = 18 \text{ Hz}$ ,  $E = 2.1 * 10^5 \text{ MPa}$ ,  $B = 2000$ ,  $L = 2250 \text{ mm}$ ,  $\rho = 7850 \text{ kg/m}^3 = 7.85 * 10^{-6} \text{ kg/mm}^3$ ,  $m_{add} = 2 * 50 = 100 \text{ kg/m}$  =  $0.1 \text{ kg/mm}$ ,  $p = 3.5 \text{ kN/m}^2 = 3.5 * 10^{-3} \text{ N/mm}^2$ ,  $\psi = 1.4$ ,  $\sigma = N/A_{eff} = 150 \text{ MPa}$ .

The computational results are summarized in Table 4.

Table 4. Optimization results: optimum dimensions in mm, number of ribs  $n$ , fulfilling the design constraints (5.11) and (5.15), as well as  $K/k_m$  - values in kg for cost in function of the ratio  $k_f/k_m$

$f_y$ [MPa]	$b$	$t$	$t_f$	$n$	(5.11)	(5.15)	$K/k_m$		
							$\frac{k_f}{k_m} = 0$	$\frac{k_f}{k_m} = 1$	$\frac{k_f}{k_m} = 2$
235	60	2	2	4	31.5 > 18Hz	0.99 < 1	520	898	1276
355	40	2	2	4	21.1 > 18Hz	0.89 < 1	486	859	1231

As can be seen from Table 1, the number of ribs and the thickness of face sheets should be minimum to achieve minimum cost. For larger yield stress the dimension of SHS can be decreased, thus the cost is also smaller. It can also be seen that the eigenfrequency constraint (5.11) is passive and the stress constraint (5.15) is active.

The optimum dimensions do not depend on the fabrication cost or on the ratio of  $k_f/k_m$ . In fabrication cost only the distance of spots depends on the structural dimensions (see 5.9), but, in all cases, the limit  $a_{max} = 50t_f$  is governing, constraint (5.9) gives much larger values for  $a$ . Since  $t_f = t_{fmin} = 2 \text{ mm}$  for all cases the fabrication cost remains the same. The fabrication cost is quite high for  $f_y = 235 \text{ MPa}$ , in the case of  $k_f/k_m = 1$  it is  $100(898-520)/898 = 42\%$  and for  $k_f/k_m = 2$  it is  $100(1276-520)/1276 = 59\%$  of the whole cost.

## 6. Conclusions

We have shown that stiffened plates play an important role in structural design. The analysis of these structures can be made for static loading and can be built into the optimization software. Cost calculation of these structures is important due to the high volume of welding. Two examples show how we can perform cost minimization using different material and fabrication cost factors. The optima of stiffened plates with compression load show that for material cost the number of stiffeners is high (13 stiffeners), for high fabrication cost the number is low (6 stiffeners). For different welding technologies, optima are different. For SMAW the cost of welding is close to

half of the total cost, for SAW the welding cost is only 20% of the total cost. For the second example where the stiffeners are square hollow sections, not only the stress and stability constraints (taking into account the effective width due to bending and compression), but the eigenfrequency constraints are also considered. In most cases the optima are determined by the thickness lower limits and the stability constraint. The fabrication cost can be more than half the total cost at the optimum.

**Acknowledgement.** The research work was supported by the Hungarian National Research Foundation (project No.: OTKA 22846 and 29326) and the Fund for Higher Education grant 8/2000.

## REFERENCES

1. FARKAS, J. and JÁRMAI, K.: *Minimum cost design of laterally loaded welded rectangular cellular plates*, Journal of Structural Optimization, Springer Verlag, **8**(4), (1994), 262-267.
2. FARKAS, J.: *Design of Welded Structures*, Mérnöki Továbbképző Intézet, Tankönyvkiadó, Budapest, p. 156, 1972. (in Hungarian)
3. LIKHTARNIKOV, Y.M.: *Metal Structures*, Stroyizdat, Moscow, 1968. (in Russian)
4. WILLIAMS, D.G.: *Analysis of double plated grillage under in-plane and normal loading*, Ph.D. thesis, University of London, Imperial College, 1969.
5. MASSONNET, CH.: *Plaques et coques cylindriques orthotropes á nervures dissymetriques*, Mémoires Assoc. Intern. Ponts at Charpentes 19, Zürich, Leeman, 201-230, 1959.
6. GIENKE, E.: *Die Berechnung von Hohlrippen-Platten*, Stahlbau, **29**, (1955), 1-11, 47-59.
7. FARKAS, J. and JÁRMAI, K.: *Analysis and Optimum Design of Metal Structures*, Balkema Publishers, Rotterdam, Brookfield, 1997.
8. JÁRMAI, K. and FARKAS, J.: *Cost calculation and optimization of welded steel structures*, Journal of Constructional Steel Research, Elsevier, **50**( 2), (1999), 115-135.
9. PAHL, G., BEELICH, K.H.: *Kostenwachstumsgesetze nach Ähnlichkeitsbeziehungen für Schweissverbindungen*, VDI-Bericht, Nr. 457, 129-141, Düsseldorf, 1992.
10. OTT, H.H. and HUBKA, V.: *Vorausberechnung der Herstellkosten von Schweisskonstruktionen (Fabrication cost calculation of welded structures)*. Proc. Int. Conference on Engineering Design ICED, Hamburg, 478-487. Heurista, Zürich, 1985.
11. COSTCOMP: *Programm zur Berechnung der Schweisskosten*,. Deutscher Verlag für Schweisstechnik, Düsseldorf., 1990.
12. BODT, H.J.M.: *The Global Approach to Welding Costs*, The Netherlands Institute of Welding, The Hague, 1990.
13. American Petroleum Institute, *API Bulletin on design of flat plate structures*, Bul. 2V, 1st edn., 1987.
14. JÁRMAI, K.: *Single- and multicriteria optimization as a tool of decision support system*, Computers in Industry, **11**(3), (1989), 249-266.
15. SURUGA, T. and MAEDA, Y.: *Selection of hollow steel plate deck*, 10th IABSE Congress, Tokyo, 1976, Final Report, 19-22.
16. DAST (Deutscher Ausschuss für Stahlbau), Richtlinie 016., *Bemessung und konstruktive Gestaltung von Tragwerken aus dünnwandigen kaltgeformten Bauteilen*, Köln, 1986.

- 
17. BLODGETT, O.W.: *Report on proposed standards for sheet steel structural welding*, Welding Journal, **57**, April, (1978), 15-24.
  18. FÜCHSEL, S., MÖBIUS, W. and STEINERT, G.: *Empfehlung zur Berechnung von MAG-Punktschweiss-verbindungen*, ZIS-Report, Halle, 1, (1990), 31-36.
  19. Eurocode 3: *Design of steel structures*, Part 1.1, CEN. European Committee for Standardization, Brussels, 1992.
  20. prEN 10219-2: *Cold formed structural hollow sections of non-alloy and fine grain structural steels, Part 2., Tolerances, dimensions and sectional properties*, European Committee for Standardization, Brussels, 1992. (German version DIN EN 10219 Teil 2. Entwurf. 1993.)



# PRINCIPLE OF COMPLEMENTARY VIRTUAL WORK AND THE RIEMANN-CHRISTOFFEL CURVATURE TENSOR AS COMPATIBILITY CONDITION

IMRE KOZÁK

Department of Mechanics, University of Miskolc  
3515 Miskolc – Egyetemváros, Hungary  
mechkoz@gold.uni-miskolc.hu

[Received: June 21, 1999]

**Abstract.** Due to the deformation of a solid body its metric tensor changes. In this paper the Riemann-Christoffel curvature tensor, considered as the compatibility field equation of the nonlinear theory of deformation and written in terms of the metric tensor of the deformed body, is derived from the principle of complementary virtual work.

*Keywords:* Riemann-Christoffel curvature tensor, principle of complementary virtual work

## 1. Introduction

The deformation tensors of a solid body are uniquely defined by its displacement field. Otherwise, when the deformation tensors are known, a single-valued continuous displacement field (without rigid body motions) can be derived only in the case when the deformation tensors satisfy the compatibility conditions. Compatibility conditions consist of compatibility field equations and compatibility boundary conditions. In this paper the compatibility field equations are investigated only.

In the infinitesimal theory of deformation, the compatibility field equation is equivalent to the vanishing of the Saint-Venant compatibility tensor. In the nonlinear deformation theory, the compatibility condition is usually expressed by the requirement that the metric tensor of the deformed body be the metric tensor of a Euclidean space (note that the metric tensor of the deformed body is the Green deformation tensor in the reference configuration and the Cauchy deformation tensor in the current configuration). This means that vanishing of the Riemann-Christoffel curvature tensor written in terms of the metric tensor of the deformed body is equivalent to the compatibility field equation.

Both the tensorial Saint-Venant equation and the zero-valued Riemann-Christoffel curvature tensor have six scalar equations. These six equations are not independent of each other. The problem of necessary and sufficient compatibility conditions arises from this fact. A partial solution for this problem was given by Washizu [1]. In the framework of the classical elasticity theory, the necessary and sufficient compatibility conditions were given by Grycz [2], the compatibility field equations and compatibility boundary conditions were derived from the principle of virtual work by the author, see Kozák [3,4].

The papers [5,6] by Bertóti established compatibility field equations and boundary conditions of the first kind in the linear theory of elasticity. For micropolar case and within the framework of the linear theory Kozák-Szeidl [7] determined the necessary and sufficient conditions the strains should meet to be compatible.

This paper derives the Riemann-Christoffel curvature tensor as the compatibility field equation of the nonlinear theory of deformation using the principle of complementary virtual work. The necessary and sufficient conditions of compatibility in the nonlinear theory of deformation are not investigated here. In this respect we refer to an earlier work of the author Kozák [8].

In the following we assume that the volume of the body is simple-connected and bounded by a closed smooth single surface. Both the invariant (symbolic) and indicial (tensorial) notation of tensor calculus will be used. When indicial notation is used, the covariant derivative of a tensor as well as the partial derivative of a two-point tensor will be denoted by a semicolon followed by an index in the subscript, whereas the total covariant derivative of a two-point tensor will be denoted by a colon followed by an index in the subscript.

## 2. Coordinate systems. Deformation gradients

**2.1.** Let the spatial point, the position vector, the spatial coordinates and the base vectors be denoted as follows:

- in the reference coordinate system (in the reference configuration of the body):

$$P^\circ, \mathbf{r}^\circ, x^{\circ k}, \mathbf{g}_{k^\circ}, \mathbf{g}^{l^\circ}, \quad \mathbf{g}_{k^\circ} = \frac{\partial \mathbf{r}^\circ}{\partial x^{\circ k}}$$

- in the spatial coordinate system (in the current configuration of the body):

$$P, \mathbf{r}, x^p, \mathbf{g}_p, \mathbf{g}^q, \quad \mathbf{g}_p = \frac{\partial \mathbf{r}}{\partial x^p}.$$

In the course of deformation the arbitrary point  $\hat{P}$  of the body, moves from the space point  $P^\circ(x^{\circ 1}, x^{\circ 2}, x^{\circ 3})$  to the space point  $P(x^1, x^2, x^3)$ . The trajectory of the point  $\hat{P}$  is determined by the motion:

$$x^p = x^p(x^{\circ 1}, x^{\circ 2}, x^{\circ 3}; t), \quad J = \det \left| \frac{\partial x^p}{\partial x^{\circ k}} \right| > 0. \quad (2.1)$$

The inverse motion is given by

$$x^{\circ k} = x^{\circ k}(x^1, x^2, x^3; t). \quad (2.2)$$

Using material coordinate system, let the point, the coordinates and the base vectors be denoted as follows

- in the reference configuration of the body:

$$\hat{P}, X^{\circ K} = X^K, \mathbf{G}_{K^\circ}, \mathbf{G}^{L^\circ}, \quad \mathbf{G}_{K^\circ} = \frac{\partial \mathbf{r}^\circ}{\partial X^{\circ K}} = \frac{\partial x^{\circ l}}{\partial X^{\circ K}} \mathbf{g}_{l^\circ}$$

– in the current configuration of the body:

$$\hat{P}, X^P = X^{\circ P}, \mathbf{G}_P, \mathbf{G}^Q, \quad \mathbf{G}_P = \frac{\partial \mathbf{r}}{\partial X^P} = \frac{\partial x^q}{\partial X^P} \mathbf{g}_q.$$

**2.2.** At arbitrary time  $t$  the direct and inverse mappings are given by

$$d\mathbf{r} = \mathbf{F} \cdot d\mathbf{r}^\circ, \quad d\mathbf{r}^\circ = \mathbf{F}^{-1} \cdot d\mathbf{r} \tag{2.3}$$

respectively, where  $\mathbf{F}$  is the deformation gradient:

$$\mathbf{F} = F^p_{l^\circ} \mathbf{g}_p \mathbf{g}^{l^\circ} = \frac{\partial x^p}{\partial x^{l^\circ}} \mathbf{g}_p \mathbf{g}^{l^\circ} = \mathbf{G}_Q \mathbf{G}^{Q^\circ} \tag{2.4}$$

and  $\mathbf{F}^{-1}$  is the inverse deformation gradient:

$$\mathbf{F}^{-1} = (F^{-1})^{k^\circ}_q \mathbf{g}_{k^\circ} \mathbf{g}^q = \frac{\partial x^{k^\circ}}{\partial x^q} \mathbf{g}_{k^\circ} \mathbf{g}^q = \mathbf{G}_{Q^\circ} \mathbf{G}^{Q^\circ}. \tag{2.5}$$

$\mathbf{F}$  and  $\mathbf{F}^{-1}$  are two-point-tensors.

In the reference configuration they can be written as

$$F_{k^\circ l^\circ} = g_{k^\circ l^\circ} + u_{k^\circ;l^\circ} = g_{k^\circ p} F^p_{l^\circ} = g_{k^\circ p} \left( \delta_{l^\circ}^p + u^p_{;l^\circ} \right) \tag{2.6}$$

and in the current configuration as

$$(F^{-1})_{pq} = g_{pq} - u_{p;q} = g_{pk^\circ} (F^{-1})^{k^\circ}_q = g_{pk^\circ} \left( \delta_q^{k^\circ} - u^{k^\circ}_{;q} \right) \tag{2.7}$$

where  $g_{k^\circ p} = g_{pk^\circ}$  is a shifter,  $\mathbf{u}^\circ = u_{k^\circ} \mathbf{g}^{k^\circ} = u_p \mathbf{g}^p = \mathbf{u}$  is the displacement vector.

### 3. The principle of complementary virtual work

**3.1.** We assume that on the surface part  $(A_t)$  loads, on the surface part  $(A_u)$  displacements are prescribed and  $(A_t) = (A_t) \cup (A_u)$  is the whole surface of the body. In addition we assume that the variation of the Cauchy stress tensor satisfies the following conditions:

$$\delta S^{pq}_{;q} = 0 \quad \text{and} \quad \delta S^{pq} = \delta S^{qp}, \quad x \in (B) \tag{3.1}$$

$$\delta S^{pq} n_q dA = 0 \quad x \in (A_t) \tag{3.2}$$

where  $n_q$  is the normal unit vector to  $(A_t)$ .

The principle of complementary virtual work states that when equation

$$\int_{(B)} \left[ g_{pq} - (F^{-1})_{pq} \right] \delta S^{pq} dV = \int_{(A_u)} \tilde{u}_p \delta S^{pq} n_q dA \tag{3.3}$$

holds for any  $\delta S^{pq}$  satisfying (3.1) and (3.2) in the current configuration  $(B)$  of the body, where  $\tilde{u}_p$  is the prescribed displacement field, then the inverse deformation gradient and the gradient of the displacement vector

$$(F^{-1})^{k^\circ} = g^{k^\circ p} (F^{-1})_{pq} \quad \text{and} \quad u^{k^\circ}_{;q} = g^{k^\circ p} u_{p;q} \quad (3.4)$$

are kinematically admissible.

**3.2.** Any tensor  $\delta S^{pq}$  satisfying (3.1) can be derived from a second-order, symmetric, otherwise arbitrary stress function tensor  $\delta H_{rs}$ :

$$\delta S^{pq} = \varepsilon^{pr m} \varepsilon^{qsn} \delta H_{rs;mn} \quad (3.5)$$

Inserting (3.5) in (3.5) we obtain:

$$\int_{(B)} \varepsilon^{pr m} \varepsilon^{qsn} \left[ g_{pq} - (F^{-1})_{pq} \right] \delta H_{rs;mn} dV = \int_{(A_u)} \tilde{u}_p \varepsilon^{pr m} \varepsilon^{qsn} \delta H_{rs;mn} n_q dA \quad (3.6)$$

Applying the Gauss-theorem twice on the volume integral, another form of the principle of complementary virtual work is obtained:

$$\begin{aligned} \int_{(B)} \varepsilon^{pr m} \varepsilon^{qsn} (F^{-1})_{pq;mn} \delta H_{rs} dV &= \int_{(A)} n_n \varepsilon^{pr m} \varepsilon^{qsn} \left[ g_{pq} - (F^{-1})_{pq} \right] \delta H_{rs;m} dA + \\ &+ \int_{(A)} n_m \varepsilon^{pr m} \varepsilon^{qsn} (F^{-1})_{pq;n} \delta H_{rs} dA - \int_{(A_u)} \tilde{u}_p n_q \varepsilon^{pr m} \varepsilon^{qsn} \delta H_{rs;mn} n_q dA . \end{aligned} \quad (3.7)$$

Taking into account that  $\delta H_{rs}$  is arbitrary in the volume of the current configuration of the body, from (3.7) we get the compatibility field equation for the inverse deformation gradient  $F^{-1}$ :

$$\varepsilon^{pr m} \varepsilon^{qsn} (F^{-1})_{pq;mn} = 0, \quad x \in (B) . \quad (3.8)$$

As mentioned in the introduction, this paper does not investigate the necessary and sufficient compatibility conditions of the nonlinear theory of deformation, therefore equation (3.7) is used for the derivation of the compatibility field equation (3.8) only.

#### 4. The compatibility field equation and the curvature tensor

**4.1.** In the following our investigations will be carried out in a material coordinate system, proposed by Lurie [9]. In this case the inverse deformation gradient can be written as

$$F^{-1} = (F^{-1})^{K^\circ}_Q \mathbf{G}_{K^\circ} \mathbf{G}^Q = \mathbf{G}_{Q^\circ} \mathbf{G}^Q \quad (4.1)$$

i.e.,

$$\left[ (F^{-1})^{K^\circ}_Q \right] = \left[ \frac{\partial X^{K^\circ}}{\partial X^Q} \right] = \left[ \delta^{K^\circ}_Q \right] = \begin{bmatrix} 1 & 0 & 0 \\ 0 & 1 & 0 \\ 0 & 0 & 1 \end{bmatrix} \quad (4.2)$$

and

$$(F^{-1})_{PQ} = G_{PK^\circ} (F^{-1})_Q^{K^\circ}, \quad (4.3)$$

where  $G_{PK^\circ}$  is a shifter.

The form of the compatibility field equation (3.8) in the material coordinate system is

$$\varepsilon^{PRM} \varepsilon^{QSN} (F^{-1})_{PQ;MN} = 0, \quad x \in (B). \quad (4.4)$$

To carry out the covariant differentiations in (4.4), the rule for the total covariant differentiation of two-point tensors will be used, taking into account that the total covariant derivative of a shifter is zero. First we obtain:

$$(F^{-1})_{PQ;M} = \left[ G_{PK^\circ} (F^{-1})_Q^{K^\circ} \right]_{;M} = G_{PK^\circ} (F^{-1})_{Q;M}^{K^\circ} \quad (4.5)$$

where

$$\begin{aligned} (F^{-1})_{Q;M}^{K^\circ} &= (F^{-1})_{Q;A^\circ}^{K^\circ} (F^{-1})_M^{A^\circ} + (F^{-1})_{Q;M}^{K^\circ} = \\ &= \Gamma_{B^\circ A^\circ}^{K^\circ} (F^{-1})_Q^{B^\circ} (F^{-1})_M^{A^\circ} - \Gamma_{QM}^U (F^{-1})_U^{K^\circ}. \end{aligned} \quad (4.6)$$

In (4.6)  $\Gamma_{B^\circ A^\circ}^{K^\circ}$  and  $\Gamma_{QM}^U$  are Christoffel symbols of the second kind.

Following from (4.5) and (4.6) we can write:

$$(F^{-1})_{PQ;MN} = G_{PK^\circ} (F^{-1})_{Q;MN}^{K^\circ}, \quad (4.7)$$

where

$$(F^{-1})_{Q;MN}^{K^\circ} = \left[ (F^{-1})_{Q;M}^{K^\circ} \right]_{;C^\circ} (F^{-1})_N^{C^\circ} + \left[ (F^{-1})_{Q;M}^{K^\circ} \right]_{;N} \quad (4.8)$$

$$\left[ (F^{-1})_{Q;M}^{K^\circ} \right]_{;C^\circ} = \frac{\partial \Gamma_{B^\circ A^\circ}^{K^\circ}}{\partial X^{C^\circ}} (F^{-1})_Q^{B^\circ} (F^{-1})_M^{A^\circ} + \Gamma_{C^\circ D^\circ}^{K^\circ} (F^{-1})_{Q;M}^{D^\circ} \quad (4.9)$$

and

$$\left[ (F^{-1})_{Q;M}^{K^\circ} \right]_{;N} = \frac{\partial \Gamma_{QM}^U}{\partial X^N} (F^{-1})_U^{K^\circ} - \Gamma_{QN}^V (F^{-1})_{V;M}^{K^\circ} - \Gamma_{MN}^W (F^{-1})_{Q;W}^{D^\circ} \quad (4.10)$$

Now we make the following transformations: first we insert (4.6) in (4.9) and (4.10), then (4.9) and (4.10) in (4.8). After some algebra, we obtain the compatibility field equation (4.4) in the current configuration in terms of material coordinates (with changed dummy indices):

$$\begin{aligned} &\varepsilon^{IMP} \varepsilon^{JNQ} (F^{-1})_{PQ;MN} = \\ &= \varepsilon^{IMP} \varepsilon^{JNQ} G_{PK^\circ} \left[ \left( \frac{\partial \Gamma_{B^\circ A^\circ}^{K^\circ}}{\partial X^{C^\circ}} + \Gamma_{C^\circ D^\circ}^{K^\circ} \Gamma_{A^\circ B^\circ}^{D^\circ} \right) (F^{-1})_M^{A^\circ} (F^{-1})_Q^{B^\circ} (F^{-1})_N^{C^\circ} \right] - \\ &\quad - \varepsilon^{IMP} \varepsilon^{JNQ} G_{PK^\circ} \left[ \left( \frac{\partial \Gamma_{QM}^U}{\partial X^N} + \Gamma_{NW}^U \Gamma_{MQ}^W \right) (F^{-1})_U^{K^\circ} \right] \end{aligned} \quad (4.11)$$

Making use of the components of the inverse deformation gradient given in (4.2), (4.11) can be written in the following form:

$$\begin{aligned} \varepsilon^{IMP} \varepsilon^{JNQ} (F^{-1})_{PQ:MN} &= \varepsilon^{IA^\circ P^\circ} \varepsilon^{JC^\circ B^\circ} G_{P^\circ K^\circ} \left( \frac{\partial \Gamma_{B^\circ A^\circ}^{K^\circ}}{\partial X^{\circ C}} + \Gamma_{C^\circ D^\circ}^{K^\circ} \Gamma_{A^\circ B^\circ}^{D^\circ} \right) - \\ &\quad - \varepsilon^{IMP} \varepsilon^{JNQ} G_{PU^\circ} \left( \frac{\partial \Gamma_{QM}^U}{\partial X^N} + \Gamma_{NW}^U \Gamma_{MQ}^W \right). \end{aligned} \quad (4.12)$$

**4.2.** The Riemann-theory states that in order to tensor  $G_{PK}$  of the material coordinate system be the metric tensor of a Euclidean space in the current configuration, it is necessary and sufficient that  $G_{PK}$  be positive definite and satisfy the following equation:

$$R_{NQM}{}^A = -\frac{\partial \Gamma_{MQ}^A}{\partial X^N} + \frac{\partial \Gamma_{MN}^A}{\partial X^Q} - \Gamma_{NB}^A \Gamma_{MQ}^B + \Gamma_{QB}^A \Gamma_{MN}^B = 0, \quad (4.13)$$

where  $R_{NQM}{}^A$  is the Riemann-Christoffel curvature tensor. If tensor  $G_{PQ}$  is defined as a metric tensor, just like in our case (see equation (4.21)), positive definiteness of  $G_{PK}$  is a priori satisfied and the only condition left to be investigated is the zero-valuedness of the Riemann-Christoffel curvature tensor (4.13).

Instead of the Riemann-Christoffel curvature tensor, the so-called Ricci tensor can also be used. Definition of the Ricci tensor is given by

$$\begin{aligned} A^{IJ} &= \frac{1}{4} \varepsilon^{IMP} \varepsilon^{JNQ} R_{NQMP} = \frac{1}{4} \varepsilon^{IMP} \varepsilon^{JNQ} G_{PA} R_{NQM}{}^A = \\ &= \frac{1}{4} \varepsilon^{IMP} \varepsilon^{JNQ} G_{PA} \left( -\frac{\partial \Gamma_{MQ}^A}{\partial X^N} - \Gamma_{NB}^A \Gamma_{MQ}^B \right) = 0. \end{aligned} \quad (4.14)$$

Both the Riemann-Christoffel curvature tensor and the Ricci tensor have six independent non-zero components:

$$\begin{aligned} A^{11} &= \frac{1}{G} R_{2323}, & A^{22} &= \frac{1}{G} R_{3131}, & A^{33} &= \frac{1}{G} R_{1212}, \\ A^{12} &= \frac{1}{G} R_{2131}, & A^{23} &= \frac{1}{G} R_{3112}, & A^{31} &= \frac{1}{G} R_{1223}, \\ & & G &= \det |G_{PA}|. \end{aligned} \quad (4.15)$$

According to (4.15), zero-valuedness of the Riemann-Christoffel curvature tensor is equivalent with the zero-valuedness of the Ricci tensor.

In the material coordinate system and reference configuration the Ricci tensor reads:

$$\begin{aligned} A^{\circ I^\circ J^\circ} &= \frac{1}{4} \varepsilon^{I^\circ A^\circ P^\circ} \varepsilon^{J^\circ C^\circ B^\circ} R_{C^\circ B^\circ A^\circ P^\circ} = \frac{1}{4} \varepsilon^{I^\circ A^\circ P^\circ} \varepsilon^{J^\circ C^\circ B^\circ} G_{P^\circ K^\circ} R_{C^\circ B^\circ A^\circ}{}^{K^\circ} = \\ &= \frac{1}{4} \varepsilon^{I^\circ A^\circ P^\circ} \varepsilon^{J^\circ C^\circ B^\circ} G_{P^\circ K^\circ} \left( -\frac{\partial \Gamma_{B^\circ A^\circ}^{K^\circ}}{\partial X^{\circ C}} - \Gamma_{C^\circ D^\circ}^{K^\circ} \Gamma_{A^\circ B^\circ}^{D^\circ} \right) = 0. \end{aligned} \quad (4.17)$$

If the space of the reference configuration is Euclidean, then  $R_{C^\circ B^\circ A^\circ}^{K^\circ} = 0$  and  $A^{\circ I^\circ J^\circ} = 0$ , and similarly, if the space of the current configuration is Euclidean then  $R_{NQM}^A = 0$  and  $A^{IJ} = 0$ .

**4.3.** Comparing the compatibility field equation (4.12) obtained from the principle of complementary virtual work and equation (4.14) for the Ricci tensor in the current configuration as well as equation (4.17) for the Ricci tensor in the reference configuration we obtain:

$$\varepsilon^{IMP} \varepsilon^{JNQ} (F^{-1})_{PQ:MN} = -2G_{I^\circ}^I G_{J^\circ}^J A^{\circ I^\circ J^\circ} + 2A^{IJ} = 0. \quad (4.18)$$

**4.4.** Then, assuming that in the case of the direct mapping the reference configuration is Euclidean, i.e.,  $A^{\circ I^\circ J^\circ} = 0$ , it follows from (4.18) and (4.14) that

$$\varepsilon^{IMP} \varepsilon^{JNQ} (F^{-1})_{PQ:MN} = 2A^{IJ} = \frac{1}{4} \varepsilon^{IMP} \varepsilon^{JNQ} G_{PA} R_{NQM}^A = 0, \quad (4.19)$$

$$\varepsilon^{IMP} \varepsilon^{JNQ} G_{PA} \left( \frac{\partial \Gamma_{MQ}^A}{\partial X^N} + \Gamma_{NB}^A \Gamma_{MQ}^B \right) = 0. \quad (4.20)$$

In other words, the compatibility field equation (4.18) is equivalent to the zero-valuedness of the Ricci, as well as - according to (4.15) - the Riemann-Christoffel curvature tensor in the current configuration, provided they are expressed in terms of the changed metric tensor  $G_{PA}$ . Tensor  $G_{PA}$  is nothing but the Cauchy deformation tensor:

$$G_{PA} = G_{P^\circ A^\circ} + 2E_{PA} \quad (4.21)$$

where  $E_{PA}$  is the Euler-Almansi strain tensor. For equation (4.20) we have to take into consideration that

$$\begin{aligned} \Gamma_{MQ}^A &= G^{AS} \Gamma_{MQ,S} = \frac{1}{2} G^{AS} \left[ \frac{\partial}{\partial X^M} G_{QS} + \frac{\partial}{\partial X^Q} G_{MS} - \frac{\partial}{\partial X^S} G_{MQ} \right] = \\ &= G^{AS} \left[ \Gamma_{M^\circ Q^\circ, S^\circ} + \left( \frac{\partial}{\partial X^M} E_{QS} + \frac{\partial}{\partial X^Q} E_{MS} - \frac{\partial}{\partial X^S} E_{MQ} \right) \right] \end{aligned} \quad (4.22)$$

where  $\Gamma_{MQ,S}$  and  $\Gamma_{M^\circ Q^\circ, S^\circ}$  are Christoffel symbols of the first kind.

**4.5.** When, in contrary to the above, the inverse mapping is considered and we assume that the space of the current configuration is Euclidean, i.e.,  $A^{IJ} = 0$  from (4.18) and (4.17) we have

$$\begin{aligned} \varepsilon^{IMP} \varepsilon^{JNQ} (F^{-1})_{PQ:MN} &= -2G_{I^\circ}^I G_{J^\circ}^J A^{\circ I^\circ J^\circ} = \\ &= -\frac{1}{2} G_{I^\circ}^I G_{J^\circ}^J \varepsilon^{I^\circ A^\circ P^\circ} \varepsilon^{J^\circ C^\circ B^\circ} G_{P^\circ K^\circ} R_{C^\circ B^\circ A^\circ}^{K^\circ} = 0 \end{aligned} \quad (4.23)$$

and

$$\varepsilon^{I^\circ A^\circ P^\circ} \varepsilon^{J^\circ C^\circ B^\circ} G_{P^\circ K^\circ} \left( -\frac{\partial \Gamma_{B^\circ A^\circ}^{K^\circ}}{\partial X^{\circ C}} - \Gamma_{C^\circ D^\circ}^{K^\circ} \Gamma_{A^\circ B^\circ}^{D^\circ} \right) = 0. \quad (4.24)$$

Thus, in this case the compatibility field equation (4.18) is equivalent to the zero-valuedness of the Ricci, as well as - according to (4.15) - the Riemann-Christoffel curvature tensor in the reference configuration, provided they are expressed in terms of the changed metric tensor  $G_{P^\circ K^\circ}$ . Tensor  $G_{P^\circ K^\circ}$  is nothing but the Green deformation tensor:

$$G_{P^\circ K^\circ} = G_{PK} - 2E_{P^\circ K^\circ}^\circ \quad (4.25)$$

where  $E_{P^\circ K^\circ}^\circ$  is the Green-Lagrange strain tensor. For equation (4.24) we have to take into consideration that

$$\begin{aligned} \Gamma_{B^\circ A^\circ}^{K^\circ} &= G^{K^\circ L^\circ} \Gamma_{A^\circ B^\circ, L^\circ} = \frac{1}{2} G^{K^\circ L^\circ} \left( \frac{\partial}{\partial X^{\circ A}} G_{B^\circ L^\circ} + \frac{\partial}{\partial X^{\circ B}} G_{A^\circ L^\circ} - \frac{\partial}{\partial X^{\circ L}} G_{A^\circ B^\circ} \right) = \\ &= G^{K^\circ L^\circ} \left[ \Gamma_{AB, L} - \left( \frac{\partial}{\partial X^{\circ A}} E_{B^\circ L^\circ}^\circ + \frac{\partial}{\partial X^{\circ B}} E_{A^\circ L^\circ}^\circ - \frac{\partial}{\partial X^{\circ L}} E_{A^\circ B^\circ}^\circ \right) \right] \end{aligned} \quad (4.26)$$

## 5. Conclusions

Applying a material coordinate system it has been pointed out that for solid bodies the compatibility field equation obtained from the principle of complementary virtual work is equivalent to the zero-valuedness of the Riemann-Christoffel curvature tensor:

- in the case of direct mapping the Riemann-Christoffel curvature tensor is expressed, according to (4.19)-(4.22), by the Cauchy deformation tensor defined as the metric tensor of the current configuration,
- in the case of inverse mapping the Riemann-Christoffel curvature tensor is expressed, according to (4.23)-(4.26), by the Green deformation tensor defined as the metric tensor of the reference configuration.

In the above statements, instead of the Riemann-Christoffel curvature tensors the Ricci tensors can equally be used.

**Note.** This paper is dedicated to I. Páczelt on the occasion of his 60th birthday since it applies one of the proposals of Prof. Lurie in his book 'Theory of elasticity' and I. Páczelt was a graduate student of Prof. Lurie in the years of 1966-1969.

## REFERENCES

1. WASHIZU, K.: *A note on the conditions of compatibility*, J. of Math. and Physics, **36**(4), (1958), 306-312.
2. GRYZ, J.: *On the compatibility conditions in the classical theory of elasticity*, Archiwum Mechaniki Stosowanej, **6**(19), (1967), 883-891.
3. KOZÁK, I.: *Remarks and contributions to the variational principles of the linearized theory of elasticity in terms of the stress functions*, Acta Technica Hung., **92**(1-2), (1981), 45-65.
4. KOZÁK, I.: *Linear Shell Theory in Terms of Stresses*, Dissertation, Miskolc, 1980, 246 p. (in Hungarian)

5. BERTÓTI, E.: *On mixed variational formulation of linear elasticity using nonsymmetric stresses and displacements*, International Journal of Solids and Structures, **34**, (1997), 1283-1292.
6. BERTÓTI, E.: *Indeterminacy of first order stress functions and the stress and rotation based formulation of linear elasticity*, Computational Mechanics, **14**, (1994), 249-265.
7. KOZÁK, I. AND SZEIDL, G.: *The field equations and boundary conditions with force stresses and couple stresses in the linearized theory of micropolar elastostatics*, Acta Technica Hung., **91**(1-2), (1980), 57-80.
8. KOZÁK, I.: *Remarks on the paper: "Determination of the necessary and sufficient compatibility conditions on the boundary"* written by G. Lámer, Alkalmazott Matematikai Lapok, 17 (1993), 329-345. (in Hungarian)
9. LURIE, A. I.: *Theory of Elasticity*, Nauka, Moscow, 1970, 939 p. (in Russian)



## **STRENGTH ANALYSIS OF HIGH PRESSURE STEEL PIPES REINFORCED BY COMPOSITE LAYERS**

LÁSZLÓ SÁRKÖZI

Department of Mechanics, University of Miskolc  
3515 Miskolc – Egyetemváros, Hungary  
mechsl@gold.uni-miskolc.hu

IMRE TÖRÖK

Department of Mechanical Technology, University of Miskolc  
3515 Miskolc – Egyetemváros, Hungary  
metti@gold.uni-miskolc.hu

[Received: April 6, 2000]

**Abstract.** Due to certain civil engineering activities, e.g. road construction, the safety factor of already working high pressure oil and gas transmitting pipes in the vicinity should be previously increased. For doing so the relatively new, but well proved, pipe guard technique is applied many times, by which several layers of glass fiber reinforced epoxy material is applied to the external cylindrical surface. For the knowledge of the mechanical behaviour and for the possibility of the standardisation of this new anisotropic and heterogeneous structure an analytical procedure and a computer program has been worked out in the frame of linear elasticity. In parallel, a number of experiments were also carried out for example for the determination of the pressure-volume change characteristics and for that of the bursting pressure. Results of the analytical calculations and experiments were compared and a good correlation was found.

*Keywords:* High pressure steel pipes, composite materials, reinforcement

### **1. Introduction**

In the practice of oil and gas transmission some sections of the high pressure steel pipes should be reinforced to avoid local damages due to the construction of civil engineering establishments like roads, railway lines etc nearby. The so-called clock spring technique is a highly recommended procedure for doing that by which several fiber reinforced epoxy layers are applied to the outer cylinder-jacket of the pipe. An analytical procedure has been worked out for predicting the expectable strength behaviour of this new complex, anisotropic and heterogeneous tube. On this base a simple computer program for the possibility of standardisation has also been developed. In this respect the basic question is the necessary number of the layers if both the initial and the attainable safety factors are known for a given tube geometry, steel material, working pressure and composite parameters. In addition to the analytical and computer analysis experimental investigations have been also carried out for the determination of the pressure – volume-change characteristics both for the original (pure steel) tube and for the reinforced tube structures. These experiments have been performed up to the ultimate bursting pressure, approx. 170-200 bar.

In the frame of the analytical procedure the model was considered as an infinitely long, complex tube constructed from inside by the original steel pipe and reinforced by an arbitrary number of epoxy-glass fiber layers from outside. The layers have the same thickness and they were reinforced by fibers with cross-bonded orientation per layer in such a way that the filling fibres were placed in circumferential and the chain fibers were placed in axial directions. Special measurements have been carried out to determine the chain and the filling direction elasticity moduli and the Poisson ratios. For controlling certain transformation formulae the elasticity modulus of the degree of 45 positioned composite layer was also investigated. The tube was assumed to be linearly elastic. Sections 2 and 3 present the closed form solutions for the radial displacements and the characteristic stress components and also the equivalent stresses in the steel tube and epoxy layer(s). Section 4 is devoted to the experimental determination of the safety factor and to the comparison of the experimental and computed results. Conclusions are presented in the last section.

## 2. The mechanical model and the computation strategy

By application of the clock spring technique we get a heterogeneous tube which is made up of the original steel pipe from inside and a multilayered glass fiber reinforced by a structural constituent made of epoxy material from outside. Mechanically the tube is considered to be infinitely long, linearly elastic, and the load is a constant pressure exerted on the internal surface. Consequently, in a cylindrical co-ordinate system the displacements in the axial direction  $z$  are free and the corresponding stresses are equal to zero. On this basis, for the computation of the characteristic displacement, strain and stress components along the thickness of the steel tube a boundary value problem should be established and analyzed making use of the data

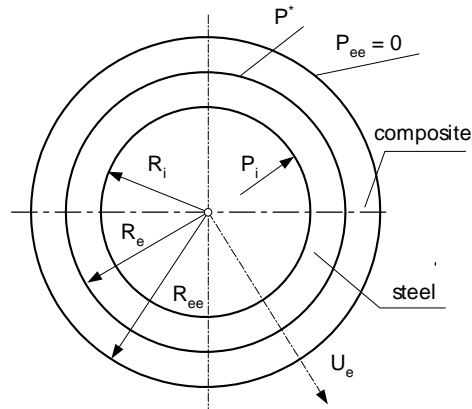


Figure 1. Boundary problem of a complex tube

shown in Figure 1. The main point of this activity is the determination of the internal pressure  $p^*$  between the steel and the epoxy as we shall see later.

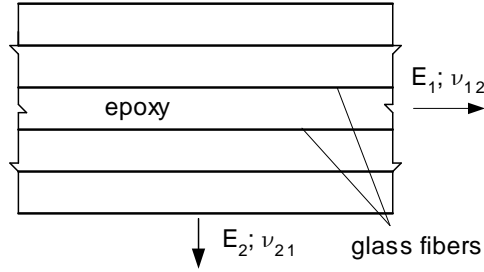


Figure 2. Composite layer reinforced in one direction

According to Figure 1 we have the following boundary conditions:

$$\begin{aligned} \sigma_R(R = R_i) &= -p_i, \\ \sigma_R(R = R_{ee}) &= 0. \end{aligned} \tag{2.1}$$

At the common radii  $R = R_e$  the radial displacement co-ordinate is denoted by  $u_e$ .

The material constants for the steel are the usual ones, i.e., the Young modulus (denoted by  $E$ ), and the Poisson ratio (denoted by  $\nu$ ). According to the literature of composite materials – see e.g.[1,2] – the material parameters for the substituting anisotropic thin layer are (see Figure 2.) as follows:

- $E_1$  is the elastic modulus in the direction of the fibers,
- $E_2$  is the elastic modulus in the direction perpendicular to the fibers,
- $\nu_{12}$  and  $\nu_{21}$  are the anisotropic Poisson ratios,
- $G$  is the shearing modulus of elasticity.

The well-known reciprocal relation reads

$$E_1\nu_{21} = E_2\nu_{12} \tag{2.2}$$

which means that only four material parameters are independent of each other. In our case the fibers are placed parallel either to the circumferential direction or to the axial direction, therefore the value of the shearing modulus has no importance.

If the material parameters are known, the geometrical data and the yield stress of the steel the computation can be based on the following ideas:

- first the function that relates the radial displacement at an arbitrary point of the external steel tube surface  $u_{e1}$  to  $p^*$ , as yet unknown contact pressure, should be determined in terms of the given internal pressure  $p_i$ ,
- secondly the function that relates the radial displacement at an arbitrary point on the internal surface of the epoxy tube  $u_{e2}$  to  $p^*$ , which can be considered as an internal pressure for this constituent, should be determined (the material of the epoxy tube is assumed to be orthogonally anisotropic),
- taking the equality  $u_e = u_{e1} = u_{e2}$  into account, we obtain a simple linear equation which can easily be solved for the unknown  $p^*$ ,
- in the following calculations we are concerned with the steel tube subjected to the internal pressure  $p_i$  and the contact pressure  $p^*$  as external pressure, then

the circumferential stress and the von Mises equivalent stress are calculated at the internal diameter which is the critical region of the tube,

- the last step is the determination of the safety factor  $n$ .

It is obvious that the above calculations can be repeated for one, two etc. clock spring layered structures in order to find the number of necessary layers for a given and improved safety factor.

### 3. Basic formulae for the computation

**3.1. The steel tube.** Following the steps of the above strategies first we have to deal with the well-known Euler type second order differential equation of a homogeneous and isotropic cylinder. Its closed form solution has been published in a number of textbooks. (See e.g. [3].) Recalling the usual notations we can write that:

- $u$  is the radial displacement,
- $\epsilon_R, \epsilon_\varphi, \epsilon_z$  are the strains in radial, tangential and axial directions, respectively,
- $\sigma_R, \sigma_\varphi, \sigma_z$  are the normal stresses in the same directions,
- $\gamma_{R\varphi}$  is the shear strain along the meridian,
- $\tau_{R\varphi}$  is the shear stresses along the meridian.

With these notations the stress and the strain vectors and also Hook's law can be constructed

$$\boldsymbol{\sigma}^T = [ \sigma_R, \sigma_\varphi, \sigma_z, \tau_{R\varphi} ] \quad \boldsymbol{\epsilon}^T = [ \epsilon_R, \epsilon_\varphi, \epsilon_z, \gamma_{R\varphi} ]$$

$$\boldsymbol{\sigma} = \mathbf{D}\boldsymbol{\epsilon} \quad (3.1)$$

where the constitutive matrix is of the form

$$\mathbf{D} = \frac{E(1-\nu)}{(1+\nu)(1-2\nu)} \begin{bmatrix} 1 & \nu & \nu & 0 \\ \nu & 1-\nu & \nu & 0 \\ \nu & \nu & 1-\nu & 0 \\ 0 & 0 & 0 & \frac{1-2\nu}{2(1-\nu)} \end{bmatrix} \quad (3.2)$$

It follows from (3.1) and (3.2) that

$$\sigma_R = \frac{E(1-\nu)}{(1+\nu)(1-2\nu)} \left[ \epsilon_R + \epsilon_\varphi \frac{\nu}{1-\nu} \right], \quad (3.3a)$$

$$\sigma_\varphi = \frac{E(1-\nu)}{(1+\nu)(1-2\nu)} \left[ \epsilon_\varphi + \epsilon_R \frac{\nu}{1-\nu} \right]. \quad (3.3b)$$

Substituting the above stress components into the geometrical formulae

$$\epsilon_R = \frac{du}{dR} \quad \text{and} \quad \epsilon_\varphi = \frac{u}{R} \quad (3.4)$$

and the results into the equilibrium equation

$$\frac{d\sigma_R}{dR} + \frac{\sigma_R - \sigma_\varphi}{R} = 0. \quad (3.5)$$

the well-known tube equation is obtained

$$\frac{d^2u}{dR^2} + \frac{1}{R} \frac{du}{dR} - \frac{u}{R^2} = 0. \quad (3.6)$$

Its general solution takes the form

$$u = K_1 R + \frac{K_2}{R} \quad \frac{du}{dR} = K_1 - \frac{K_2}{R^2} \quad (3.7)$$

where  $K_1$  and  $K_2$  are constants of integration which depend on the boundary conditions. Making use of the above relations but omitting the details we shall find that

$$u_{e1} = p^* I + J \quad (3.8)$$

in which the constants  $I$  and  $J$  can be given in terms of other constants  $A, \dots, H$ :

$$I = AR_e + \frac{D}{R_e} \quad J = - \left( BR_e + \frac{F}{R_e} \right) \quad (3.9a)$$

$$A = \frac{1}{C} \frac{R_e^2}{(R_i^2 - R_e^2)} \quad B = \frac{1}{H} \frac{p_i R_e^2}{(R_i^2 - R_e^2)} \quad (3.9b)$$

$$D = \frac{1}{C} \frac{R_e^2}{(R_i^2 - R_e^2)} \quad F = \frac{1}{H} \frac{p_i R_e^2 R_i^2}{(R_i^2 - R_e^2)} \quad (3.9c)$$

$$C = \frac{E(1-\nu)}{(1+\nu)(1-2\nu)} \quad H = \frac{E}{1+\nu} \quad (3.9d)$$

**3.2. The epoxy tube.** For the anisotropic epoxy tube produced by the clock spring technique the constitutive matrix can be taken from the book [4] by Lekhnitsky:

$$\mathbf{D} = \hat{H} \begin{bmatrix} n(1-\nu_2^2) & \nu_1 + n\nu_2^2 & n\nu_2(1+\nu_1) & 0 \\ \nu_1 + n\nu_2^2 & n(1-n\nu_2^2) & n\nu_2(1+\nu_1) & 0 \\ n\nu_2(1+\nu_1) & n\nu_2(1+\nu_1) & 1-\nu_1^2 & 0 \\ 0 & 0 & 0 & n(1-\nu_1^2)(1-2n\nu_2^2) \end{bmatrix} \quad (3.10)$$

where

$$\hat{H} = \frac{E_2}{(1+\nu_1)(1-\nu_1+2n\nu_2^2)}$$

and

$$\nu_1 = \nu_{12}; \quad \nu_2 = \nu_{21}; \quad m = \frac{G_2}{E_2}, \quad n = \frac{E_1}{E_2}.$$

Here the indexes 1 and 2 denote the principal material directions. These are parallel with the circumferential and axial directions.

Following the chain of ideas leading to equation (3.6), we arrive at the Euler type differential equation

$$\frac{d^2u}{dR^2} + \frac{1}{R} \frac{du}{dR} - \frac{1-n\nu_2^2}{1-\nu_1^2} \frac{u}{R^2} = 0 \quad (3.11)$$

which the radial displacement  $u$  within the anisotropic tube should meet. The general solution to this equation takes the form

$$u = C_1 e^{\sqrt{s}R} + C_2 e^{\sqrt{s}\frac{1}{R}} \quad (3.12)$$

where

$$s = \frac{1 - nv_2^2}{1 - v_2} . \quad (3.13)$$

As one can expect for  $n = 1$  differential equation (3.11) is that of the isotropic tube. From the technical point of view just the positive value of  $s$  is taken into consideration.

The constants of integration  $C_1$  and  $C_2$  in (3.12) can be calculated from the boundary conditions

$$\begin{aligned} \sigma_R &= -p^* & \text{if } R &= R_e , \\ \sigma_R &= 0 & \text{if } R &= R_{ee} . \end{aligned} \quad (3.14)$$

Making use the above formulae and the boundary conditions (3.14) but omitting again the details we shall find that

$$u_{e2} = Tp^* \quad (3.15)$$

where the constant  $T$  is given in terms of the constants  $P, Q, S$  and  $C$ :

$$\begin{aligned} T &= \frac{s}{(P-s)Q} e^{\sqrt{s}R_i} + \frac{1}{s-P} e^{\sqrt{s}\frac{1}{R_i}} \\ P &= \frac{1}{R_e^2} C e^{\sqrt{s}} (2nv_2^2 - n + v_1) ; & Q &= C e^{\sqrt{s}} (n + v_1) \\ S &= \frac{1}{R_{ee}^2} C e^{\sqrt{s}} (2nv_2^2 - n + v_1) ; & C &= \frac{E_2}{(1+v_1)(1-v_2-2nv_2)} . \end{aligned} \quad (3.16)$$

**3.3. The contact pressure and the safety factor.** Recalling the third point of our computation strategy, i.e., using the equality (3.8) to (3.15) the contact pressure  $p^*$  can be determined as

$$p^* = \frac{J}{T-I} . \quad (3.17)$$

With this value the strain and stress components  $\epsilon_R, \epsilon_\varphi, \sigma_R$  and  $\sigma_\varphi$  can easily be determined at the external diameter  $D_e$  and the internal diameter  $D_i$  which is the critical surface of the steel tube.

Then the equivalent stress can also be computed

$$\bar{\sigma} = \sigma_\varphi - \sigma_R . \quad (3.18)$$

Taking the equivalent stress on  $D_i$  the safety factor can be obtained from the relation

$$n = \frac{\sigma_{allowable}}{\bar{\sigma}} \quad (3.19)$$

#### 4. Parametric study

Making use of the formulae (3.3a,b), (3.7), (3.9a, . . . , d), (3.16), (3.17) and (3.19) a simple program has been developed in order to compute all the mechanical quantities and the safety factors both for an ‘original’ tube and for a clock spring reinforced tube by superimposing one, two etc. layers. As a parametric study a 12“ gas transmitting steel pipe was investigated provided that it is reinforced up to maximum six clock spring layers. The operational pressure  $p_i = 6$  MPa. The other input and output data are summarized below.

Data for the original steel pipe:

The inside diameter is  $D_i = 326$  mm and the outside diameter is  $D_e = 338$  mm. The Young modulus is  $E = 2.1 \cdot 10^5$  MPa, the Poisson ratio is  $\nu = 0.33$ , and the yield stress is  $\sigma_Y = 300$  MPa. The following data were calculated:

$\epsilon_{Re}$	$\epsilon_{\varphi e}$	$\sigma_{Re}$	$\sigma_{\varphi e}$		
-0.000338	0.000678	0.	160.0		
$\epsilon_{Ri}$	$\epsilon_{\varphi i}$	$\sigma_{Ri}$	$\sigma_{\varphi i}$	$\bar{\sigma}$	$n$
-0.000376	0.000716	-6.0	166.0	172.1	1.74

Table 1.

Data for the clock spring layers (1 and 2 identify the axial and tangential directions):  $E_1 = 1 \cdot 10^5$  MPa,  $E_2 = 2,5 \cdot 10^4$  MPa,  $\nu_{12} = 0,44$ ,  $\nu_{21} = 0,11$ ,  $G = 7,5 \cdot 10^3$ MPa. The maximum number of layers were 6 and the thickness of one layer was 1.0 mm.

The computational results are presented in Table 2:

No of layers	$\sigma_{Ri}$	$\sigma_{\varphi i}$	$\bar{\sigma}$	$n$
1	-6.0	157.0	157.0	1.91
2	-6.0	138.0	144.0	2.08
3	-6.0	128.0	134.0	2.25
4	-6.0	119.0	125.0	2.41
5	-6.0	111.0	117.0	2.57
6	-6.0	104.0	110.0	2.73

Table 2.

According to the expectations the more layers we have, the higher the safety factor is. The functional connection is linear.

#### 5. Experiments, measurements and validation of the computation strategy

The authors had a chance to make experiments in lab circumstances with the so called cross-bonded plies of thickness 0.75 mm. The quality, diameter and density of the

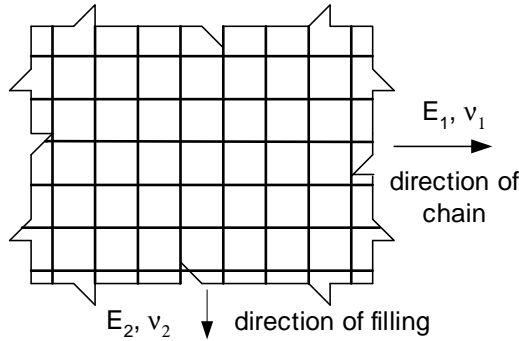


Figure 3. Composite layer reinforced in two direction

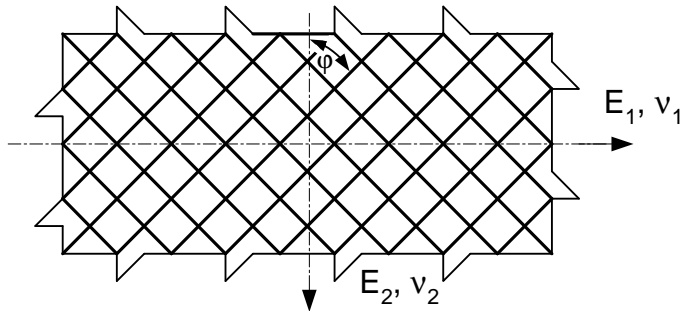


Figure 4. Composite layer reinforced in direction  $45^\circ$

fibers were equal both in the chain direction and in the filling direction along a ply as is shown in Figure 3. Previously, by using flat samples with 2, 3 and 4 reinforced layers, tests were carried out for the determination of the unidirectional tension strength applying the load in chain direction, then in filler direction and finally in a 45 degree oblique direction – see Figure 4. It is easy to see that in these cases the samples should behave like an isotropic material. The measurements are in good agreement with this expectation since the data measured are nearly equal to each other – see Table 3. For the practical determination of the volume – pressure characteristic and the elastic limit and bursting pressure an experimental investigation was carried out by using a compressor testing set at the Department of Mechanical Technology, University of Miskolc. The facility is characterized by a maximum pressure limit of 40 MPa and a maximum volume change of  $2500 \text{ cm}^3$  per one stroke of the piston. Both an original tube and a six layer reinforced tube were measured. The length of the tube

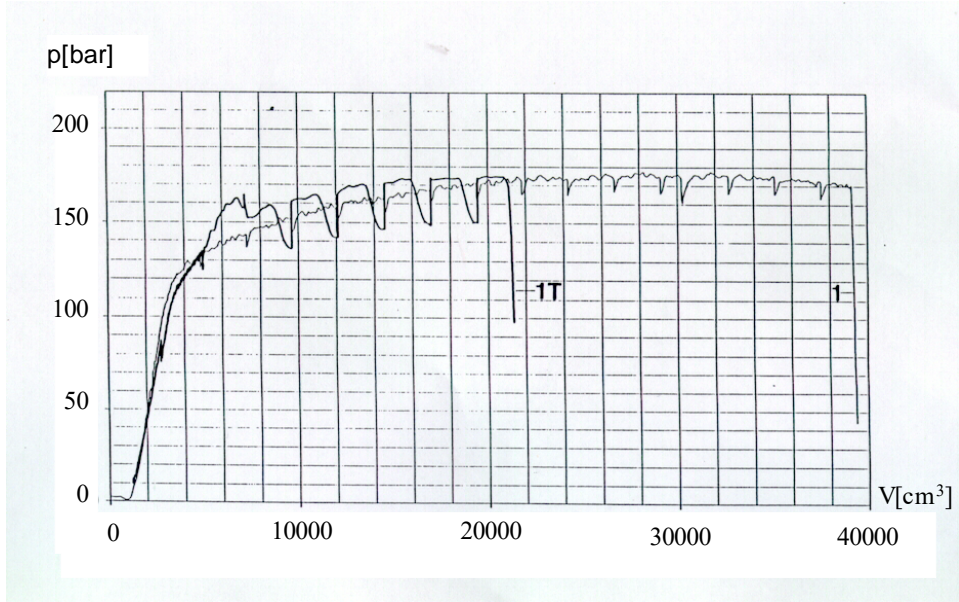


Figure 5. Pressure against volume for steel and a reinforced tube (curves 1 and 1T)

Direction of force	Strength in tension [MPa]		
	Layers		
	2	3	4
chain	238	241	249
filling	254	245	251
oblique	237	241	247

Table 3.

sample was 2115 mm, the external diameter 325 mm, and the thickness of the steel pipe was 5,5 mm. The normal operational pressure of this pipe is 6.5 MPa. The material parameters of the steel were  $E_{steel} = 2.0 \cdot 10^5$  MPa,  $\nu_{steel} = 0.33$ , and  $\sigma_{allowable} = 360$  MPa, while the parameters of the composite layers were  $E = E_1 = E_2 = 5 \cdot 10^4$  MPa,  $\nu = \nu_1 = \nu_2 = 0.44$ ,  $G = 7.5 \cdot 10^3$  MPa, the number of layers was 6 and the thickness of one layer was 0.75 mm.

As can be seen in Figure 5. the pressure increase was continued to the total burst of the specimens. This value for the homogeneous pipe (curve 1) is 178 bar and for the heterogeneous pipe reinforced by six composite layers (curve 1T) is 175 bar. They are practically the same. The elastic limit for curve 1 is 134 bar. On the other hand the elastic limit is 163 bar for curve 1T, which clearly shows that there is an increase of 21.6%.

Numerical calculations for a maximum of six plies have been also performed with the results shown in Tables 4 and 5.

Tube made only of steel

$\varepsilon_{Re}$	$\varepsilon_{\varphi e}$	$\sigma_{Re}$	$\sigma_{\varphi e}$
-0.000380	0.000760	0.	180

$\varepsilon_{Ri}$	$\varepsilon_{\varphi i}$	$\sigma_{Ri}$	$\sigma_{\varphi i}$	$\sigma$	$n$
-0.000420	0.000801	-6.4	186	192.3	1.87

Table 4.

Number of layers	$\sigma_{Ri}$	$\sigma_{\varphi i}$	$\sigma$	$n$
1	-6.4	180	186	1.93
2	-6.4	174	180	2.00
3	-6.4	168	175	2.06
4	-6.4	163	170	2.12
5	-6.4	159	165	2.18
6	-6.4	154	161	2.24

Table 5.

According to the computation the improvement in the safety factor for the case of six layers is 19.7%, which is very close to the previous value.

## 6. Concluding remarks

Both the analytical and experimental investigations and results proved the applicability of the clock spring technique by which the safety factor of high pressure transporting steel pipes can be improved. In the algorithm an arbitrary number of layers and arbitrary fiber orientation can be taken into consideration, however, up to the moment only orthotropic and transversely isotropic problems have been solved. Making use of the computational procedure we have developed the necessary number of the composite layers for given geometrical and material data can also be determined. As far as the value of the pressure  $p^*$  is known from the analysis, a future task could be the determination of the strains and stresses in the composite plies. On the other hand, taking the non-linear behavior of the steel into consideration (for example by assuming an elastic-ideally plastic constitutive law) the bursting pressure could analytically be determined and the results could also be compared with experimental data. This work is in progress.

## REFERENCES

1. CHAWLA, K. K.: *Composite Materials: Science and Engineering*, Springer-Verlag, New York, London 1987.
2. HERAKOVICH, C. T.: *Mechanics of Fibrous Composites*, John Wiley & Sons, Inc. New York, 1998.
3. THIMOSSENKO, S. P.: *Theory of Elasticity*, Third Edition, McGraw-Hill, 1970.
4. LEKHNITSKY, S. G.: *Theory of Elasticity of Anisotropic Bodies*, Holden-Day, San Francisco, 1963.

## **COST-EFFECTIVE STRUCTURAL OPTIMIZATION**

JÓZSEF FARKAS

Department of Materials Handling and Logistics, University of Miskolc  
3515 Miskolc – Egyetemváros, Hungary  
altfar@uni-miskolc.hu

[Received: August 15, 1999]

*Dedicated to Professor István Páczelt on the occasion of his sixtieth birthday*

**Abstract.** A special cost function enables designers to separate the material and fabrication costs to estimate a realistic minimum cost design of welded structures and to show the achievable cost savings. As a review of our research results in this field, numerical examples of I-beams, stiffened box beams, stiffened plates loaded by hydrostatic pressure, Vierendeel trusses, silos and bridge decks illustrate that significant cost savings can be achieved by minimum cost design.

*Keywords:* Cost function, welded structures

### **1. Introduction**

The aim of optimum design is to find better structural solutions, which are safe and economic. The safety is guaranteed by fulfilling the design constraints and the economy is achieved by minimization of a cost function. Thus, a structural optimization needs a realistic cost function as well as design constraints, which express all the important engineering aspects. The constrained function minimization problem defined above can be solved using efficient computerized mathematical methods.

The aim of the present study is to show that, to bridge the gap between the optimization theory and design practice, it is necessary to include in the optimum design procedure a cost function, which contains not only the material, but also the fabrication costs. The effectiveness of the minimum cost design is illustrated by cost savings achieved for several structural examples.

### **2. Main phases of the structural optimization**

A structural solution is characterized by materials used, dimensions, geometry, topology, profiles, production technology, connections, erection and maintenance. The cost function and the design constraints should contain these characteristics. Certain combinations of these characteristics give possible structural versions and the most suitable optimum solution is selected from these versions. The selection is made by means of comparisons, but only optimized versions can be realistically compared to each other.

The formulation of a cost function as well as the design constraints needs a large analytical research. Optimization means that the designer, on the basis of analytical results, knows the behaviour of a structure in a wide range of loads and characteristics mentioned above.

The optimum design procedure has three main phases as follows:

1. preparation: selection of candidate structural versions, definition of the cost function and the design constraints;
2. constrained function minimization using computerized mathematical methods;
3. evaluation: comparisons, working out design rules and expert systems.

### 3. The cost function

In the past the aim of aircraft designers was to minimize the structural weight, but now the optimization procedure is much more complex. Schmit [1] has emphasized that, for the development of structural synthesis, cost functions should be used instead of minimum weight design.

In the industrial practice the cost relating to the total weight of a structure is usually calculated. With these data only the minimum weight design can be solved. For a realistic cost minimization the material and fabrication costs should be separated. This necessity can be illustrated by the example of a welded stiffened plate. In this case different numbers of stiffeners give minimum weight and minimum cost. Minimum weight design means many thin stiffeners (like a honeycomb sandwich), but, because of the high welding cost, the optimum number of stiffeners for minimum cost is much smaller. The greater the ratio fabrication cost/total cost, the greater the difference between the minimum weight and cost designs.

In the cost function the material and fabrication costs are included

$$K = K_m + K_f = k_m \rho V + k_f \sum T_i \quad (3.1)$$

where  $\rho$  is the material density,  $V$  is the volume of structure,  $k_m$  and  $k_f$  are the material and fabrication cost factors, respectively,  $T_i$  are the production times. Equation (3.1) can be written in the form

$$\frac{K}{k_m} = \rho V + \frac{k_f}{k_m} (T_1 + T_2 + T_3) . \quad (3.2)$$

Time for preparation, assembly and tacking can be expressed as

$$T_1 = C_1 \Theta_d (\kappa \rho V)^{1/2} \quad (3.3)$$

where  $C_1 = 1 \text{ min/kg}^{0.5}$ ,  $\Theta_d$  is a difficulty factor expressing the complexity of the structure (planar or spatial, constructed from simple plate elements or profiles),  $\kappa$  is number of structural elements to be assembled.

Time for welding can be expressed as

$$T_2 = \sum C_{2i} a_{wi}^n L_{wi} \quad (3.4)$$

where  $a_w$  is the weld size,  $L_w$  is the weld length. Formulae for  $C_{2i}a_w^n$  are developed using the COSTCOMP database for different welding technologies and weld types – [2,3].

The additional time for electrode changing, deslagging and chipping can be calculated as

$$T_3 = 0.3T_2 \tag{3.5}$$

The final form of the cost function is

$$\frac{K}{k_m} = \rho V + \frac{k_f}{k_m} \left( C_1 \Theta_d (\kappa \rho V)^{1/2} + 1.3T_2 \right) \tag{3.6}$$

The following data of cost factors are used:  $k_m = 0.5 - 1.2$  \$/kg,  $k_f = 0 - 60$  \$/manhour = 0-1 \$/min. To give internationally usable results, values of  $k_f/k_m = 0, 1$  and  $2$  kg/min are considered, the value of 0 means minimum weight design.

E.g. for fillet welds the welding cost formulae are given in Table 1 – Farkas-Jármai [4], Jármai-Farkas [5].

Welding technology	$a_w$ (mm)	$10^3 C_2 a_w^n$ (min/mm)
SMAW	0-15	$0.7889a_w^2$
GMAW-C	0-15	$0.3394a_w^2$
GMAW-M	0-15	$0.3258a_w^2$
SAW	0-15	$0.2349a_w^2$

Table 1. Welding times for a weld length unit  $T_2/L_w$  (min/mm) of longitudinal fillet welds in normal position in the function of weld size and welding technology

The used abbreviations are as follows: SMAW – shielded metal arc welding, GMAW-C -gas metal arc welding with CO2, GMAW-M- gas metal arc welding with mixgas, SAW- submerged arc welding.

The above described cost function cannot give generally valid values, but it is suitable for realistic comparisons of structural versions. In the cost function only those parts should be considered, which contain the structural parameters to be optimized. For instance, times required for transportation of product elements between fabrication places in a manufacture is not necessary to calculate, since the structural dimensions to be optimized do not vary in such measure, which could affect the transportation times.

#### 4. Design constraints

The development of structural optimization always needs new design aspects to be included in the procedure. In some recent studies we have considered a new design constraint on the limitation of the residual welding distortions. We have shown that our calculation method for residual welding stresses and distortions is suitable for estimation of these phenomena [6] and we have used our simple formulae in the structural optimization to guarantee the quality of welded structures containing eccentric welds, which can cause large deformation due to their shrinkage.

In the mathematical formulation of constraints on stress, fatigue, stability and fabrication requirements we need the up-to-date rules of related design standards. These rules express the safety and quality requirements in relatively simple forms, which are suitable for effective computations. The rules are based on international theoretical and experimental research results. The problem is that standards do not give all important details for design, thus, we should use in many cases more standards to include all the important constraints. For instance, Eurocode 3 [7, EC3 1992] is not completed for all the structural types yet, so we need to use BS (British), DIN (German) or API (American Petroleum Institute) rules as well.

To illustrate the measure of cost savings achievable by structural optimization some examples are shown from our recent studies.

## 5. Examples of application

**5.1. Rolled and welded I-beams.** The characteristics of the rolled I-section of UB I 914x419x388 – [7], [8, BS4 1993] – are as follows: the cross-section area is  $A = 49400 \text{ mm}^2$ , the elastic section modulus is  $W_x = 15.63 \times 10^6 \text{ mm}^3$ . The optimum web height of the welded I-section having the same section modulus can be calculated as [4,9]

$$h = (3W_0/2\beta)^{1/3} \quad (5.1)$$

where  $W_0$  is the required section modulus. The limiting web slenderness for pure bending according to EC3 is

$$\frac{1}{\beta} = 124\varepsilon \quad \varepsilon = \left(\frac{235}{f_\theta}\right)^{1/2} \quad (5.2)$$

For the yield stress  $f_y = 355 \text{ MPa}$  we obtain  $h = 1335 \text{ mm}$  and the web thickness is  $t_w = \beta h = 13 \text{ mm}$ . The limiting slenderness of the flange  $1/\delta = 28\varepsilon$  is and the flange width

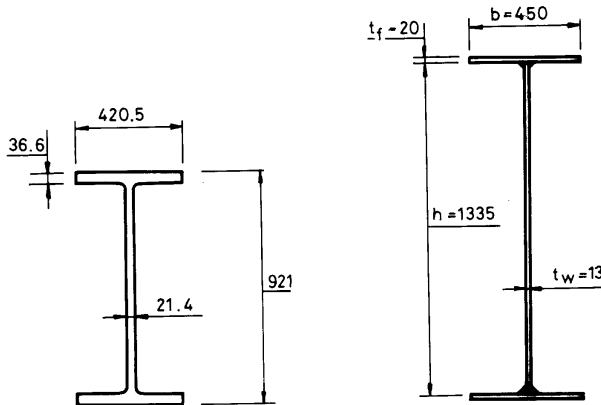


Figure 1: Comparison of a rolled and a welded I beam

is  $b = h(\beta/2\delta)^{1/2} = 450$  mm, the flange thickness is  $t_f = \delta b = 20$  mm. The cross-section area of the welded I-beam is  $A = 35355$  mm<sup>2</sup>, which is 40% smaller, than that of a rolled beam.

The cost of the welded I-beam of span length 10 m can be calculated using equations (3.2-3.6). Data:  $\rho = 7850$  kg/m<sup>3</sup>,  $k_f/k_m = 1$  kg/min,  $\Theta_d = 2$ , double fillet welds of size  $a_W = 6$  mm, GMAW-M. With these data  $K/km = 3567$  kg. For the rolled I-beam we obtain 3878 kg, thus, the welded

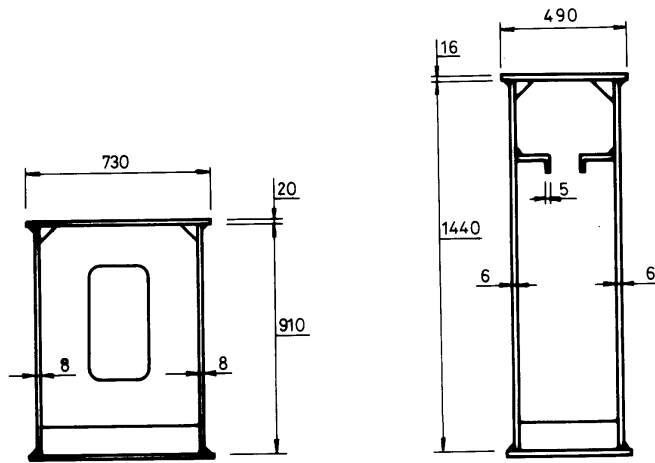


Figure 2: Comparison of box beams without and with longitudinal stiffeners

beam is 9% cheaper than the rolled one. It can be seen from the Figure 1 that this saving is achieved using thinner plates. It should be mentioned that this result is valid for beams in which the effect of shear can be neglected.

**5.2. Welded box beams without and with longitudinal stiffeners.** The limiting slenderness of a welded box beam loaded in bending can be increased by using longitudinal stiffeners in the 1/5 of the web height (Fig.2), therefore the web thickness can be decreased. The detailed minimum cost design procedures for box beams without and with longitudinal stiffeners, in which the transversal diaphragms and their welds are also considered [10], show that the cost of the box beam with stiffeners is 20% smaller than that of the beam without stiffeners.

**5.3. Welded stiffened plates loaded in bending by hydrostatic pressure.** For a simply supported base plate the equidistant arrangement of horizontal stiffeners is not optimal, since in this case the base plate parts of equal thickness are loaded by different maximal bending moments. The optimum positions of stiffeners can be calculated using the condition that all the base plate parts should be stressed to yield strength. In the numerical example treated in our study [11] the optimum number of stiffeners is determined as well, which gives the minimum cost of the whole plate structure. Trapezoidal stiffeners designed for bending are considered and the cost of vertical butt welds joining the

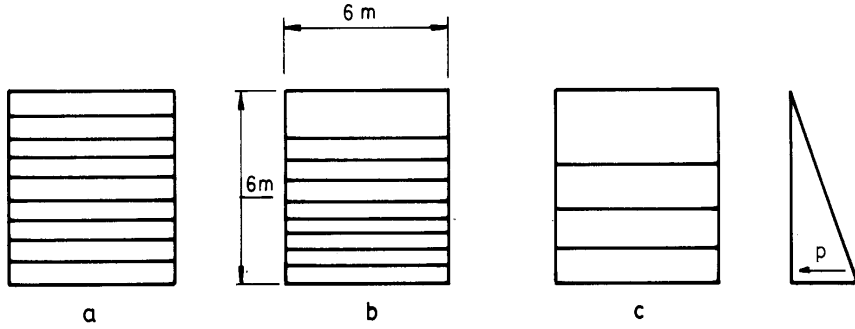


Figure.3: Values of  $K/k_m$  (kg) for a stiffened steel plate loaded by hydrostatic pressure: (a) 6972 for 8 stiffeners in equidistant position, (b) 6111 for 8 stiffeners in optimized position, (c) 7749 for 3 stiffeners in optimized position

base plate parts is also taken into account. The detailed calculations show that the optimum number of stiffeners is 8, using optimized stiffener positions 18% cost savings can be achieved compared with 8 stiffeners in equidistant position ( $k_f/k_m = 1$ ). Using 8 stiffeners instead of 3 in optimum positions 31% cost savings can be achieved ( $k_f/k_m = 1$ ), since the plate thicknesses can be decreased (Fig.3).

**5.4. Optimum number of columns of a Vierendeel truss.** In a numerical example of a simply supported Vierendeel truss (Fig.4.) welded from square hollow section rods the detailed calculations [12] show that the minimum cost can be achieved using 12 columns. The cost difference between structural versions of 10 and 12 columns is 30%.

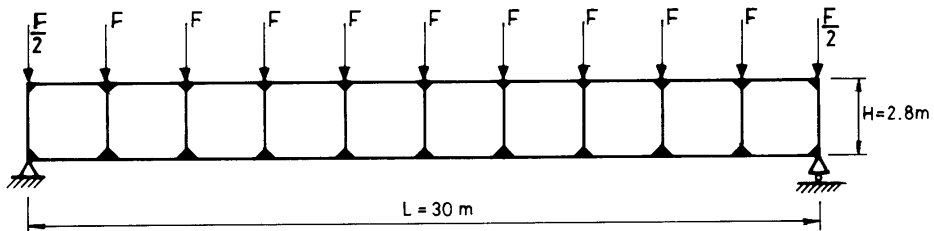


Figure 4: A simply supported Vierendeel truss with parallel chords welded from square hollow section rods

**5.5. Welded steel silo.** A detailed cost analysis is performed in the case of a silo of capacity 500 m<sup>3</sup> loaded by cement powder consisting of a roof, cylindrical bin, ringbeam, hopper and columns [13]. The calculations show that the total cost depends on the ratio bin height/bin radius. The optimal value of this ratio was 6.20, the cost difference between the structural versions of ratio 1.76 and 6.20 was 8%.

**5.6. Welded highway bridge deck with trapezoidal longitudinal stiffeners.** Most of structural dimensions of a bridge deck should be determined according to standard prescriptions, but the distance of transverse stiffeners can be optimized. In the case of a numerical example treated in our study [14] the optimal distance was 2.5 m. The cost difference between the structural versions of distances 2.5 and 4.0 m was 20%.

## 6. Conclusions

A relatively simple cost function is proposed for the calculation of material and fabrication costs of welded structures. This cost function enables designers to show the difference between structural versions corresponding to minimum weight and minimum cost. The treated numerical examples show that significant cost savings can be achieved using optimization methods.

**Acknowledgement.** This work has been supported by grants OTKA 19003 and OTKA 22846 of the Hungarian Fund of Scientific Research.

## REFERENCES

1. SCHMIT, L.A. jr.: *Structural optimization – some key ideas and insights*. In “New Directions in Optimum Structural Design. Eds. Atrek, E., Gallagher, R.H. et al. Wiley & Sons, Chichester etc.”, 1984, pp.1-45.
2. COSTCOMP: *Programm zur Berechnung der Schweisskosten*. Deutscher Verlag für Schweisstechnik, Düsseldorf, 1990.
3. BODT, H. J. M.: *The Global Approach to Welding Costs*. The Netherlands Institute of Welding, The Hague, 1990.
4. FARKAS, J. and JÁRMAI, K.: *Analysis and Optimum Design of Metal Structures*, Rotterdam - Brookfield, Balkema, 1997.
5. JÁRMAI, K. and FARKAS, J.: *Cost calculation and optimisation of welded steel structures*, Journal of Constructional Steel Research, 50, (1999), 115-135.
6. FARKAS, J. and JÁRMAI, K.: *Analysis of some methods for reducing residual beam curvatures due to weld shrinkage*, Welding in the World, 41, (1998), 385-398.
7. The Steel Construction Institute: *Section Properties and Member Resistances to Eurocode 3*. Publ. 158. Berkshire, UK, 1997.
8. BS 4: Part 1.: *Structural Steel Sections – Specification for Hot Rolled Sections*, 1993.
9. FARKAS, J.: *Optimum Design of Metal Structures*, Budapest Akadémiai Kiadó, Chichester, Ellis Horwood, 1984.
10. JÁRMAI, K. and FARKAS, J.: *Optimum cost design of welded box beams with longitudinal stiffeners using advanced backtrack method*, 3rd World Congress of Structural and Multidisciplinary Optimization, Buffalo, New York. Short paper proceedings. Vol.2. (1999), 363-365.  
FARKAS, J. and JÁRMAI, K.: *Optimum design of welded stiffened plates loaded by hydrostatic normal pressure*. 3rd World Congress of Structural and Multidisciplinary Optimization, Buffalo, New York. Short paper proceedings. Vol.2. (1999), 493-495.
11. FARKAS, J. and JÁRMAI, K.: *Minimum cost design of SHS Vierendeel trusses*, Tubular

Structures VII. Proc. 7th Int. Symposium on Tubular Structures, Miskolc, 1996. Eds. Farkas, J. and Jármai, K. Rotterdam-Brookfield, Balkema.

12. FARKAS, J. and JÁRMAI, K.: *Fabrication cost calculation and optimum design of welded steel silos*, *Welding in the World*, 37(5), (1996), 225-232.
13. JÁRMAI, K., HORIKAWA, K., and FARKAS, J.: *Economic design of steel bridge decks*, *Welding in the World*, 41(1), (1998), 49-59.

## Notes for Contributors

### to the Journal of Computational and Applied Mechanics

**Aims and scope.** The aim of the journal is to publish research papers on theoretical and applied mechanics. Special emphasis is given to articles on computational mechanics, continuum mechanics (mechanics of solid bodies, fluid mechanics, heat and mass transfer) and dynamics. Review papers on a research field and materials effective for teaching can also be accepted and are published as review papers or classroom notes. Papers devoted to mathematical problems relevant to mechanics will also be considered.

**Frequency of the journal.** Two issues a year (approximately 80 pages per issue).

**Submission of Manuscripts.** Submission of a manuscript implies that the paper has not been published, nor is being considered for publication elsewhere. Papers should be written in standard grammatical English. Two copies of the manuscript should be submitted on pages of A4 size. The text is to be 130 mm wide and 190 mm long and the main text should be typeset in 10pt CMR fonts. Though the length of a paper is not prescribed, authors are encouraged to write concisely. However, short communications or discussions on papers published in the journal must not be longer than 2 pages. Each manuscript should be provided with an English Abstract of about 50–70 words, reporting concisely on the objective and results of the paper. The Abstract is followed by the Mathematical Subject Classification – in case the author (or authors) give the classification codes – then the keywords (no more than five). References should be grouped at the end of the paper in numerical order of appearance. Author's name(s) and initials, paper titles, journal name, volume, issue, year and page numbers should be given for all journals referenced.

The journal prefers the submission of manuscripts in  $\text{\LaTeX}$ . Authors should prefer the standard  $\text{\LaTeX}$  article style and are not recommended to define their own  $\text{\LaTeX}$  commands. Visit our home page for further details concerning the issue how to edit your paper.

For the purpose of refereeing, two copies of the manuscripts should initially be submitted in hardcopy to an editor of the journal. The eventual supply of an accepted-for-publication paper in its final camera-ready form (together with the corresponding files on an MS-DOS diskette) will ensure more rapid publication. Format requirements are provided by the home page of the journal from which sample  $\text{\LaTeX}$  files can be downloaded:

<http://www.uni-miskolc.hu/home/web/pumns/mechanics>

These sample files can also be obtained directly (via e-mail) from a member of the Editorial Board Gy. Szeidl (mechszgy@gold.uni-miskolc.hu), upon request.

Twenty offprints of each paper will be provided free of charge and mailed to the correspondent author.

The Journal of Computational and Applied Mechanics is abstracted in the Russian Referativnij Zhurnal.

Responsible for publication: Rector of the University of Miskolc Published by the Miskolc University Press under the leadership of Dr. József PÉTER Responsible for duplication: works manager Mária KOVÁCS Number of copies printed: 200 Put to the Press on August 22, 2000 Number of permission: TU 2000-800-ME **HU ISSN 1586-2070**

## **A Short History of the Publications of the University of Miskolc**

The University of Miskolc (Hungary) is an important center of research in Central Europe. Its parent university was founded by the empress Maria Teresia in Selmechánya (today Banská Štiavnica, Slovakia) in 1735. After the first world war the legal predecessor of the University of Miskolc moved to Sopron (Hungary) where, in 1929, it started the series of university publications with the title *Publications of the Mining and Metallurgical Division of the Hungarian Academy of Mining and Forestry Engineering* (Volumes I.-VI.). From 1934 to 1947 the Institution had the name Faculty of Mining, Metallurgical and Forestry Engineering of the József Nádor University of Technology and Economical Sciences at Sopron. Accordingly the publications were given the title *Publications of the Mining and Metallurgical Engineering Division* (Volumes VII.-XVI.). For the last volume before 1950 – due to a further change in the name of the Institution – *Technical University, Faculties of Mining, Metallurgical and Forestry Engineering, Publications of the Mining and Metallurgical Divisions* was the title.

For some years after 1950 the Publications were temporarily suspended.

After the foundation of the Faculty of Mechanical Engineering in Miskolc in 1949 and the movement of the Sopron Mining and Metallurgical Faculties to Miskolc, the Publications restarted with the general title *Publications of the Technical University of Heavy Industry* in 1955. Four new series - Series A (Mining), Series B (Metallurgy), Series C (Machinery) and Series D (Natural Sciences) - were founded in 1976. These came out both in foreign languages (English, German and Russian) and in Hungarian.

In 1990, right after the foundation of some new faculties, the university was renamed to University of Miskolc. At the same time the structure of the Publications was reorganized so that it could follow the faculty structure. Accordingly, three new series were established: Series E (Legal Sciences), Series F (Economical Sciences) Series G (Humanities and Social Sciences). The seven series are formed by some periodicals and such publications which come out with various frequencies.

Papers on computational and applied mechanics were published in the

### **Publications of the University of Miskolc, Series D, Natural Sciences.**

This series was given the name Natural Sciences, Mathematics in 1995. The name change reflects the fact that most of the papers published in the journal are of mathematical nature though papers on mechanics also come out.

The series

### **Publications of the University of Miskolc, Series C, Fundamental Engineering Sciences**

founded in 1995 also published papers on mechanical issues. The present journal, which is published by the support of the Faculty of Mechanical Engineering as a member of the Series C (Machinery), is the legal successor of the above journal.



# Journal of Computational and Applied Mechanics

Volume 1, Number 1 (2000)

---

## Contents

### Contributed Papers

Edgár BERTÓTI: Applicability of a constant Young's modulus in geometrically nonlinear elasticity	3–12
István ECSEDI: Stress functions for torsion-free axisymmetric state of stress	13–21
János ÉGERT: Iterative algorithms for the solution of frictionless contact problems	23–36
László FORRAI: A finite element model for stability analysis of symmetrical rotor systems with internal damping	37–47
Károly JÁRMAI: Optimum design of stiffened plates	49–69
Imre KOZÁK: Principle of complementary virtual work and the Riemann-Christoffel curvature tensor as compatibility condition	71–79
László SÁRKÖZI: Strength analysis of high pressure steel pipes reinforced by composite layers	81–90

### Review Paper

József FARKAS: Cost-effective structural optimization	91–98
---	-------